ANNUAL RESEARCH REPORT

July 2023-June 2024

Bangladesh Space Research and Remote Sensing Organization (SPARRSO)

Bangladesh Space Research and Remote Sensing Organization (SPARRSO)
Ministry of Defence
Government of the People's Republic of Bangladesh

ANNUAL RESEARCH REPORT

July 2023-June 2024

SPARRSO

Advisor

Mr. Md. Rashedul Islam

Chairman (Additional Secretary)

Editorial Committee

Mr. Jashim Uddin Haider, Member (Joint Secretary)	Convener
Dr. Md. Abdus Salam, Chief Scientific Officer	Member
Dr. B. M. Refat Faisal, Principal Scientific Officer	Member
Ms. Farhana Tazneen, Senior Scientific Officer	Member
Mr. Md Farid Uddin, Scientific Officer	Member
Mr. Naim Islam Talukder, Scientific Officer	Member
Mr. Rubel Kanti Dey, Information Officer	Member-Secretary

Published by

Bangladesh Space Research and Remote Sensing Organization (SPARRSO)

Agargaon, Sher-e-Bangla Nagar, Dhaka-1207, Bangladesh.

Phone: +88-02-48117692

Fax: +88-02-48111169

E-mail: admin@sparrso.gov.bd

October 2024

Table of Content

Mapping Tree Covers in Bangladesh

Md. Mahmudur Rahman*, Md. Abu Taleb Pramanik, Mehedi Hasan Peas, M. Ziaul Islam

Bangladesh Space Research and Remote Sensing Organization (SPARRSO), Agargaon, Sher-e-Bangla Nagar, Dhaka-1207, Bangladesh.
**Corresponding author E-mail: mahmud@sparrso.gov.bd*

Abstract

Tree resources in many countries are changing because of natural and man-made interventions. Earlier efforts for preparing country-scale forest cover maps in Bangladesh used visual interpretation and on-screen digitizing techniques, satellite image segmentation, etc., which are time-consuming. The objectives of this study are (a) to develop a methodology for mapping forests and tree covers with Landsat data using a pixel-based classification approach and (b) to prepare tree cover maps for entire Bangladesh using Landsat-8/9 data. The training samples were collected from all the major spectral sub-classes, completed the classification with a guided clustering process, and later the spectral subclasses were merged into the original land cover classes. Several classification algorithms, including the maximum likelihood classification, minimum distance classification, and machine learning techniques, like random forests, were considered to map forest, bamboo or shrub cover, cropland, water-bodies, and other land to non-forest classes. The generation of tree cover maps during the 2023-2024 financial year was implemented for Landsat scenes 138-042, 138-043, and 138-043. Within the next financial year, the classification of all the remaining scenes should be completed.

Keywords: Trees, Pixel-based classification, Algorithm, Landsat, Bangladesh.

Introduction

Trees are important as they provide numerous goods and services to society. They provide timber for construction and furniture, fuelwood for cooking, fodder for pasture, and fruits for humans. Besides these goods, trees purify our air, provide housing to millions of species that protect us from disease, cool our streets and cities, protect against floods and water pollution, and ease our minds during stressful times. Trees act as a reservoir of terrestrial carbon stocks and assist in combating global climate change.

Tree resources in many countries are changing because of natural and man-made interventions. Therefore, it is important to monitor tree resources in a country over time. Bangladesh located in the Ganges-Brahmaputra delta basin is also experiencing changes in tree resources. The natural vegetation of Bangladesh consists of tropical moist ever-green and semi-evergreen forests, tropical moist deciduous forests, mangroves, and freshwater wetlands which are rich in biodiversity, and some of them are

connected to Indo-Burma biodiversity hotspots (Myers et al., 2000; Olson et al., 2001; Potapov et al., 2017). However, the natural vegetation of this developing and densely-populated country is undergoing a negative change due to tremendous pressure and demand for forest-based products such as timber, fuel-wood, and agricultural land expansion (Reddy et al., 2016). Despite this decreasing trend in natural vegetation, planted areas such as village woodlots, homestead trees, and small-scale plantations are increasing (Potapov et al., 2017).

Therefore, preparing tree cover maps and statistics for a periodical time frame is an important task to understand the dynamics of tree covers over time. However, earlier efforts for preparing country-scale forest cover maps in Bangladesh used visual interpretation and on-screen digitizing techniques, satellite image segmentation, etc., which are time-consuming techniques. These practices usually make it difficult and require higher budgets for preparing county-scale forest cover maps. The current effort is dedicated to working on the generation of tree cover maps and statistics using automated digital classification techniques that will ease the preparation of tree cover maps on a country scale spending a shorter amount of time and resources.

Bangladesh's Bangladesh Forest Department (BFD) implemented the first National Forest Assessment (NFA) in 2005–2007, covering national forests, whereas previous management inventories were limited to selected forest areas only (FD & FAO 2007). In a systematic design, it included remote sensing analyses which were done by SPARRSO (Bangladesh Space Research and Remote Sensing Organization), and a ground inventory with sampling plots across the country. Later BFD launched the first BFI (Bangladesh Forest Inventory) cycle in 2015. All land uses in the country (not only forest land) are taken into consideration.

The National Land Cover Map 2015 was produced under the National Land Representation System (NLRS) development process of Bangladesh where tree cover mapping was done under the class-vegetated area. This class was further sub-classed into five levels such as terrestrial and aquatic, then to natural and cultivated, further to tree-dominated areas, shrub-dominated areas, evergreen forests, mixed forests, plantations, etc. SPOT 6/7 images of 6 m resolution were used for this purpose (Jalal et al., 2019).

Following the above-mentioned attempts for national tree cover mapping in Bangladesh, there is a recent initiative to update the map with 2023 satellite images. The above study used a vector segmentation to prepare the National Land Cover Map of 2023. However, this study on national tree cover mapping utilizes 30m Landsat data and uses a raster-

based classification approach. Upon completion, both of these maps can be compared. The objectives of this study are

(i) to develop a methodology for mapping forests and tree covers with Landsat data using a pixel-based classification approach; information from different vegetation indices and global tree height data was incorporated to discriminate trees from shrub land, cropland, and other vegetated land.
(ii) to prepare tree cover maps for Bangladesh using Landsat-8/9 data. The country has different types of forests, Hill Forest, Sal Forest, Sundarbans Mangrove, Coastal Plantation, Trees outside Forests (TOF), etc.

Materials and Methods

Study area

The study area covered the entire Bangladesh which has different types of forests, namely,

- Hill Forests (Chittagong, Chittagong Hill Tracts and Sylhet),
- Sal Forest (central region and north-western Bangladesh),
- Sundarbans Mangrove,
- Mangrove Plantation (along the coastal belt of Bangladesh) and
- Village Forests or Trees Outside Forests

Hill Forests

The forests of Chittagong, Chittagong Hill Tracts, Cox's Bazar, and Sylhet regions belong to the Hill Forest types. Hill Forest is a natural terrestrial forest thriving evergreen, semi-evergreen, and deciduous trees; some trees retain the foliage throughout the year and some trees shed their leaves in the dry period to reduce the loss of water through transpiration. It consists of moist tropical evergreen and semi-evergreen trees and is generally uneven-aged. Shrubs and herbs occur fewer in number as undergrowth in this forest, however many areas are covered by this class because of the removal of trees by human intervention. The major tree species of this class are Chaplish (*Artocarpus chaplasha*), Garjan (*Dipterocarpus* spp.), *Syzigium* species, Jarul (*Legarstromia speciosa*), Gamar (*Gmelina arborea*), Koroi (*Albizzia spp*), Civit (*Swintonia floribunda*), Toon (*Cedrela toona*), Bandorhola (*Duabanga grandiflora*), Telsur (*Hopea odorata*), Uriam (*Mangifera sylyatica*), Dhakijam (*Syziqium grande*), etc.

Sal Forest

The tropical moist deciduous forest is dominated by Sal (*Shorea robusta*) trees and is located in the relatively high land of Madhupur and Barind tracts. Sal trees naturally rejuvenate by coppice and are present all over the forest. This forest is located in Gazipur, Tangail, Mymensingh, Jamalpur, Comilla, Dinajpur, Thakurgaon, Rangpur, and Rajshahi districts of the country. Parts of the natural forest were cleared by logging activities and replaced by the plantations of rubber (*Hevea brasiliensis*) trees, Acacia (*Acacia auriculiformis*), and other fast-growing tree species.

Sundarbans Mangrove

The geographical area which is dominated by natural mangrove forests and the forest floor is usually inundated twice daily by brackish water. These forest types belonging to the Sundarbans are the largest single tract of natural mangroves in the world. The forest area is intersected by numerous rivers and creeks. A major part of Sundarbans is located in Bangladesh. This forest is located in the southern part of Satkhira, Khulna, and Bagerhat districts. The dominant mangrove species is Sundri (*Heritiera fomes*). Other species include *Avicennia* spp., *Xylocarpus mekongensis*, *Xylocarpus granatum*, *Sonneratia apetala*, *Bruguiera gymnorrhiza*, *Ceriops decandra*, *Aegiceras corniculatum*, *Rhizophora mucronata*, and *Nypa fruticans* palms.

Mangrove Plantation (along the coastal belt of Bangladesh)

The mangroves are planted on the newly accreted land in the estuaries of the Bay of Bengal to protect against tropical cyclones and storm surges as well as protect land from coastal erosion. Major species in the plantation are Keora (*Sonneratia apetalla*), Baen (*Avecinia alba*), Gewa (*Excoecaria agallocha*). In older plantations, other species like *Rhizophora* spp., *Exochorea* spp., *Ceriops* spp. are also found.

Village Forests or Trees Outside Forests (TOF)

Village Forests (TOF) usually represent the aggregation of scattered trees grown on cropland, grazing land, marginal land, canal banks, roadsides, along railways, and in human settlements. These trees cannot be included in the category “forests” or “other wooded land” in forest mapping (Bellefontaine et al., 2002, Rawat et al., 2003 cited in Rahman et al., 2016). This forest is scattered throughout the plain land of the country. Their density varies with regions; in some parts of the country TOF coverage is high and in other parts this is low.

Methodology

Landsat-8 Operational Land Imager (OLI)/ Landsat-9 Operational Land Imager-2 (OLI-2) level 1 terrain-corrected data (L1T) for 2022-2023 were downloaded from the United States Geological Survey (USGS) archive. Images were processed in the steps including (1) image resampling, (2) cloud/shadow/water screening and quality assessment (QA), (3) conversion of raw digital numbers (DN) to top of atmosphere (TOA) reflectance and (4) atmospheric correction.

In order to minimize differences in Landsat-8/9 OLI/OLI-2 sensor calibration, sun-earth distance, and sun elevation, the L1T Landsat image DN values were converted to TOA reflectance (for reflective bands) and brightness temperature (for thermal bands) using the approach Dark Object Subtraction as described in Chander et al., (2009). One-percent reflectance is usually considered as the reflectance of the dark object (Moran et al., 1992; Chavez, 1996). In this procedure, TOA reflectance was converted to surface reflectance; one-percent surface reflectance was subtracted from blue, green, red, and near-infrared (NIR) equivalent bands of Landsat. Since longer wavelengths like shortwave infrared (SWIR) are little affected by atmospheric scattering, it is not necessary to subtract from those bands. TOA reflectance (0–100%) and brightness temperature values (240–320 K) were scaled to 1–255 and stored as 8-bit data layers.

We applied the guided clustering technique, which is a hybrid classification. This classification technique is particularly useful where a complex variability in spectral response is present for individual cover types (Lillesand et al., 2015). We took the training samples from all the major spectral sub-classes, completed the classification with a guided clustering process, and later spectral subclasses were merged into the original land cover classes.

Several classification algorithms including the maximum likelihood classification, minimum distance classification, and machine learning techniques, like random forests (a decision trees algorithm, Breiman *et al.,* 1984) considered mapping forest/non-forest classes, and then mapping forest classes within the generic forest mask and bamboo or shrub cover, cropland, and other land to non-forest class. The following parameters of Landsat image pixels were considered in the analysis: (i) band reflectance value; (ii) normalized difference vegetation index (NDVI; Tucker, 1979); (iii) tasseled cap (Baig et al., 2014) (iv) thermal infrared band values and (v) elevation data (vi) normalized difference water index (NDWI), (vii) modified normalized difference water index (NDWI2), (viii) simple ratio, (ix) green

chlorophyll vegetation index, and (x) tree height data generated by University of Maryland (Potapov et al., 2021).

To build the classification tree model, extensive training sets located in different land covers were created by visual interpretation of the cloud-free observation of Landsat-8/9 OLI/OLI-2 images of 2022-2024. Additional datasets that include freely available VHSR images from Google Earth, selected samples of procured VHSR images, and expert judgment were used as reference materials to aid image interpretation and select training samples. Forests are defined as the tree cover 5 meters or more in height.

The vast majority of image interpretation efforts were focused on distinguishing tree canopy from other vegetation like shrubs, tea gardens, and agricultural crops. With the initial set of training, the classification results were assessed; misclassified pixels were identified and added to the training set. The process will be repeated until the quality of the tree cover map was considered as sufficient. The objectives of the study are to prepare Land Use and Land Cover (LULC) maps and the LULC considered in this study are enumerated in Table 1. Different types of tree resources are mapped in the LULC map.

Field trips were conducted to (i) collect Ground Control Points (GCPs) for validating positional accuracy of Landsat and VHSR imagery, (ii) visit different locations of tree covering areas and possible confusing classes and collect GCPs and (iii) investigate whether there is any visible sign of changes of tree cover areas. Camera photographs were taken to record all ground verification and validation. The generation of tree cover maps during the 2023-2024 financial year was implemented for Landsat scenes 138-042, 138-043, and 138-043. All the scenes covered the western part of the country and part of the scenes belonged to outside Bangladesh.

Table 1. Land use and land cover (LULC) types used in the study

Code	Label	Label	Description
1	Tree-covered area	Tree cover, broadleaf evergreen and semi-evergreen, closed, closed to open	Tropical wet evergreen and semi-evergreen forests of Chittagong, Chittagong Hill Tracts and Sylhet
		Tree cover, deciduous, closed, closed to open	Tropical moist deciduous forest/Sal Forest of central region & North Bengal
		Tree cover, plantations, or rubber garden	Plantations are distributed in different parts of the country. This class has been merged with the forest class.

Code	Label	Label	Description
			Rubber garden, distributed in the central region, north-eastern and south-eastern part of the country
		Mosaics, trees, shrubs, and houses	Trees Outside forest (TOF) / Village forest, distributed throughout the country
2	Grassland	Mosaic, Tree, and shrubs / Tea garden	Tea gardens are distributed in the north-eastern, south-eastern and north-western of the country
		Bamboo	Bamboo forests are often mixed with scattered trees and distributed in Chittagong, Chittagong Hill Tracts, and Sylhet region of the country
3	Cropland	Cropland, rain-fed or irrigated	
		Tree or shrub cover, mango orchard, guava orchard, betel nut orchard	Distributed in north Bengal and different parts of the country
4	Wetland	Tree cover, aquatic or regularly flooded in fresh-water	Freshwater swamp forest located in the north-eastern part of the country
		Tree cover, aquatic or regularly flooded in salt water, mangrove, natural	Sundarbans mangrove is located in the south-western part of the country
		Tree cover, aquatic or regularly flooded in salt-water, mangrove, plantation	Planted primarily with Keora, Bain; distributed in the coastal belt of the country
5	Artificial surfaces	Urban areas	Distributed throughout the country
6	Other land	Bare land	Bare land, distributed throughout the country
7	Water bodies	Water bodies	Rivers, haor, baor, lake, pond, ditches, beels; distributed throughout the country

Results and Discussion

Tree cover map of 138-042

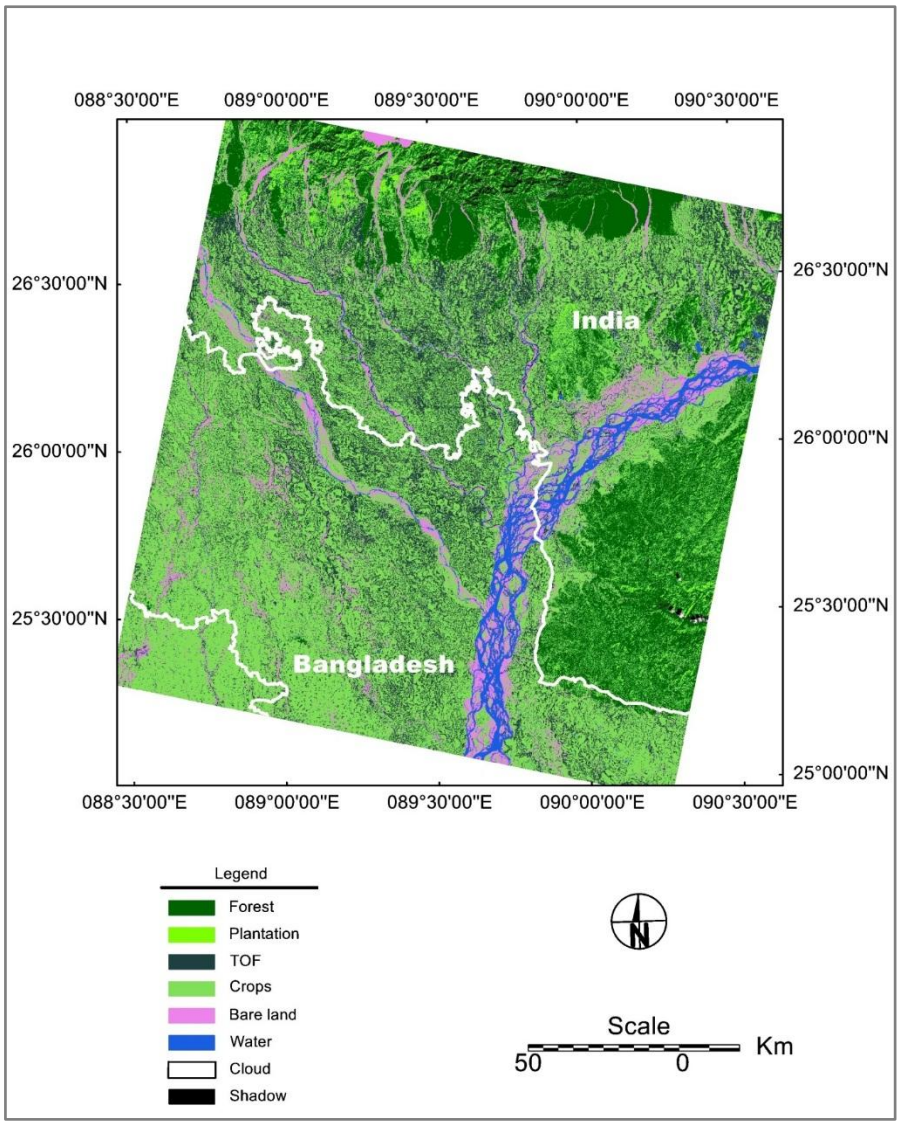

Fig. 1. Tree cover map of Landsat scene 138-042

The Landsat scene covered the entire Kurigram, Lalmonihat, Nilphamari, and Rangpur districts, and most parts of Gaibandha, Sherpur Dinajpur districts. Among different classification techniques, the Min Distance Classification technique was finally selected to apply in this image. Tree height data of 2019 developed by the University of Maryland was also included in the classification process (Potapov et al., 2020). Different classes like forest, plantation, Trees Outside Forests (TOFs), crops, bare land (near the riverside and other areas), and water (dark and blue; appeared in 6 5, and 4 band combinations in a Landsat scene) were selected.

Finally, the following land use and land cover classes were considered as the final class: forest, plantation, TOF, cropland, bare land, water, cloud and shadow. We checked visually different classes and found that the class,

TOF was better identified on the University of Maryland tree height database, and it was superimposed to our derived classification results except in some places, including the rivers and the adjacent areas where there are recent changes and the forest areas where the forest class should be kept as forest. Tree cover map of Landsat scene 138-042 is presented in Fig. 1.

Tree cover map of 138-043

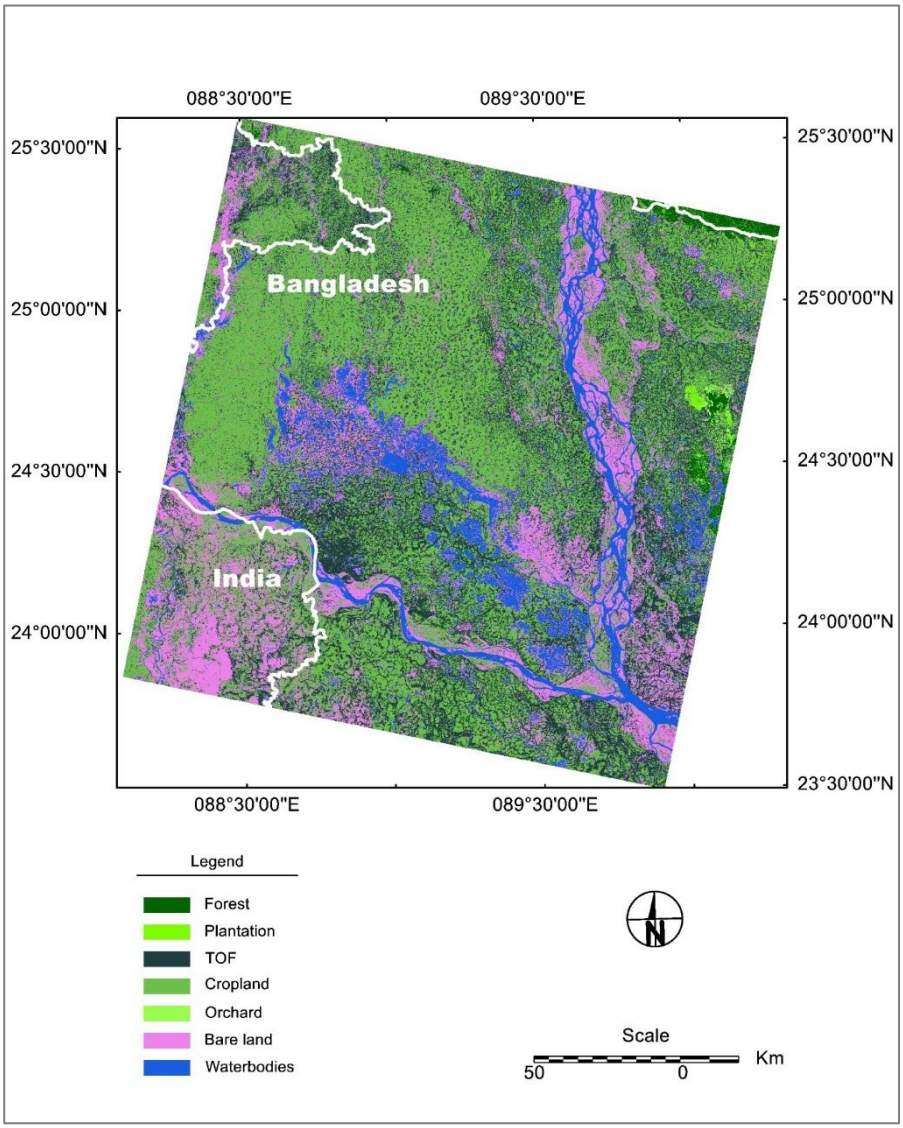

Fig. 2. Tree cover map of Landsat scene 138-043

Landsat image of 01 November 2023 was used in the classification procedure. The area includes Sherpur, Bogra, Joypurhat, Naogaon, Rajshahi, Natore, Shirajganj and Pabna districts and most part of Jamalpur, Tangail and Gaibandha districts. Minimum Distance Classification algorithm was applied to separate Sal forest, plantations, rubber plantations, TOF, crops, bare soil and water. In this scene, three types of crops, two types of bare

soil and two types of water were identified and these were later merged to the appropriate classes like cropland, bare land, and water classes (Fig. 2).

Tree cover map of 137-044

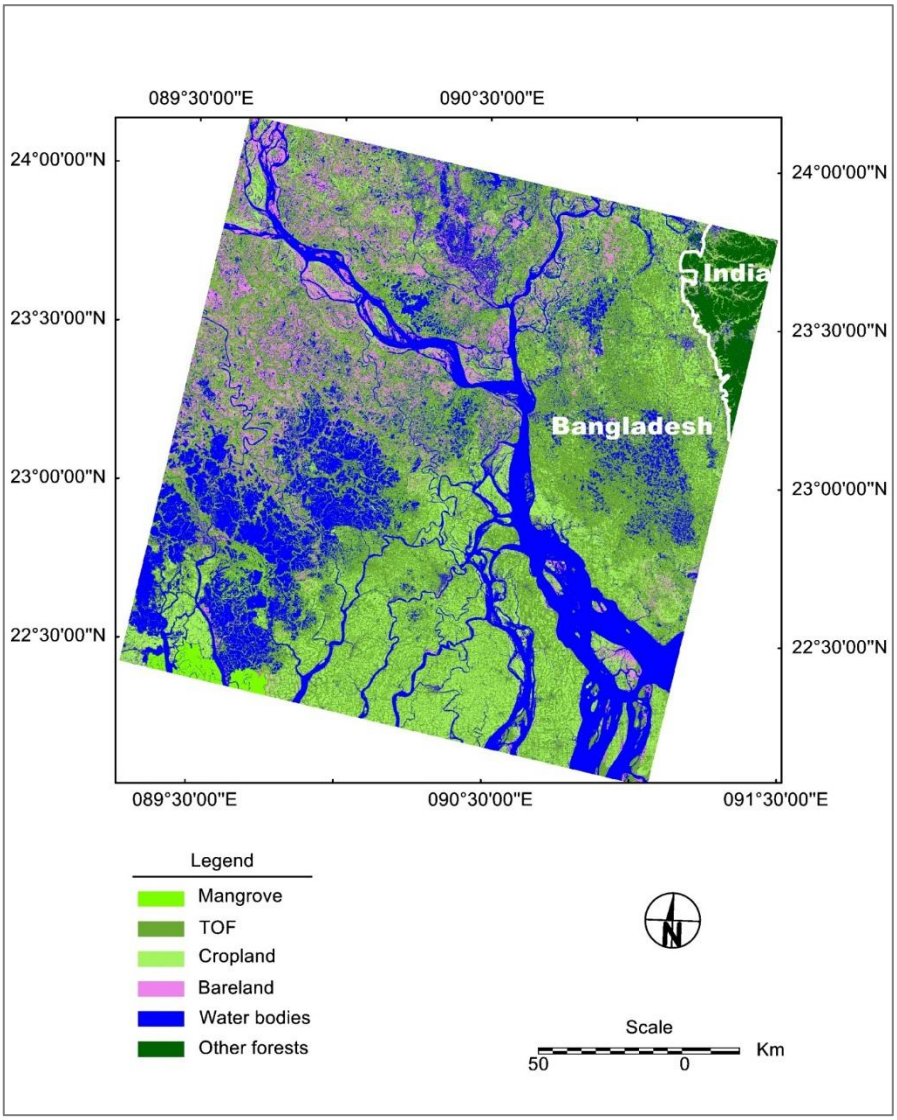

Fig. 3. Tree cover map of Landsat scene 137-044

We have tried to classify two Landsat scenes, acquired in February (03 February 2023) and November (26 November 2023). Finally, the November scene was selected for the final classification. In the guided clustering technique, the following classes were identified on the Landsat scene: mangrove bight mangrove dark, TOF, other forests (mostly located outside Bangladesh), crops, dry bare soil, inundated cropland, shrimp farms, and water. These classes were later merged into mangroves, other forests, TOF, cropland, bare land, waterbodies, and other forests. A maximum likelihood classification algorithm was applied in the classification procedure. All multispectral bands, NDVI, NDWI, and NDWI2 were considered in the image

classification process. Tree cover map of Landsat scene 137-044 is presented in Fig. 3.

Conclusions

Within the pilot study in 2022-2023, we completed the following three Landsat scenes: 136-043, 137-043, and 137-045. In this financial year (2023-2024), we completed the following Landsat frames: 137-044, 137-042, and 137-043. Within the next financial year, the classification of all the remaining scenes needs to be completed. All these remaining scenes usually covered some parts of Bangladesh. Most of these scenes cover a major part of outside Bangladesh belonging to India, Myanmar, and the Bay of Bengal.

Acknowledgments

Landsat-8 and Landsat-9 data were downloaded from the United States Geological Survey (USGS) website. We would like to thank Global Land Analysis & Discovery (GLAD) Laboratory, University of Maryland (UMD) for the Global Forest Canopy Height Map of 2019.

References

Bellefontaine, R., Petit, S., Pain-Orcet, M., Deleporte, P., Bertault, J.G. (2002). Trees outside forests. Towards better awareness. FAO Conservation Guide 35, FAO, Rome, pp. 216. [online] URL: http://www.cabdirect.org/cabdirect/abstract/2 0046798932

Baig, M. H. A., Zhang, L. F., Shuai, T. and Tong, Q. X. (2014). Derivation of a Tasselled Cap Transformation Based on Landsat 8 At-Satellite Reflectance. *Remote Sensing Letters*, 5 (5), 423–431.

Breiman, L., Friedman, J. H., Olshen, R. A. and Stone, C. J. (1984) Classification and Regression Trees (Monterey, CA: Wadsworth and Brooks/Cole).

Chander, G., Markham, B. L., and Helder D. L. (2009). Summary of current radiometric calibration coefficients for Landsat MSS, TM, ETM+, and EO-1 ALI sensors. *Remote Sensing of Environment*, 113, 893–903.

Chavez P. S., Jr. (1996). Image-based atmospheric corrections—revisited and revised. *Photogrammetric Engineering & Remote Sensing*, 62(9), 1025-1036.

FD & FAO. (2007). National forest and tree resources assessment 2005 – 2007, Bangladesh. https://www.fao.org/forestry/17847/en/bgd/

Jalal, R., Golam Mahboob, M., Udita, T. S., Aziz, T., Masum, S. M., Costello, L., Saha, C. R., Chowdhury, A. A. M., Salam, A., Shahrin, F., Sumon, F.

R., Iqbal, Z., Rahman, M., Siddique, M. A., Rahman, M. M., Jahan, M. N., Shaunak, M. F., Rahman, M. S., Islam, M. R., … Hossain, M. A. (2019). Toward Efficient Land Cover Mapping: An Overview of the National Land Representation System and Land Cover Map 2015 of Bangladesh. *IEEE Journal of Selected Topics in Applied Earth Observations and Remote Sensing*, 12(10), 3852–3861. https://doi.org/10.1109/JSTARS.2019.2903642

Lillesand, T.M., Kiefer, R.W., and Chipman, J.W. (2015). Remote sensing and image interpretation (7th edition). New York: John Wiley & Sons, Inc.

Moran, M. S., Jackson, R. D., Slater, P. N. and Teillet, P. M. (1992). Evaluation of simplified procedures for retrieval of land surface reflectance factors from satellite sensor output. *Remote Sensing of Environment*, 41, 169-184.

Myers, N., Mittermeier, R. A., Mittermeier, C. G., da Fonseca, G. A. B., & Kent, J. (2000). Biodiversity hotspots for conservation priorities. *Nature*, 403(6772), 853–858. https://doi.org/10.1038/35002501

Olofsson, P., Foody, G. M., Stehman, S. V. and Woodcock, C. E. (2013). Making better use of accuracy data in land change studies: estimating accuracy and area and quantifying uncertainty using stratified estimation. *Remote Sensing of Environment*, 129, 122–31.

Olson, D. M., Dinerstein, E., Wikramanayake, E. D., Burgess, N. D., Powell, G. V. N., Underwood, E. C., D'amico, J. A., Itoua, I., Strand, H. E., Morrison, J. C., Loucks, C. J., Allnutt, T. F., Ricketts, T. H., Kura, Y., Lamoreux, J. F., Wettengel, W. W., Hedao, P., & Kassem, K. R. (2001). Terrestrial Ecoregions of the World: A New Map of Life on Earth: A new global map of terrestrial ecoregions provides an innovative tool for conserving biodiversity. *BioScienc*e, 51(11), 933–938. https://doi.org/10.1641/00063568(2001)051[0933:TEOTWA]2.0.CO;2

Potapov, P., Li, X., Hernandez-Serna, A., Tyukavina, A., Hansen, M. C., Kommareddy, A., Pickens, A., Turubanova, S., Tang, H., Silva, C. E., Armston, J., Dubayah, R., Blair, J. B., & Hofton, M. (2021). Mapping global forest canopy height through integration of GEDI and Landsat data. *Remote Sensing of Environment*, 253, 112165. https://doi.org/10.1016/j.rse.2020.112165

Potapov, P., Siddiqui, B. N., Iqbal, Z., Aziz, T., Zzaman, B., Islam, A., Pickens, A., Talero, Y., Tyukavina, A., & Turubanova, S. (2017). Comprehensive monitoring of Bangladesh tree cover inside and outside of forests, 2000–2014. *Environmental Research Letters*, 12(10), 104015.

Rahman, M. M., Islam, M. S., & Pramanik, M. A. T. (2018). Monitoring of changes in woodlots outside forests by multi-temporal Landsat imagery. *IForest*, 11(1), 162–170. https://doi.org/10.3832/ifor2021-010

Rawat, J., Dasgupta, S., Kumar, R., Kumar, A., Chauhan, K. (2004). Assessment of tree resources outside forest based on remote sensing satellite data. Proceedings of Map India 2004, GISdevelopment. net, Web site. [online] URL: http://citeseerx.ist.psu.edu/viewdoc/download?doi=10.1.1.585.9534&rep=rep1&type=pdf

Reddy, C. S., Pasha, S. V., Jha, C. S., Diwakar, P. G., & Dadhwal, V. K. (2016). Development of national database on long-term deforestation (1930–2014) in Bangladesh. *Global and Planetary Change*, 139, 173–182. https://doi.org/10.1016/j.gloplacha.2016.02.003

Tucker, C. J. (1979). Red and photographic infrared linear combinations for monitoring vegetation. *Remote Sensing of Environment*, 8, 127–50.

Developing an Agricultural Drought Monitoring Model Based on Multi-Source Remote Sensing Data

Nasrin Sultana*, Md. Abdus Salam, Tofayel Ahammad, Md Adil Shahriar

Bangladesh Space Research and Remote Sensing Organization (SPARRSO), Agargaon, Shere Bangla Nagar, Dhaka-1207, Bangladesh.
**Corresponding author E-mail: nasrin@sparrso.gov.bd*

Abstract

Droughts have significantly impacted agricultural production, leading to a decline in total yield. This study evaluates drought fluctuations from 2000 to 2022 in Dhaka and Khulna divisions using the Integrated Weighted Drought Index (IWDI). The IWDI, developed through the Analytical Hierarchy Process (AHP), incorporates multiple variables to assess different types of droughts. These variables include CHIRPS precipitation data for calculating the Precipitation Condition Index (PCI), soil moisture and Land Surface Temperature (LST) for the Soil Moisture Condition Index (SMCI) and Temperature Condition Index (TCI), NDVI for the Vegetation Condition Index (VCI), and Enhanced Vegetation Index (EVI) with Land Surface Temperature (LST) for the Vegetation and Soil Water Index (VSWI). Our findings indicate that, overall, Dhaka and Khulna divisions experienced predominantly favorable agricultural conditions. Most years exhibit a high percentage of land categorized as drought-free, supporting optimal crop growth. Districts such as Kishoreganj, Tangail, Dhaka, and Gazipur demonstrated stability with minimal drought fluctuations, highlighting their resilience to climate variability. In contrast, districts including Faridpur, Rajbari, Chuadanga, Jhenaidah, Kushtia, Meherpur, Narail, Bagerhat, and Khulna faced recurring drought conditions. These areas frequently reported mild to moderate droughts, with some years experiencing severe drought, posing challenges to agricultural sustainability.

Keywords: Agricultural drought, Monitoring, RS-Model, Crop Yield, Bangladesh.

Introduction

Food, energy, and water security are major concerns due to population growth of the whole world. Global climate change has exacerbated these difficulties (Qu et al., 2019). Regarding climate change, South Asia is regarded as one of the world's most vulnerable regions (Sarmah et al., 2018). High temperatures and low land precipitation have generated increasingly severe and extended droughts in the previous 30 years. Droughts were categorized as meteorological, agricultural, hydrological, and socioeconomical (Wilhite et al., 1985). Meteorological dryness is usually characterized by abnormal precipitation. The hydrological drought refers to deficiencies in surface and subsurface water supplies based on streamflow

and lake, reservoir, and groundwater levels, while the agricultural drought occurs when soil moisture is insufficient to meet a crop's needs at a specific time due to prolonged precipitation deficits. Drought typically affects agriculture after a meteorological drought but before a hydrological one (Kamruzzaman et al., 2019). Drought has affected 31% of south asian cultivated land since 1990, threatening plant biodiversity. Drought has increased in many parts of South Asia since the 20th century (Shahzaman et al., 2021). Bangladesh is one of the South Asian countries and largely dependent on agriculture (Aziz et al., 2021). Drought is currently regarded as one of the most common natural disasters in Bangladesh (Alamgir et al., 2015).

Drought condition in Bangladesh reveals a complex picture. Aridity and drought are common in the country, particularly in the north-western and western regions (Chowdhury & Hussain, 1983). Due to high poverty rates, dependence on agriculture, low adaptive capacity, and high variability of annual and seasonal rainfall, the Barind tract and Teesta floodplain regions of northern and northwestern (North Bengal) Bangladesh are particularly affected by drought (Shahid and Behrawan, 2008; Habiba et al, 2014). In North Bengal, droughts have become more severe, frequent, and variable over time (Miyan, 2015; Kamruzzaman et al., 2019). A study (Islam, 2009) has found that in recent decades, North Bengal has undergone considerable increases in rainfall variability, protracted seasonal-scale dry spells, and several occurrences of below-normal rainfall, which has hampered crop growth. Additionally, the yields of crops (such as rice and wheat) in North Bengal are significantly impacted by temperature variations. Different studies have investigated spatiotemporal aspects of droughts in Bangladesh following traditional and remote sensing approaches. The country is mostly affected by drought during the Kharif seasons (Dey et al., 2012) among the three (Kharif I, Kharif II, and Rabi) cropping seasons. Recently, Kamruzzaman et al. (2019) addressed the central region of the country as vulnerable to droughts, including northern and north-western regions as identified earlier. In Bangladesh, the Pre-Kharif season (March to June) is characterized by variable rainfall, a protracted dry spell, high temperatures (over 40 °C from March to June), and increased evapotranspiration (Kamruzzamana et al., 2018; Kamruzzaman et al., 2019).

Drought monitoring in Bangladesh involves the use of various drought indices such as the Standardized Precipitation Index (SPI), Standardized Precipitation Evapotranspiration Index (SPEI), and Vegetation Condition Index (VCI) (Foyez et al., 2020; Zaher et al., 2021) These indices are used to assess drought characteristics, including intensity, frequency, and

duration, at different temporal and spatial scales (Liu & Li., 2011). Multi-source remote sensing drought monitoring involves the use of various remote sensing images and data to detect and monitor drought conditions. The effectiveness is significant in multi-sensor remote sensing in revealing the occurrence, development, and disappearance of drought, as well as in characterizing drought-related phenomena and mechanisms (Niaz, et al., 2021). Integrated Weighted Drought Index (IWDI) works in drought monitoring by integrating multiple drought indices to provide a comprehensive assessment of drought conditions. The IWDI combines different multiscale drought indices to reduce uncertainty and improve the accuracy of drought monitoring. It uses various weighting schemes and statistical methods to integrate data from different meteorological & remote sensing products (Zhang et. al., 2022). The IWDI has been shown to have strong correlations with individual drought indices and is effective in characterizing drought processes and spatial patterns (Sultana, 2021). It has been used for regional drought monitoring and early warning systems, providing valuable information for drought mitigation policies and water resource management. Additionally, satellite-based assessments using indices such as the Vegetation Health Index (VHI), Temperature Vegetation Dryness Index (TVDI), and Shortwave Infrared Dryness Index (VSDI) have provided insights into the spatial distribution and severity of drought in the north-western regions of Bangladesh (Pettorelli et al., 2011). All those indices are not considering climate data, like precipitation variation, which is one of the influencing factors of drought in semi-arid areas. Remote sensing precipitation products of tropical rainfall measuring mission (TRMM) data are used as an alternative data of meteorological station and monitoring drought and flood (Lingtong et al., 2013). Therefore, the remote sensing-based drought indices synthesizing precipitation is developed and use to monitor the complex process of drought. Rhee et al. (2010) proposed a new multi-sensor drought index, the scaled drought condition index (SDCI), which used NDVI, LST and TRMM data. The best SDCI is defined by the formula: SDCI = (1/4) × scaled LST + (2/4) × scaled TRMM + (1/4) × scaled NDVI, and its performance is better than the existing indices such as VHI in different climate divisions.

As we know, drought is a slow process which begins with precipitation deficit, then it leads to soil moisture deficit and a higher land surface temperature, and at last the vegetation growth will be influenced by this process (Lingtong et al., 2013). Therefore, to monitor the comprehensive drought we must consider these parameters which are derived from precipitation, soil and vegetation. In this study, we used CHIRPS data as a component from precipitation to calculate PCI, used soil moisture & LST as

a component from soil to calculate SMCI & TCI, used NDVI as a component from vegetation to calculate VCI and used EVI & LST as a component from vegetation and soil to calculate VSWI. In this study, integrated weighted drought index (IWDI), based on these remotely sensed data was used to develop and to evaluate the drought conditions over the selected study area.

This research work aims to develop a model that would integrate various remote sensing products available, including weather observations, processed satellite data, etc. The domain of the model covers Dhaka & Khulna Division. The model has the provision for processing, analyzing, and visualizing these datasets for monitoring the drought situation for a specific month or a season. On the other hand, the model used to investigate meteorological factors triggering droughts. The specific objectives are (a) to identify drought indices and remote sensing products capable of detecting drought events, (b) to investigate significant meteorological factors triggering drought events, and (c) to generate an updated cropland layer.

Drought Classification

According to Wilhite et al. (1985), droughts are classified as meteorological, agricultural, hydrological, and socio-economic droughts depending on climatological and hydrological factors.

i. Meteorological drought: emerges from a prolonged dry spell, high temperatures, and low humidity, which raises evapotranspiration in a specific region.

ii. Agricultural drought: droughts have an impact on crop production. This usually happens when there is a shortage of precipitation and soil moisture. When that happens, the plant's water needs are not being met.

iii. Hydrological drought: a slow-moving drought that happens when reservoirs, streams, lakes, and aquifers' supplies of surface or deep water decrease below usual levels.

iv. Socio-economic drought: due to prolonged dryness, there is an increase in demand for items like drinking water supply and hydroelectric power, which has a significant socioeconomic impact.

Since the lack of precipitation affects all of these droughts, they are related.

History of Drought in Bangladesh

Bangladesh has a history of drought, which has had significant impacts on

the country's agriculture, economy, and food security. Droughts in Bangladesh are often associated with the dry season, which typically occurs from November to April. The country's vulnerability to drought is exacerbated by factors such as climate change, deforestation, and unsustainable water management practices.

Table 1: History of drought in Bangladesh based on literature

Year	Drought Location	Reason of Drought	Drought Severity	Method of Drought Measurement	Reference
1967, 1972, 1973, 1976, and 1982	Rangpur		extreme drought	(SPI B -2)	Dash et al., 2012
1981 to 1984	whole country		moderate	SPI	Dash et al., 2012
1992, 1999, 2006	Dhaka	Groundwater Extraction	extreme	(SPI >-2)	Rahman & Lateh, 2016
1972,1973, 1999	Khulna	Low Rainfall	extreme	(SPI >-2)	Rahman & Lateh, 2016
1972,1989, 1999, 2006	Jessore		extreme	(SPI >-2)	Rahman & Lateh, 2016
1972,1973, 1978	Chandpur		Excessive Drought	De Mortone Aridity Index (idM < 23)	Keka et al., 2012
1992,1994	Dhaka	Low Rainfall &Temperature	Moderate	Rainfall Deficiency	Keka et al., 2012
2002,2014	northwestern part				Sultana et al., 2021
1979,1981, 1984,1989, 1992,1994, 1996,2001, 2004,2009	Tista Floodplain and Barind Tract			EDI	Mondol et al., 2021

Various papers provide information on the occurrence of drought in Bangladesh (Table1). The Standardized Precipitation Index (SPI) method to analyze drought conditions from 1981 to 2010 and found that drought was a recurrent phenomenon during this period, with notable drought years in 1981, 1982, 1985, and others. Dash et al. (2012) also used SPI and the Palmer Drought Severity Index (PDSI) to diagnose meteorological drought events from 1961 to 1990 and found that moderate drought occurred more frequently across the country. Rahman & Lateh (2016) assessed and mapped drought hazards using SPI and GIS, identifying the northern, north-

western, western, and south-western parts of Bangladesh as the most drought-prone areas. Brammer 1987 discussed the 1978-1979 drought and highlighted the need for flexible production plans, monitoring of environmental factors, and recording farmers' disaster-mitigating practices. Overall, these papers collectively indicate that drought has occurred in Bangladesh in various years, with regional variations in severity and frequency.

Materials and methods

Study area

Dhaka & Khulna division is the study area for this research. The Dhaka division consists of thirteen districts: Dhaka, Narayanganj, Faridpur, Gazipur, Gopalganj, Kishoreganj, Madaripur, Manikganj, Narsingdi, Rajbari, Shariatpur, and Tangail.

Dhaka is the most populated division of Bangladesh, with 44 million people. This division is surrounded by four major rivers: the Buriganga, the Dhaleshwari, the Shitalakshya, and the Turag. The main agricultural products of the Dhaka Division, which are grown in large amounts, include rice, wheat, maize, potatoes, sugarcane, pulses, jute, and mustard. The Khulna division is the third largest division of Bangladesh, covering an area of 22,285 km². It is situated between 21°40' to 24°12' north latitude and 88°34' to 89°57' east longitude. According to BBS 2015, from 2001 to 2011 the annual population growth rate was 0.68 in Khulna. With the increment of population, the land use pattern and the environment of Khulna is changing every year.

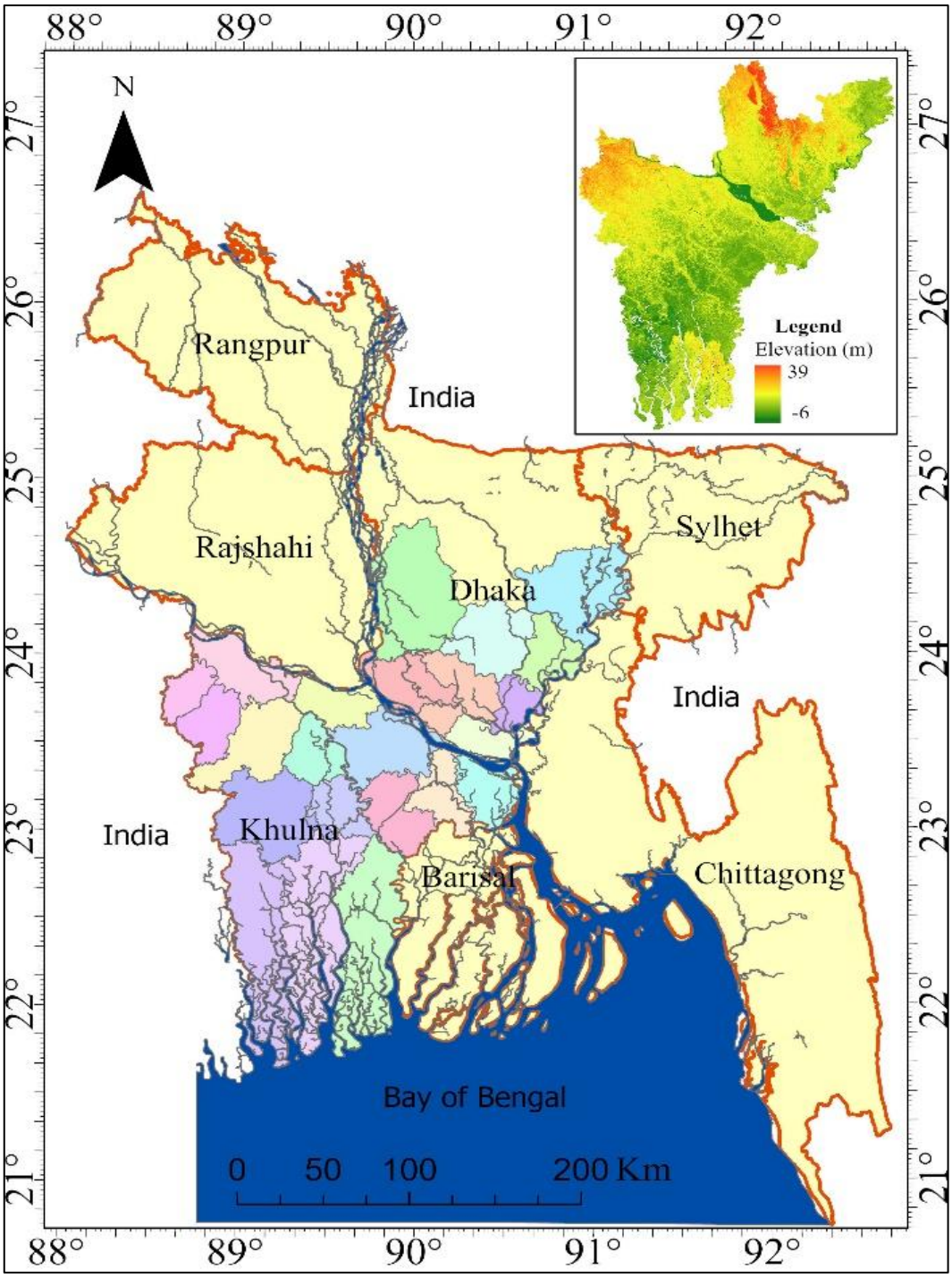

Fig. 1. Study area.

Methodology

Datasets

To develop the integrated weighted drought index, in situ and remote sensing data were collected from different sources. In situ meteorological data, i.e., (precipitation) of 11 stations from 2000 to 2022 were obtained from the Bangladesh Meteorological Department (BMD, http://bmd.gov.

bd). MOD11A2 V6.1 product of Terra Land Surface Temperature (LST), CHIRPS daily rainfall data product at 0.05° resolution, Soil Moisture (SM) data of GLDAS-2.1: Global Land Data Assimilation System, and MOD13Q1.006 product of Terra Vegetation Indices (NDVI and EVI) at 16-Day Global and 250m resolution were used in this study using Google Earth Engine (GEE) platform.

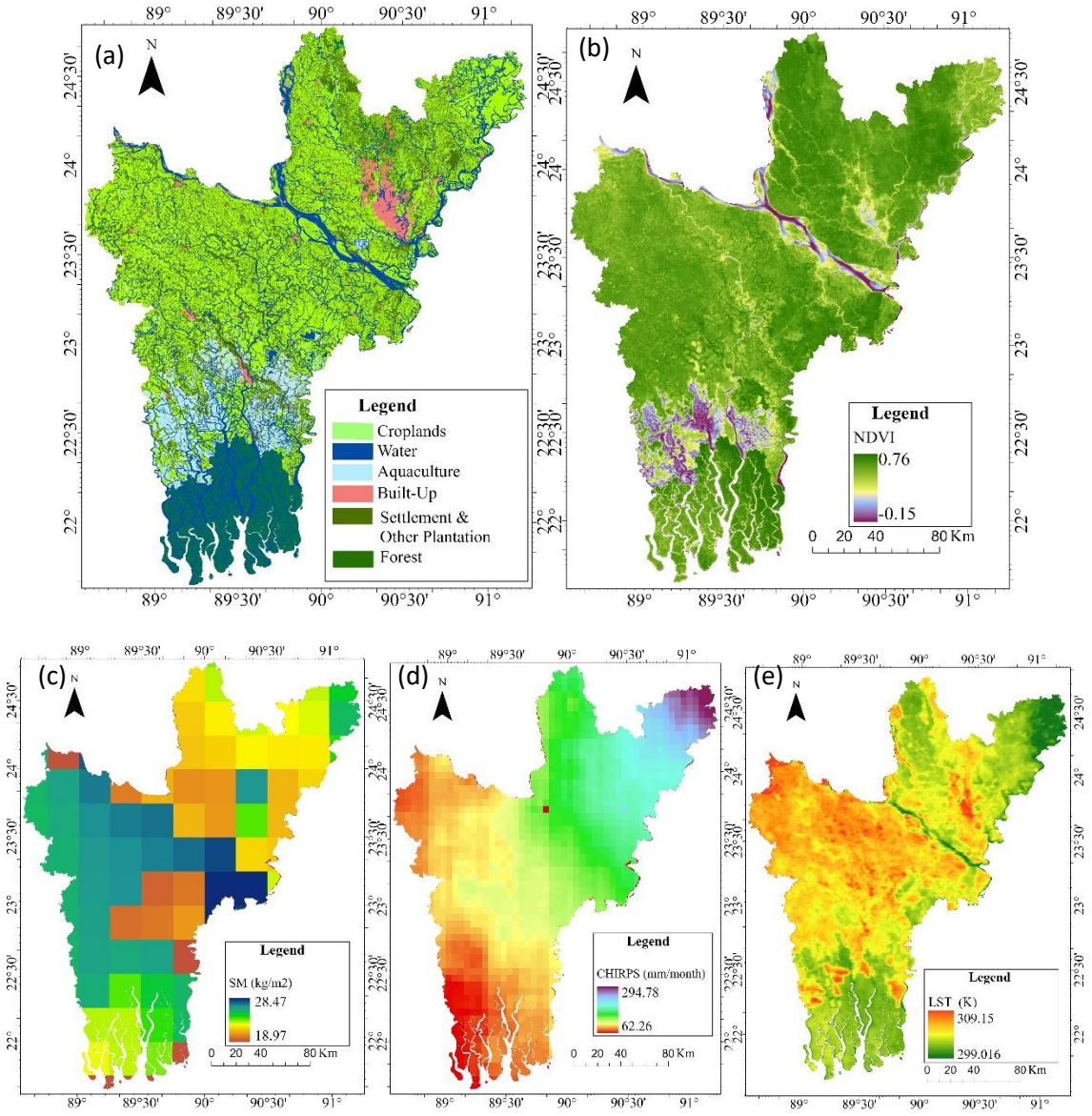

Fig. 2. (a) Map of land cover classification (GoB), (b) average NDVI, (c) average soil moisture, (d) average precipitation, and (e) average temperature from 2000 to 2022.

Table 2: Dataset used in this study

Dataset	Start Time	End Time	Spatial Resolution (m)	Temporal Resolution	Description
LST	2000	Present	1000	8 Day	MOD11A2.061 Terra Land Surface Temperature and Emissivity 8-Day Global 1km
CHIRPS	1981	Present	5566	1 day	CHIRPS Daily: Climate Hazards Group InfraRed Precipitation with Station Data (Version 2.0 Final)
SM	2000	Present	27830	3 Hour	GLDAS-2.1: Global Land Data Assimilation System
NDVI	2000	Present	250	16 Day	MOD13Q1.061 Terra Vegetation Indices 16-Day Global 250m
Rainfall	2000	2022	-	Monthly total/ average	Station data from Bangladesh Meteorological Department (BMD)

Field Survey

We carried out field survey (Fig. 3) twice in Shariatpur and Satkhira district. For the paddy rice sites, we went into the paddy rice field at least 10 m away from the border in each direction and took the geo-referenced photo and collected field information in 31 locations (Table 3 and 4).

Fig. 3. Field data collection

Table 3: Summary of Field Data Collection in Shariatpur District

S.N	District: Upazilla:	Date	Union: Village:	Latitude	Longitude	LAI	Soil Moisture (%)	PAR(mol/sqr. m/s), Above Canopy (AC), Below Canopy (BC)	Chlorophyll	Present Land Cover	Crop	Harvesting
1	Shariatpur Gosairhat	20/05/24	Pourosoba, Uttar Haturia	23°03'11.2"	90°26'16.0"	0.45	35.5	AC-980, BC-625	23.1	Jute	Fallow	
											Jute	
											Aman	
2			chormonpura	23°01'08.18"	90°25'37.07"	0.03	29.7	AC-1345, BC-1088	43.6	Soyabean	Fallow	
											Soyabean	
											Aman	
3			Edilpur, Basudevchap	23°03'10.95"	90°24'48.0"	0.97	34.3	AC-1689, BC-673	31.7	Boro	Boro	1-10 May
											Fallow	
											Aman	
4	Shariatpur Damudya	21/05/24	East Damudya, Haldarkandi	23°06'43.68"	90°26'57.23"	2.16	12.7	AC-1703, BC-425	34.7	Jute/ Soyabean	Fallow	
											Jute/ Soyabean	
											Aman	
5			East Damudya, Boro Naogaon	23°08'04.37"	90°26'41.57"	0.65	35.3	AC-1556, BC-775	13.4	Jute/ Soyabean	Fallow	
											Jute/ Soyabean	
											Aman	
6			Banesshor, Mazirtech	23°08'50.38"	90°25'07.32"	0.40	46.7	AC-1420, BC-625	15.1	Boro	Boro	1-10 May
											Fallow	
											Fallow	
7	Shariatpur Sadar	21/05/24	Rudrokor, Devok	23°10'50.28"	90°22'28.13"	0.34	35.4	AC-1285, BC-255	44.0	Boro	Boro	1-10 May
											Fallow	
											Fallow	
8			Chitolia, Kashipur	23°11'11.04"	90°18'25.08"	1.34	37.2	AC-1420, BC-775	42.6	Boro	Boro	1-10 May
											Fallow	
											Aman	
9				23°10'41.79"	90°17'47.37"	2.01	35.29	AC-1224,	34.7	Boro	Boro	1-10 May

S.N	District: Upazilla:	Date	Union: Village:	Latitude	Longitude	LAI	Soil Moisture (%)	PAR(mol/sqr. m/s), Above Canopy (AC), Below Canopy (BC)	Chlorophyll	Present Land Cover	Crop	Harvesting
			Chitolia, Hindupara					BC-880			Fallow	
											Aman	
10	Shariatpur Bhedarganj	22/05/24	Chawga, Sanirbor	23°11'25.06"	90°24'28.47"	0.20	42.00	AC-1581, BC-649	42.0	Boro	Boro	1-10 May
											Fallow	
											Fallow	
11			Rambodropur, Koroltoli	23°11'59.37"	90°28'09.19"	0.58	34.0	AC-1978, BC-1651	38.3	Boro	Boro	1-10 May
											Fallow	
											Fallow	
12			Digar Mohishkhali, Charchandra	23°12'58.47"	90°29'34.0"	0.57	20.2	AC-2235, BC-276	35.6	Jute	Fallow	
											Jute	
											Fallow	
13	Shariatpur Naria	22/05/24	Vijari, Kanchonlura	23°13'26.86"	90°25'49.16"	0.79	43.3	AC-1841, BC-156	21.8	Boro	Boro	1-10 May
											Fallow	
											Fallow	
14			Fotehjongapur, Sirongol	23°16'28.95"	90°23'25.20"	2.01	34.6	AC-2094, BC-806	29.0	Boro	Boro	1-10 May
											Fallow	
											Aman	
15			Pourosoba, Bismillahnagor	23°18'03.00"	90°24'52.70"	1.56	42.0	AC-2074, BC-533	26.1	Boro	Boro	1-10 May
											Fallow	
											Aman	
16			Ragnagor, Paragao	23°25'01.25"	90°35'00.00"	1.23	39.3	AC-1362, BC-720	45.2	Boro	Boro	1-10 May
											Fallow	
											Aman	
17	Shariatpur Zajira	23/05/24	Munsikandi	23°33'51.96"	90°32'51.30"	1.35	37.2	AC-1356, BC-649	38.6	Boro	Boro	1-10 May
											Fallow	
											Aman	
18								AC-2235, BC-276	35.6	Jute	Fallow	
											Jute	
											Fallow	

Table 4: Summary of Field Field Data Collection in Satkhira district

S.N	District: Upazilla:	Date	Union: Village:	Latitude	Longitude	Soil Moisture(%)	Present Land Cover	Crop
1	Satkhira Kolaroa	03/06/24	Pourosoba, Mirzapur	22°51'54.45"	89°03'14.21"	40.7	Fallow	Boro Fallow Aman
2			Pourosoba, Patna	22°51'51.88"	89°03'16.05"	44.1	Fallow	Boro Fallow Aman
3			Juikhali, Hamidpur	22°52'4.54"	89°03'35.74"	55.4	Plum Garden	
4		04/06/24	Jalalabad, Pasna	22°52'14.53"	89°03'49.12"	44.9	Fallow	Boro Fallow Aman
5			2 No Jalalabad, Faijullahpuri	22°52'22.68"	89°04'23.60"	38.7	Fallow	Boro Fallow Aman
6			Jubakhali, Bamonkhali	22°52'14.06"	89°04'48.86"	31.2	Tomato	Boro Tomato Fallow
7		05/06/24	Jalalabad, Jalalabad	22°51'31.84"	89°04'25.97"	45.7	Water	Boro Fallow Fallow
8			Jalalabad, West Jalalabad	22°51'31.39"	89°03'19.20"	44.6	Rice	
9			Helatona, Helatona	22°52'35.08"	89°01'39.73"	39.8	Rice	
10			Helatona, Helatona	22°52'26.50"	89°01'22.01"	28.9	Plum garden	
11	Satkhira Assasuni	06/06/24	Dumuria, Haribanga	22°30'24.8"	89°09'25.92"	48.7	Fish cultivation	
12			Dumuria, Dumurpota	22°32'59.43"	89°11'25.16"	45.2	Fish cultivation	
13			Chandi, Bamondanger Bill	22°31'56.87"	89°11'24.14"	35.2	Boro	Boro Fallow Fallow

Data Processing

All the satellite data products were accessed in GEE and then the dataset was filtered for the study area during the periods of 2000-2022 Pre-Kharif (March-May) seasons. Different datasets are available in different spatiotemporal resolutions, which cannot be used directly (Mustafa et al., 2020, 2021). This study's datasets were resampled and projected into homogeneous spatiotemporal resolution using GEE (Kulkarni et al., 2020; Shahzaman et al., 2021). Indices (i.e., Precipitation Condition Index (PCI), Soil Moisture Condition Index (SMCI), Standardized Precipitation Index (SPI), Vegetation Condition Index (VCI), Temperature Condition Index (TCI) and Vegetation Supply Water Index (VSWI) were executed using JavaScript in Google Earth Engine (GEE) platform. Weight calculation in AHP. Finally, the outputs were analyzed and visualized as figures, graphs, maps, and tables using different tools such as Erdas Imagine, ArcGIS, MS Excel etc. Fig. 4 shows the research flowchart.

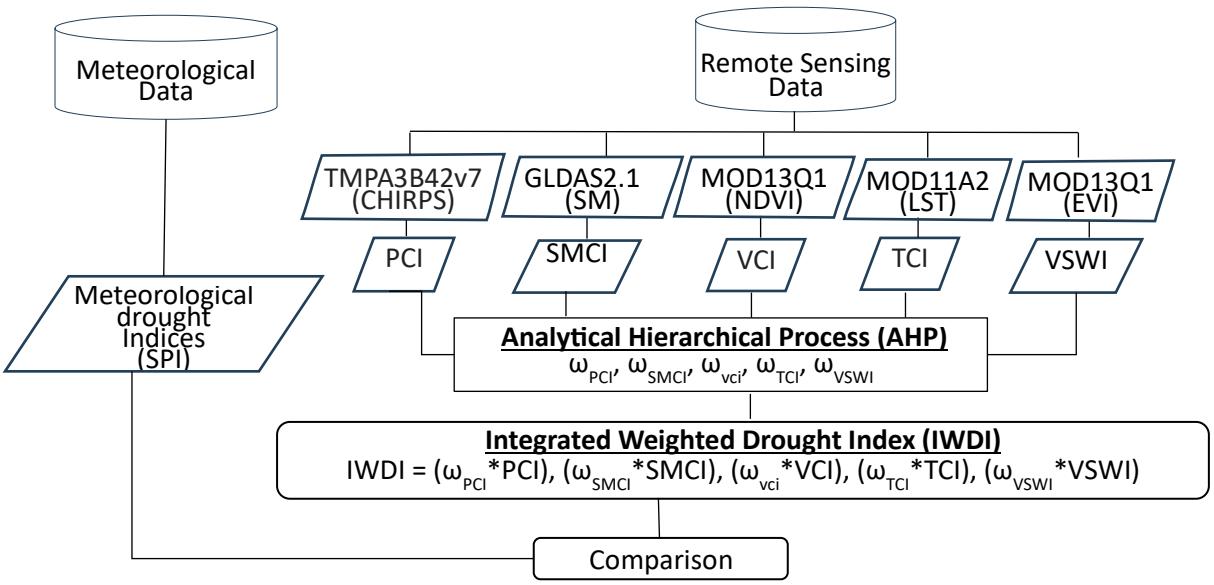

Fig. 4. Agricultural drought determination procedures. ω shows the weight of each drought indices, i.e., PCI, VCI, VSWI, TCI, and SMCI.

Standardized Precipitation Index (SPI)

SPI is computed as normalized values of the probability distribution of rainfall recorded in an area (usually > 30 years rainfall) for a certain period and quantifies the precipitation deficits as dry events of different degrees of severity (Mckee et al., 1993). SPI has wide use on drought intensity / severity assessment and other applications such as estimation of soil moisture. SPI solely makes use of data on precipitation. According to McKee's table values, a negative SPI value denotes dryness and a positive

number denotes wetness. The following formula was used to determine the SPI.

$$\mathrm{SPI} = \frac{(\mathrm{P} - \mathrm{Pm})}{\sigma}$$

Where, Pm is the long-term mean precipitation for the same time period, is the standard deviation of the precipitation for that time period, and P is the precipitation value for that time period. The 30-year record commonly used in the SPI calculation serves as the long-term climate normal. The overall SPI value, which is given in terms of standard deviations, is a standardized measurement of the precipitation's departure from the long-term average.

Table 5. Classification of SPI drought categories.

SPI Values	Category
>= +2.0	Extremely wet
+1.5 to +1.99	Very wet
+1.0 to +1.49	Moderately wet
-0.99 to +0.99	Near normal
-1.0 to -1.49	Moderately dry
-1.5 to -1.99	Severely dry
<= -2.0	Extremely dry

Precipitation Condition Index (PCI)

The daily rainfall product of the CHIRPS dataset with 0.05° × 0.05° spatial resolution was used. The datasets were resampled to 250 m spatial resolution and used to calculate the PCI following the Equation

$$PA = \mathrm{Precipitation} - \mathrm{Precipitation}_{\min} / \mathrm{Precipitation}_{\max} - \mathrm{Precipitation}_{\min}$$

Where $\mathrm{Precipitation}_{min}$ and $\mathrm{Precipitation}_{max}$ represent the minimum and maximum historical values at every chosen time during the study period, and Precipitation represents the seasonal mean precipitation in a year.

Soil Moisture Condition Index (SMCI)

Based on the monthly GLDAS-2.1 Noah 0.25 degree datasets from 2000 to 2022 resampled to 250m, the monthly SMCI values were determined as developed by Kogan, 1995, as following the Equation

$$\mathrm{SMCI} = \mathrm{SM} - \mathrm{SM}_{min}/\mathrm{SM}_{max} - \mathrm{SM}_{min}$$

where SMmin and SMmax are the minimum and maximum values at every chosen time during the study period, SM represents the seasonal mean soil moisture in a year.

Vegetation Condition Index (VCI)

The vegetation condition index is to achieve the objective of drought monitoring by monitoring on surface vegetation growth conditions, while the year-to-year change in NDVI of a region is capable to reflect the interannual fluctuation in productivity of each ecosystem resulting from differences in meteorological conditions, and the maximum and minimum of perennial NDVIs reflect the best and the worst meteorological conditions in these years. Based on these features, Kogan et al define VCI as

$$VCI = \mathrm{Precipitation}_{\max} - \mathrm{Precipitation}_{\min}/\mathrm{NDVI}_{\max} - \mathrm{NDVI}_{\min}$$

where NDVI is the mean NDVI value for the month of March-May of a particular year; NDVI_{max} and NDVI_{min} are the maximum and minimum values of NDVIs for the study period respectively; the maximum and minimum in the denominator reflect the best and worst conditions for vegetation growth; their difference, in a sense, represents the growth environment of local vegetation; and the smaller difference between the NDVI for a year and the minimum in the numerator denotes the worse vegetation growth. VCI ranges from 0-1; VCI≤0.3 means a bad vegetation growth condition, 0.3≤VCI≤0.7 means a good vegetation growth condition.

Temperature Condition Index (TCI)

The Temperature Condition Index (TCI) is another index used for drought monitoring that focuses on the temperature conditions of vegetation. The Land Surface Temperature (LST) measured from brightness temperature was utilized for assessing TCI. The index measures the vegetation stress associated with temperature and intense wetness (Singh et al., 2003). Kogan (1995) also determined the TCI index based on brightness temperature. Higher TCI values represent stress vegetation conditions (Singh et al., 2003). The index was derived using MOD11A2 LST as:

$$TCI = LST_{\max} - \mathrm{LST}/\mathrm{LST}_{\max} - \mathrm{LST}_{\min}$$

where LST is the mean LST value for the month of March-May of a particular year; LST_{max} and LST_{min} are the maximum and minimum values of LST for the study period respectively. The temperature threshold is the minimum

temperature required for the specific crop to grow, and it varies for different crops. Smaller TCI means more severe drought.

Vegetation Supply Water Index (VSWI)

The Vegetation Supply Water Index (VSWI) is a crucial metric used to estimate the extent of drought in agricultural fields by analysing the ratio between the vegetation index (EVI) and land surface temperature (LST). The higher the VSWI value, the lower the crop canopy temperature. However, if the vegetation index is higher, it indicates that the more vigorous transpiration of vegetation, the higher soil moisture content. The lower VSWI also indicates high crop canopy temperature, which further indicates water supply is insufficient to meet the vegetation demand.

$$VSWI = \frac{EVI}{LST}$$

where EVI & LST is the mean EVI & LST value for the month of March-May of a particular year.

Weight Calculation

Analytical hierarchical process (AHP) is a structured technique, which can be used for establishing and evaluating complicated decisions (Saaty, 1988). In this study 5 (five) parameters i.e. CHIRPS data as a component from precipitation to calculate PCI, soil moisture & LST as a component from soil to calculate SMCI & TCI, NDVI as a component from vegetation to calculate VCI and EVI & LST as a component from vegetation and soil to calculate VSWI are selected. These inputs are crucial for selecting appropriate drought indicators. The initial step involves a data quality check; if the data fails this check, it is rejected. For data that passes, preprocessing is carried out to prepare the dataset for further analysis. This includes normalizing the indicators to ensure consistency across different scales and units. Following normalization, weights are assigned to each indicator based on their relative importance by experts. The weight matrix comprises five criteria: PCI, SMCI, VCI, TCI and VSWI. The matrix includes pairwise comparisons among these criteria, with values indicating their relative importance. For instance, Soil Moisture is twice as important as PCI, reflected by a value of 2/1 in the matrix. The right-hand section of the figure displays the normalized principal eigenvector derived from the comparison matrix, which represents the relative weights assigned to each criterion. The weights are calculated as follows: PCI (0.14), SMCI (0.25),

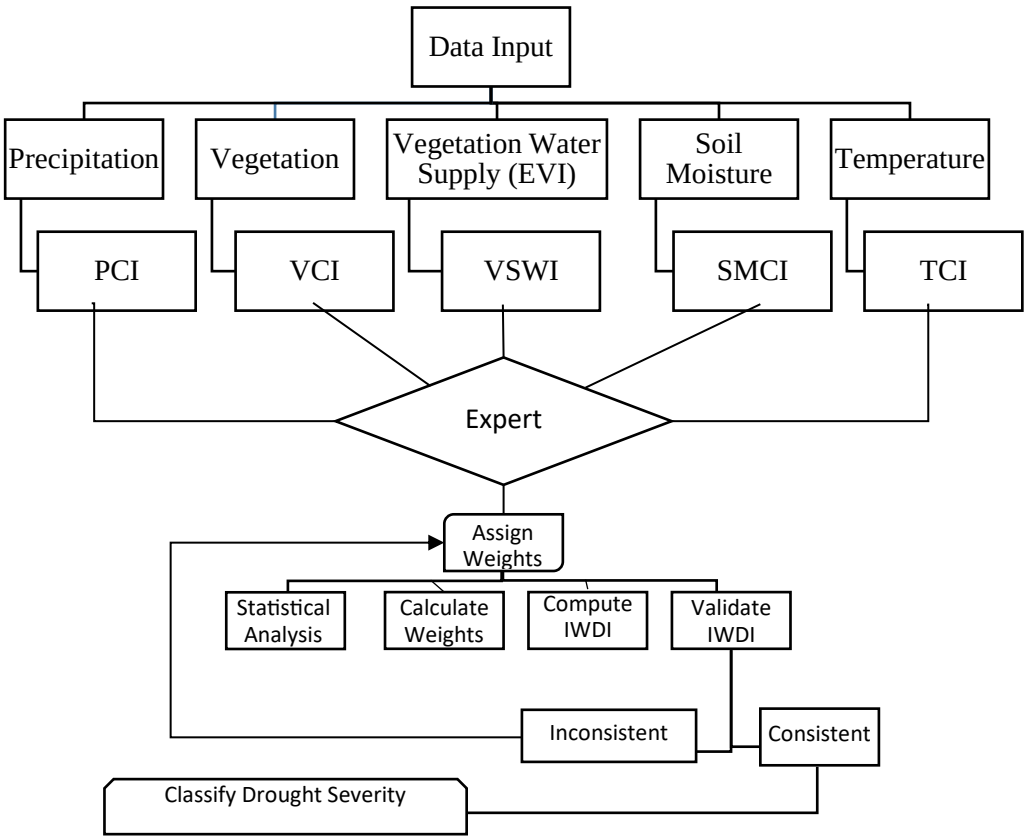

Fig. 5. Represents the weight calculation process for the IWDI using the Analytic Hierarchy Process (AHP).

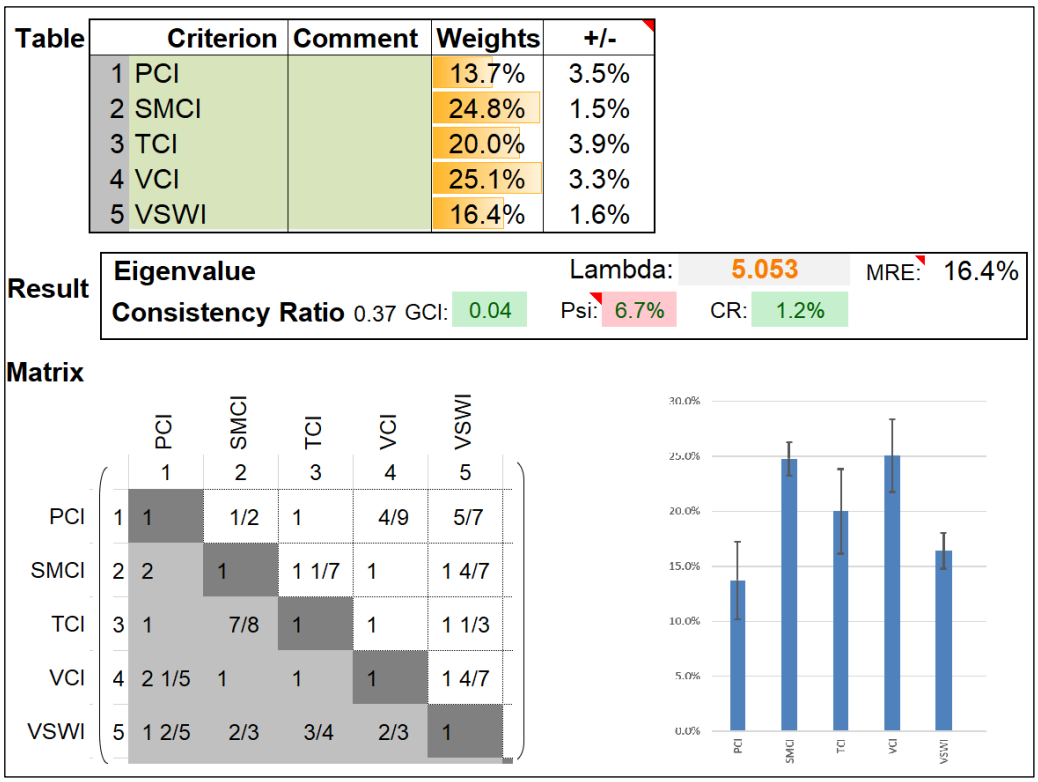

Table

	Criterion	Comment	Weights	+/-
1	PCI		13.7%	3.5%
2	SMCI		24.8%	1.5%
3	TCI		20.0%	3.9%
4	VCI		25.1%	3.3%
5	VSWI		16.4%	1.6%

Result

Eigenvalue Lambda: 5.053 MRE: 16.4%

Consistency Ratio 0.37 GCI: 0.04 Psi: 6.7% CR: 1.2%

Matrix

		PCI	SMCI	TCI	VCI	VSWI
		1	2	3	4	5
PCI	1	1	1/2	1	4/9	5/7
SMCI	2	2	1	1 1/7	1	1 4/7
TCI	3	1	7/8	1	1	1 1/3
VCI	4	2 1/5	1	1	1	1 4/7
VSWI	5	1 2/5	2/3	3/4	2/3	1

Fig. 6. Weight calculation using AHP.

VCI (0.25), TCI (0.2) and VSWI (0.16). The next step involves validating the IWDI to ensure it accurately reflects drought conditions. If inconsistencies are found during validation, the weights are adjusted, and the IWDI is recalculated. Once validated, the IWDI is used to classify drought severity across different regions, facilitating targeted drought mitigation and management efforts.

Process of Integrated Weighted Drought Index (IWDI) construction

The Integrated Weighted Drought Index (IWDI) is calculated by considering all possible variables relevant to different types of droughts, such as meteorological, agricultural, and soil moisture drought indices (Kanthavel, et.al., 2022). It integrates multiple drought indices, including meteorological, remote sensing multi-sensor, soil moisture conditions, and climate variables, to develop a comprehensive index for monitoring and assessing droughts (Ali et al, 2022). The IWDI has been found to have a significant correlation with meteorological and agricultural drought indices, making it a reliable indicator for monitoring agricultural droughts (Shi, X., et.al., 2022). The integration of different indices, as done in the IWDI, is considered a better option for understanding and monitoring agricultural drought losses (Uddin, et. al., 2020).

The IWDI is computed as the weighted average of the

$$IWDI = 0.14PCI + 0.25SMCI + 0.25VCI + 0.2TCI + 0.16VSWI$$

Where: PCI = Precipitation Condition Index
SMCI = Soil Moisture Condition Index
VCI = Vegetation Condition Index
TCI = Temperature Condition Index
VSWI = Vegetation Supply Water Index

Results and Discussions

Drought Trend Based on SPI

Precipitation data were derived from monthly rainfall measurements for a period of 22 years (2000–2022). These monthly rainfall data were used to compute the SPI for each station. In situ rainfall data were collected from Bangladesh Meteorological Department (BMD). The number of rainfall stations between 2000 and 2006 was 5, from 2007 to 2017 the number of these stations had increased to and reached 11 in 2018. The SPI is an index normally calculated on the basis of selected periods of time (typically 1, 2, 3, 6, 9, 12, 24 and 48 months of total precipitation) and indicates how the precipitation for a specific period compares with the complete record

(possibly 25 or 50 or 100 years) at a given station. SPI at different time scales, e.g. 1- or 3-month SPI of a particular month represents deviation in precipitation totals for the same month and current plus previous two months, respectively. Positive values indicate greater than mean precipitation and negative values indicate less than mean precipitation.

The 3-month SPI was calculated for 11 rainfall stations using monthly rainfall data of the pre-kharif season (March–May) for the period of 2000–2022. The SPI data shows significant variability in precipitation across the 11 weather stations, indicating both dry and wet periods. Drought and wet events are summarized in Table 6. Multiple stations experienced periods of drought, indicated by negative SPI values. Notable drought years include 2009, 2014, and 2018, where several stations showed extended dry spells, as in 2013 and 2017, several stations experienced wet spells. The early 2000s to 2010 showed alternating periods of drought and excess moisture, with no clear trend towards drier or wetter conditions. However, some stations like Dhaka and Faridpur recorded a gradual increase in drought conditions towards the end of this period. 2010-2022 period shows more frequent and intense precipitation anomalies, with both extreme wet and dry conditions becoming more pronounced. For example, Mongla recorded extremely high SPI values in 2009 and 2013, indicative of unusually wet periods, while Khulna experienced significant droughts in 2011 and 2021.

Dhaka exhibits a mix of dry and wet periods, with notable droughts in 2009 and 2014, and wetter conditions in 2017. Faridpur shows a trend towards drier conditions, particularly in 2008 and 2014, with intermittent wet periods like in 2017. In Tangail data from 2007 onwards reveals alternating dry and wet periods, with significant droughts in 2011 and 2014, and wetter conditions in 2017 and 2020. Khulna experiences both extreme droughts and wet periods, notably a severe drought in 2021 and an unusually wet period in 2017. Mongla marked by extreme precipitation anomalies, including an exceptionally wet period in 2009 and 2013, and severe droughts in 2014 and 2021. Satkhira shows more consistent fluctuations with noticeable droughts in 2009, 2014, and 2018, and wet periods in 2013 and 2017. 2009 is a critical year where many stations, including Faridpur and Satkhira, recorded severe drought conditions. 2013 marked by significant wet periods across several stations, particularly in Mongla and Khulna. 2017 a wetter year for most stations, indicating a region-wide trend of increased precipitation.

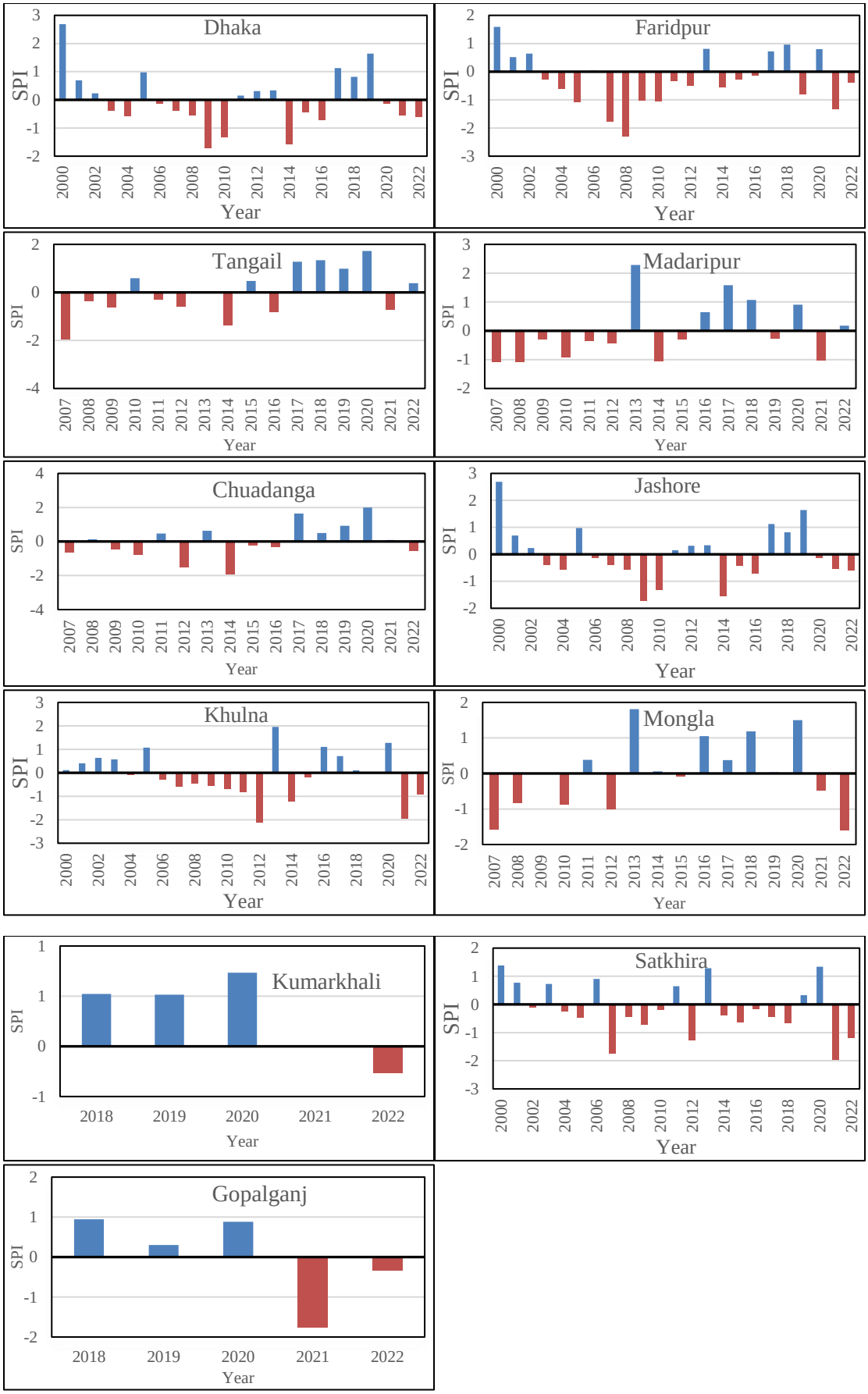

Fig. 7. Bar Plot of SPI observed in various stations

Table 6: List of years representing various drought classes

Station	Extremely Dry	Severe Dry	Moderate Dry	Normal	Extremely Wet	very wet	Moderately wet
Dhaka		2009	2010 2014			2000 2019	
Faridpur	2008	2007	2005 2009 2010 2021				2000
Tangail		2007	2014			2020	2017 2018
Madaripur			2007 2008 2014 2021		2013	2017	2018
Chuadanga		2012 2014				2017 2020	
Jessore			2012				2001 2002 2016
Khulna		2012 2021	2014				2013 2020
Mongla		2007 2022	2012			2013	2016 2018 2020
Satkhira		2021	2007 2022				2000 2013
Gopalganj Kumarkhali		2021					

Drought Trend Based on IWDI

To enumerate the drought stages, this study used Balint et al., 2013 interval to define the range of IWDI classification levels (Table 7).

Table 7: Classification of drought categories based on the value of the IWDI

IWDI Value	Drought Severity
>1.0	No drought
1.0–0.8	Mild drought
0.8–0.6	Moderate drought
0.6–0.4	Severe drought
<0.4	Extreme drought

PCI, SMCI, VCI, TCI and VSWI maps were produced. By using these indices IWDI were produced for Dhaka and Khulna divisions of Bangladesh from 2000 to 2022, providing a comprehensive temporal and spatial analysis of drought conditions (Fig. 8 & 9). The maps focus on the region encompassing Dhaka and Khulna division, using a color-coded scale

ranging from red (<0.4, indicating extreme drought), medium coral light (0.6-0.4, indicating severe drought), yellow (0.8-0.6, indicating moderate drought), Lemongrass (1.0-0.8, indicating mild drought) and leafgreen (>1.0 no drought). Over the twenty-three-year period, significant variations in drought patterns are observed. From 2000 to 2022, the drought patterns across different districts, as indicated by IWDI data, reveal significant fluctuations in the severity and extent of droughts.

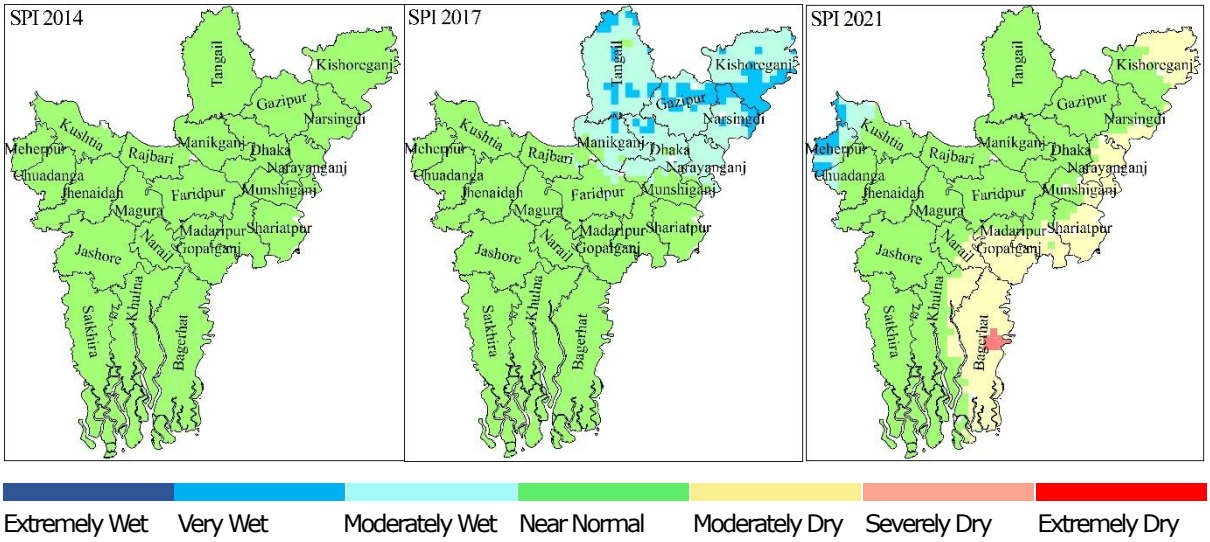

Fig. 8. Spatial distribution of pre-kharif SPI across the study area for the years 2014, 2017, and 2021.

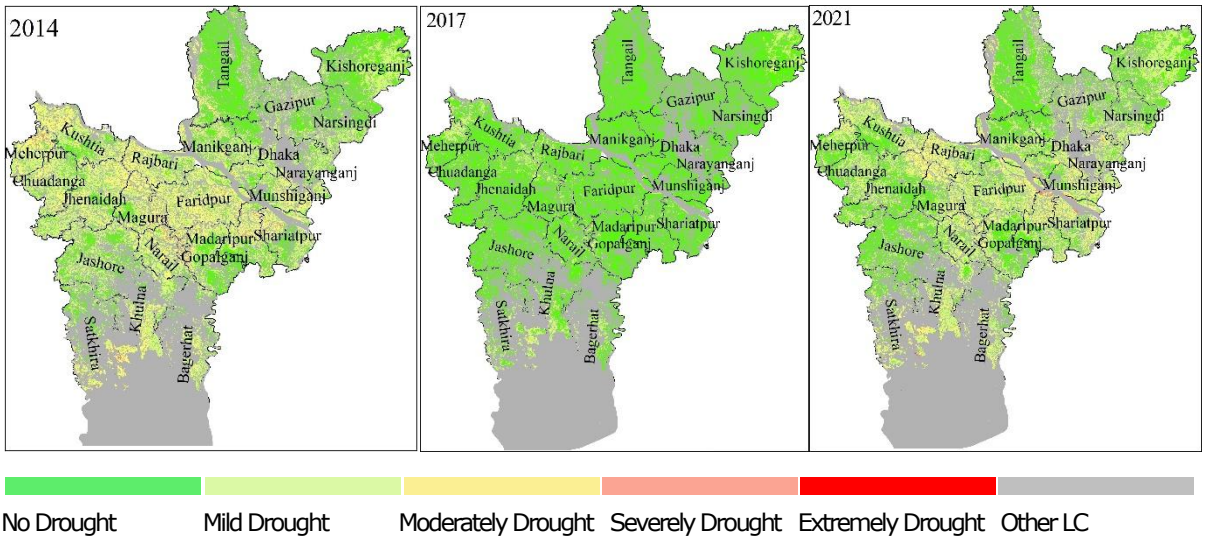

Fig. 9. Spatial distribution of pre-kharif IWDI across the study area for the years 2014, 2017, and 2021.

Based on the analysis of the SPI and IWDI data, the drought patterns in Bangladesh's Dhaka and Khulna divisions show clear temporal variability over the years 2014, 2017, and 2021. According to IWDI data, 2014 was a notable year for drought severity across several districts. IWDI data

highlights that Faridpur had only 4.26% of its land under no drought, with a significant 48.80% experiencing mild drought and 45.67% in moderate drought. Khulna faced similar conditions, with 33.63% of land experiencing moderate drought. More than 80% of cropland experienced mild to moderate drought, with some areas facing severe drought, particularly in districts like Faridpur, Chuadanga, Rajbari, Jhenaidah, Meherpur, Kushtia, and Narail. Drought conditions improved considerably in 2017. SPI data shows a wet year for most districts, with IWDI confirming widespread recovery. Dhaka reported 90.20% of land under no drought, and Gazipur showed 97.03% of cropland free from drought. Khulna experience significant improvement, with 56.61% of its land under no drought. Despite this, Faridpur continued to struggle, with 54.83% of land experiencing mild drought. Favorable conditions prevailed in most districts, with Dhaka (96.39% no drought) and Tangail (99.66% no drought) showing minimal drought impact. Khulna's condition further improved, with 62.56% of land experiencing no drought. Drought severity increased again in 2021, with notable stress in some areas. Dhaka had 32.59% of its land under no drought, while 52.85% was in mild drought. Khulna faced worsening conditions, with 60.31% of land in mild drought and 26.08% in moderate drought. Similar to 2014, districts like Faridpur, Rajbari, and Khulna experienced high drought conditions.

Cropland Layer

The cropland layer represents a binary map legend of crop/non-crop that highlights the separation between annual cropland and non-cropland areas. Cropland layers have been created for 23 districts of Dhaka and Khulna division. To create a cropland layer upazila-wise high resolution (0.5m) georeferenced Google Earth Image was downloaded using Tile+ plugins of QGIS. After that, the multi-resolution segmentation algorithm of the eCognition software was used to develop image objects using the Google Earth Image. The algorithm uses three parameters: scale, shape weighting, and compactness weighting. Segmentation parameters were determined through a combination of trial and error, and experience.

Parameters used in this study were scale parameter: 50, shape weighting: 0.6, compactness weighting: 0.7. Since Google Earth provides archive imagery in many places, it is not possible to create a cropland layer of the current time using only Google Earth Image. So, to identify the objects, the Sentinel-2 image of the period from Jan'23 to Mar'23 has been used along with the Google Earth Image. If an object represents cropland in Google Earth Image but non-cropland in Sentinel-2 images, that object

is assigned with the non-cropland class. Each object was manually identified using ArcGIS. In case of mixed object cut polygon feature of ArcGIS was used to separate cropland from non-cropland.

To generate an updated high resolution cropland layer for Dhaka district, WorldView-2 (WV02) and WorldView-3 (WV03) satellite images of Dhaka for 2023-2024 years were purchased from Maxar. By using these images, the cropland layer of Dhaka district was generated. The remaining 22 districts of Dhaka and Jessore divisions, Google Earth and Sentinel-2 imagery were utilized to generate the cropland layer. These cropland layers are expected to enhance the accuracy of crop monitoring in the future.

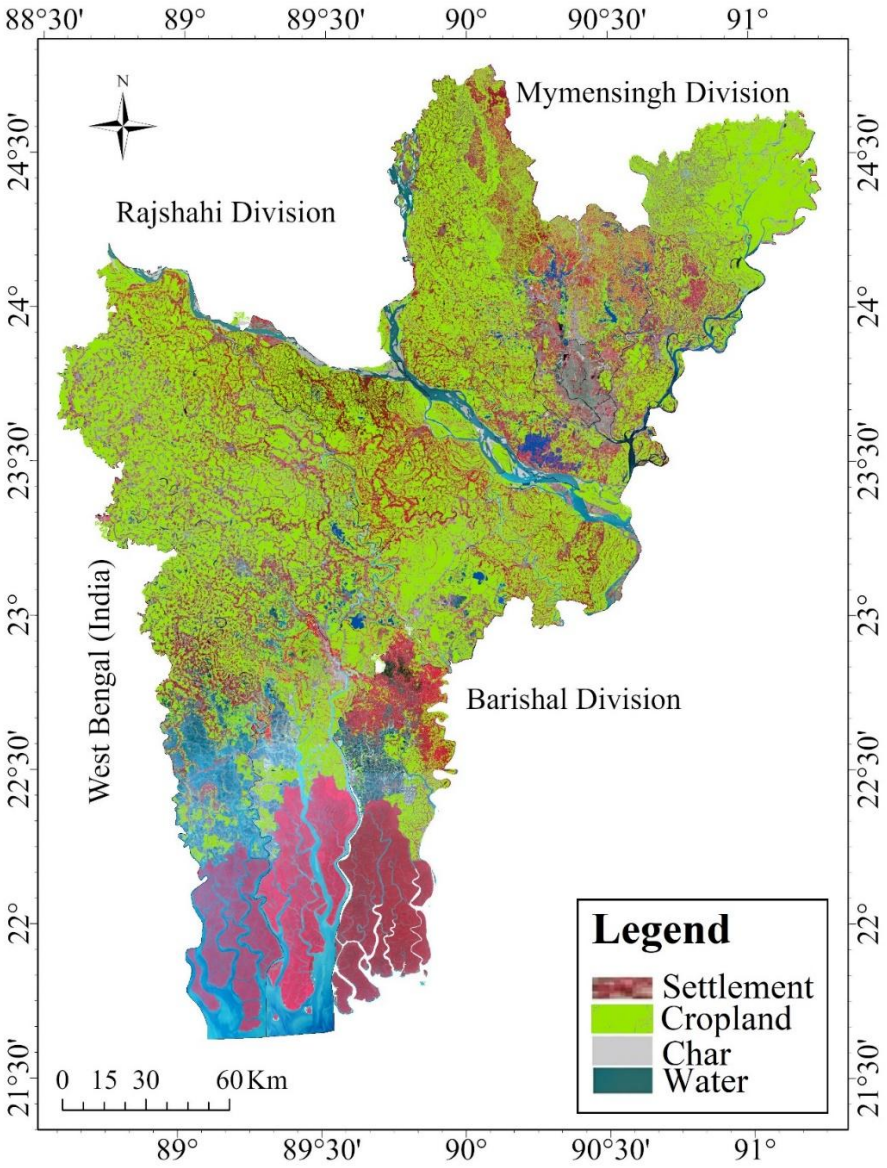

Fig. 10. Spatial distribution of cropland layer across Dhaka and Khulna Divisions.

Conclusions

This study provides a comprehensive analysis of drought conditions in Dhaka and Khulna division of Bangladesh from 2000 to 2022, utilizing the Integrated Weighted Drought Index (IWDI) to assess spatial and temporal variability. The methodology integrates key drought indicators—precipitation, soil moisture, SPI, TCI, VCI, and VSWI—ensuring a robust and multifaceted evaluation. The weight calculation process, underpinned by the Analytic Hierarchy Process (AHP), emphasizes the relative importance of each indicator, thereby enhancing the accuracy of the IWDI. The results reveal significant annual and regional variations in drought severity. The impact of drought varied significantly across districts. The overall trend across the Khulna and Dhaka divisions indicates a predominance of favorable agricultural conditions, with most years showing high percentages of land under no drought. Districts like Kishoreganj, Tangail, Dhaka and Gazipur consistently exhibited stable conditions, with minimal fluctuations in drought severity. These regions exhibit relatively high percentages of agricultural land under no drought throughout the years, reflecting their resilience to climatic variability. Conversely, districts such as Faridpur, Rajbari, Chuadanga, Jhenaidah, Kushtia, Meherpur, Narail, Bagerhat and Khulna experienced recurrent drought conditions. These areas frequently reported significant portions of agricultural land under mild to moderate drought, and in some years, even severe drought.

Acknowledgements

The author is extremely grateful to the Honorable Chairman of SPARRSO, the Members, Advisors and Project Investigator for their continuous support and funding. The author would also express gratitude to all who worked in the team and supported until the completion of this research.

References

Ali, F., Saba, R., Zulfiqar, A., Sadia, Q., Bing, L., Muhammad, A.K. (2022). The spatiotemporal weighted efficient drought index—a new generalized procedure of regional drought indicator. *Ecohydrology*, 15(7), e2454. https://doi.org/10.1002/eco.2454

Alamgir, M., Shamsuddin, S., Manzul, K.H., Syams, N., Sobri, B.H., and Supiah, S. (2015). Analysis of meteorological drought pattern during different climatic and cropping seasons in Bangladesh. *Journal of the American Water Resources Association*, 51(3), 794–806, https://doi.org/10.1111/jawr.12276

Aziz, M. A., Hossain, A.B.M.Z., Moniruzzaman, M., Rokib, A., Taslima, Z., Saiful, A., Qayum, M.A., Mamun, M.A.A., Kader, M.A., Rahman, N.M.F. (2022). Mapping of agricultural drought in bangladesh using geographic information system (GIS). *Earth Systems and Environment*, 6, 657–667. https://doi.org/10.1007/s41748-021-00231-8

Balint, Z., Francis, M., Peris, M., and Christian, T.O. (2013). Monitoring drought with the combined drought index in kenya, developments in earth surface processes kenya: a natural outlook. *Geo-Environmental Resources and Hazards,* 16, 341–356. https://doi.org/10.1016/B978-0-444-59559-1.00023-2

Brammer, H. (1987). Drought in Bangladesh: Lessons for planners and administrators. *Disasters,* 11(1), 21–29 https://doi.org/10.1111/j.1467-7717.1987.tb00611.x

Chowdhury, M.H.K. and Hussain, M.A. (1983). On the aridity and drought conditions of Bangladesh. *MAUSAM*, 34(1), 71–76, https://doi.org/10.54302/mausam.v34i1.2334

Dey, N.C., Alam, M.S., Sajjan, A.K., Bhuiyan, M.A., Ghose, L., Ibaraki, Y., and Kari, F. (2012). Assessing environmental and health impact of drought in the northwest Bangladesh. *Journal of Environmental Science and Natural Resources*, 4(2), 89–97. https://doi.org/10.3329/jesnr.v4i2.10141

Dash, B.K., Rafiuddin, M., Khanam, F. (2012). Characteristics of meteorological drought in Bangladesh. *Nat. Hazards,* 64, 1461–1474. https://doi.org/10.1007/s11069-012-0307-1

Foyez, A., Prodhan, J., Zhang, Y., Bai, T., Prasad, P., Sharma, U., Ashish, K. (2020). Monitoring of drought condition and risk in bangladesh combined data from satellite and ground meteorological observations. *IEEE Access*, 8(1):93264-93282. DOI: 10.1109/ACCESS.2020.2993025

GoB (2020), 2015 (in support of REDD+), Forest Department, Ministry of Environment, Forest and Climate Change, Government of the People's Republic of Bangladesh, Dhaka, Bangladesh. ISBN: 978-984-34-4277-2

Habiba, U., Shaw, R. and Takeuchi, Y. (2014). Farmers adaptive practices for drought risk reduction in the northwest region of Bangladesh,

Natural Hazards, 72(2), 337–359. https://doi.org/10.1007/s11069-013-1011-5

Islam, M. N. (2009). Rainfall and temperature scenario for Bangladesh. *The Open Atmospheric Science Journal*, 3(1), 93–103. DOI: 10.2174/1874282300903010093

Kamruzzaman, M., Syewoon, H., Jaepil, C., Min-Won, J. and Hanseok, J. (2019). Evaluating the spatiotemporal characteristics of agricultural drought in Bangladesh using effective drought index. *Water,* 11(12), 2437; https://doi.org/10.3390/w11122437

Kamruzzamana, M., Jang, M., Hwang, S., Jang, T. (2018). Evaluating the agricultural drought for pre-kharif season in Bangladesh using MODIS vegetation health index. *Journal of The Korean Society of Agricultural Engineers*, 60(6), 55–63, https://doi.org/10.5389/KSAE.2018.60.6.055

Kanthavel, P., Saxena, C. K., Singh, R.K. (2022). Integrated drought index based on vine copula modelling. *International Journal of Climatology*, 42 (16), 9510-9529. https://doi.org/10.1002/joc.7840

Keka, I.A., Matin, I., Rahman, M., and Banu, D. A. (2012). Analysis of drought in eastern part of Bangladesh. *Daffodil international university journal of science and technology*, 7(1), DOI:10.3329/DIUJST.V7I1.9643.

Kogan, F.N. (1995). Droughts of the Late 1980s in the United States as derived from NOAA polar orbiting satellite data. *Bull. Amer. Meteor. Soc.*, 76, 655–668. https://doi.org/10.1175/1520-0477(1995)076<0655:DOTLIT>2.0.CO;2

Kogan, F.N., (1995). Application of vegetation index and brightness temperature for drought detection. *Advances in Space Research* Volume 15(11), 91-100. https://doi.org/10.1016/0273-1177(95)00079-T

Kulkarni, S.S., Brian, D.W., Yared, A.B., Tsegaye, T., Mark, D.S., and Shirishkumar, S.G. (2020). Developing a remote sensing-based combined drought indicator approach for agricultural drought monitoring over Marathwada, India. *Remote Sensing*, 12 (13). https://doi.org/10.3390/rs12132091

Liu, S., & Li, W. (2011). The study on drought monitoring based on multi-

source remotely sensed images. *Eighth International Conference on Fuzzy Systems and Knowledge Discovery (FSKD)*, 4, 2641-2644, DOI: 10.1109/FSKD.2011.6020050.

Lingtong, D., Qingjiu, T., Tao Y., Qingyan, M., Tamas, J., Peter, U., Yan, H. (2013), A comprehensive drought monitoring method integrating MODIS and TRMM data. *International Journal of Applied Earth Observation and Geoinformation* 23 (2013) 245–253, https://doi.org/10.1016/j.jag.2012.09.010

McKee, T.B., Doesken, N.J., Kleist, J. (1993). The relationship of drought frequency and duration to time scales. In: Proceedings of Eighth Conference on Applied Climatology, Anaheim, CA. *American Meteorological Society*, 179–184.

Mustafa, F., Lingbing, B., Qin, W., Ali, M.A., Bilal, M., Shahzaman, M. and Qiu, Z., (2020). Multi-year comparison of CO_2 concentration from NOAA carbon tracker reanalysis model with data from GOSAT and OCO-2 over Asia. *Remote Sensing*, 12(15). https://doi.org/10.3390/rs12152498

Mustafa, F., Huijuan, W., Lingbing, B., Qin, W., Muhammad, S., Muhammad, B., Minqiang, Z., Rashid, I., Rana, W.A., Ali, M.A. and Qiu, Z. (2021). Validation of gosat and oco-2 against in situ aircraft measurements and comparison with carbontracker and geos-chem over Qinhuangdao, China. *Remote Sensing*, 13(5), 1–15, https://doi.org/10.3390/rs13050899

Mondol, M.A.H., Xuan, Z., David, D., Benjamin, J.H. (2021). Observed meteorological drought trends in Bangladesh identified with the Effective Drought Index (EDI). *Agricultural Water Management*, Volume 255, 107001. https://doi.org/10.1016/j.agwat.2021.107001

Miyan, M.A. (2015). Droughts in asian least developed countries: Vulnerability and sustainability. *Weather and Climate Extremes*, 7, 8–23, https://doi.org/10.1016/j.wace.2014.06.003

Niaz, M., Faiz, M.A., Wei, Y., (2021). Development of an integrated weighted drought index and its application for agricultural drought monitoring. *Arabian Journal of Geosciences*, 14, 455. https://doi.org/10.1007/s12517-021-06879-w

Pettorelli, N., Ryan, S.J., Mueller, T., Bunnefeld, N., Jędrzejewska, B., Lima, M., & Kausrud, K. (2011). The Normalized Difference Vegetation

Index (NDVI): unforeseen successes in animal ecology. *Climate Research*, 46, 15-27, DOI: 10.3354/cr00936

Qu, C., Hao, X. and Qu, J. J. (2019). Monitoring Extreme Agricultural Drought over the Horn of Africa (HOA) Using Remote Sensing Measurements. *Remote Sensing*, 11(8), 902, https://doi.org/10.3390/rs11080902

Rahman, M.R., Lateh, H. (2016). Meteorological drought in Bangladesh: assessing, analysing and hazard mapping using SPI, GIS and monthly rainfall data. *Environ Earth Sci* 75, 1026 https://doi.org/10.1007/s12665-016-5829-5

Rhee, J., Im, J., Carbone, G.J. (2010). Monitoring agricultural drought for arid and humid regions using multi-sensor remote sensing data. *Remote Sensing of Environment* 114(12), 2875–2887, https://doi.org/10.1016/j.rse.2010.07.005

Saaty, T. L. (1988). What is the Analytic Hierarchy Process?. In: Mitra, G., Greenberg, H.J., Lootsma, F.A., Rijkaert, M.J., Zimmermann, H.J. (eds) Mathematical models for decision support. NATO ASI Series, Springer, vol 48, https://doi.org/10.1007/978-3-642-83555-1_5

Sarmah, S., Jia, G. and Zhang, A. (2018). Satellite view of seasonal greenness trends and controls in South Asia. *Environmental Research Letters*, 13(3). DOI: 10.1088/1748-9326/aaa866

Sultana, M.S., Gazi, M.Y., Mia, M.B. (2021). Multiple indices based agricultural drought assessment in the northwestern part of Bangladesh using geospatial techniques. *Environmental Challenges*, Volume 4. https://doi.org/10.1016/j.envc.2021.100120

Shahzaman, M., Zhu, W., Bilal, M., Habtemicheal, B.A., Mustafa, F., Arshad, M., Ullah, I., Ishfaq, S., and Iqbal, R., (2021). Remote sensing indices for spatial monitoring of agricultural drought in south asian countries. *Remote Sensing*, 13(11). https://doi.org/10.3390/rs13112059

Singh, R.P., Roy, S., Kogan, F.N. (2003). Vegetation and temperature condition indices from NOAA AVHRR data for drought monitoring over India*. Int. J. Remote Sens.* 24 (22), 4393–4402, https://doi.org/10.1080/0143116031000084323

Shahid, S., and Behrawan, H. (2008). Drought risk assessment in the western part of Bangladesh. *Natural Hazards*, 46(3), 391–413, DOI:

10.1007/s11069-007-9191-5.

Shi, X., Hao, D., Mengyue, W., Mengqi, S., Fei, C., Yi, L., Yuanqi, Y. (2022). A comprehensive drought monitoring method integrating multi-source data. *PeerJ,* https://doi.org/10.7717/peerj.13560

Uddin, M.J., Jichao, H., Abu, R.M., Towfiqul, I., Abu, R., Islam, M.T., Kutub, U. E., Zahan, M.N. (2020). A comprehensive statistical assessment of drought indices to monitor drought status in Bangladesh. *Arabian Journal of Geosciences,* 13, 323. https://doi.org/10.1007/s12517-020-05302-0

Wilhite, D.A., Glantz, M. H. (1985). Understanding the drought phenomenon: the role of definitons. *Water Int* 10(3), 111-120, DOI: 10.1080/02508068508686328

Zaher, M.Y., Mumtaz, A., Ahmad, S., Nadhir, A., Shamsuddin, S. (2021). Forecasting standardized precipitation index using data intelligence models: regional investigation of Bangladesh. *Scientific Reports*, 11(1), 3435. https://doi.org/10.1038/s41598-021-82977-9

Zhang, Q., Rui, S., Chong-Yu, X., Peng, S., Huiqian, Y., Jiaqi, Z. (2022). Multisource data-based integrated drought monitoring index: model development and application. *Journal of hydrology,* 615, 128644. https://doi.org/10.1016/j.jhydrol.2022.128644

Air Quality Monitoring Using Remote Sensing and GIS Technologies in Major Cities of Bangladesh

Mohammad Shohidul Islam*, Md. Farid Uddin, Fahmida Yeasmin Sami

Bangladesh Space Research and Remote Sensing Organization (SPARRSO), Agargaon, Shere Bangla Nagar, Dhaka-1207, Bangladesh.
**Corresponding author E-mail: shohidul@sparrso.gov.bd*

Abstract

Air quality monitoring has become increasingly critical in urban areas due to rapid industrialization and urbanization. This study focuses on assessing air quality in major cities of Bangladesh using remote sensing (RS) and Geographic Information System (GIS). Air quality monitoring using RS & GIS technologies has emerged as a powerful approach to assess and manage air pollution in urban environments. Remote sensing enables the acquisition of high-resolution, real-time data on various air pollutants, such as carbon monoxide (CO), particulate matter ($PM_{2.5}$ and PM_{10}), and other harmful substances, by capturing reflected or emitted electromagnetic radiation from the Earth's surface and atmosphere. These data are obtained through satellites or airborne sensors, which provide extensive spatial coverage that ground-based monitoring systems alone cannot achieve. GIS offers robust tools to store, analyze, and visualize the spatial and temporal distribution of these pollutants. By integrating RS data into GIS, researchers can generate detailed pollutant distribution maps, identify pollution hotspots, and monitor changes over time. Landsat-8, Sentinel-5P, ground networks, and continuous atmospheric monitoring station (CAMS) data are used to measuring the concentration of air pollutants such as CO, $PM_{2.5}$, and PM_{10} in the regions of Dhaka, Narayanganj, Munshiganj, and Gazipur in Bangladesh. The study correlated satellite reflectance with ground-based measurements of air pollutants, yielding correlation values of 0.59 for CO, 0.60 for $PM_{2.5}$, and 0.54 for PM_{10}. The correlation values indicate a moderate relationship, suggesting that remote sensing can be a viable tool for monitoring air quality. Utilizing these correlations, pollutant distribution maps were generated to visualize the spatial distribution and concentration of air pollutants across the major cities. These maps provide a comprehensive understanding of pollution patterns, which can aid in effective urban planning and pollution control strategies in Bangladesh.

Keywords: Air pollutants, satellite reflectance, Pollution patterns, Bangladesh.

Introduction

Air pollution is the presence of substances, whether chemical, physical, or biological, that contaminate indoor and outdoor environments, leading to detrimental effects on the natural components of the surroundings (Halim et al., 2020).

Air pollution has emerged as significant health risk, primarily stemming from sources like industrial operations and vehicle exhaust. Individuals exposed to air pollution are more susceptible to both psychological issues such as stress, mood fluctuations, anxiety, depression, dementia, bipolar disorder, and schizophrenia, as well as physical health ailments like premature birth, lung cancer, cardiovascular diseases, and respiratory disorders (Brunekreef & Holgate, 2002; Pereira et al., 2007, Gurjar et al., 2010; Koas, 2010; Abdullah et al., 2018).

Meanwhile, the World Health Organization (WHO) has reported that 4.2 million deaths have occurred due to health complications attributed to air pollution(WHO, 2020). They also assert that 93% of children worldwide are regularly exposed to harmful air pollution. Due to rising population levels and the proliferation of pollution sources, air pollution has emerged as a critical issue, especially in urban centers. A significant percentage of urban areas have failed to meet the air quality standards set by the WHO in recent times. Human activities like traffic congestion and industrial emissions predominantly contribute to air pollution in urban settings. With the expansion of urban areas, these challenges are anticipated to intensify (Zhang & Batterman, 2013; Heald & Spracklen, 2015).

With urbanization forecasted to rise from 52% to 67% by 2050, the global population residing in urban areas is anticipated to expand significantly. Consequently, urban areas are expected to triple in size over the next twenty years (Suzuki et al., 2010; UNDESA, 2014). As rapid urbanization occurs, land use patterns extend outward from small urban centers to their original boundaries, eventually merging to form extensive conurbations of urban areas. While traffic congestion and industrial emissions remain the primary sources of urban air pollution, alterations in land use have also been linked to air quality changes within urban regions (Huang et al., 2013; Li et al., 2019). Due to the impact of air pollutant concentrations stemming from various sources tied to land use practices, alterations in land use have a significant correlation with air quality (Sun et al., 2016).

Urban land use patterns typically reflect the dispersion of air pollutants and air quality within urban environments (Huang & Du, 2018). Air pollution originating from human activities is released directly and indirectly from developed land, where most socio-economic activities occur. Natural land surfaces such as vegetation, farmland, and water bodies have a beneficial effect, enhancing air quality in urban regions. Regrettably, the rapid expansion of urban areas has led to a decline in the positive effects of natural land surfaces, as natural vegetation is replaced and water bodies

are covered by urban development (Gurjar et al., 2010; Irga et al., 2015; Xu et al., 2016). Modifications in how land is utilized can directly or indirectly impact natural land cover surfaces, which can influence the transportation and dispersal of air pollutants, as well as the quality of air in urban areas. Previous studies have found that developed areas tend to be associated with higher levels of emissions and, consequently, increased air pollution (Li et al., 2016; Zahari et al., 2016; Wang et al., 2018).

A study on Malaysia, it has a limited number of air quality monitoring stations, which restricts the initial strategy of pollution prevention programs, especially at a micro-scale level. The existing technique used to monitor air quality involves manually measuring pollution concentrations within the area of the measuring station. The authors have proposed a new technique that integrates satellite remote sensing and Geographic Information System (GIS) to continuously monitor air quality at a micro-scale level. This technique uses images from Landsat 7 Enhanced Thematic Mapper Plus (ETM+) and data from eight (8) Continuous Air Quality Monitoring Stations (CAQM) to determine the relationship between the digital number (DN) of the thermal infrared band and two air pollutant parameters: Carbon Monoxide (CO) and Particulate Matter (particle less than 10 microns in size – PM_{10}) (Koas, 2010).

The authors have developed several models to relate the DN of Landsat 7 ETM+ to the air pollutant parameters. Since the number of CAQM stations is limited, the authors introduced the concept of "virtual stations" to increase the density of CAQM stations. Based on these virtual stations, the kriging interpolation method (available in GIS software) is used to generate air quality maps of the study area. This method allows for a more detailed assessment of air quality within urban areas with limited CAQM stations. The generated maps of pollution concentrations from virtual stations using the kriging interpolation method produce a more realistic distribution of air pollution. The concentration of CO and PM_{10} is highest in the industrial zones of the study area. This method can be used by environmental managers and local authorities to continuously monitor air quality in urban areas(Koas, 2010).

The objective of this research is to establish the relationship between satellite spectral reflectance and air quality parameters in Bangladesh's largest urban conurbation areas (Dhaka, Narayanganj, Munshiganj, Gazipur), which have undergone several stages of urbanization since the year 2000. The study utilizes air quality data from five continuous air quality monitoring stations. Essentially, the primary goal of this research is to provide policymakers with research data to aid in the adoption of

sustainable land use policies aimed at improving air quality in the study area. The goal of this study is to develop the relation between satellite spectral reflectance and air quality parameters CO, $PM_{2.5,}$ $PM_{10,}$ and to analyze and create maps of CO, $PM_{2.5,}$ and PM_{10} concentrations of the selected area.

Materials and Methods

The methodology of this research is divided into four key phases. Firstly, selection of the study areas; secondly, data acquisition; thirdly, preliminary data processing and finally, data analysis, in the Fig. 1 the diagram has shown the research process. Bangladesh is administratively divided into 64 districts and seven divisions, with the Dhaka division situated at the center of the country. The Dhaka division is further divided into 17 districts. This study focuses on three specific districts within the Dhaka division: Dhaka, Narayanganj and Gazipur. The geographical coordinates of the study area are 90° 24.4464′ E longitude and 23° 42.624′ N latitude (Hossain et al., 2016) and the UTM zone 46N projection system. In Figure 2, a location map has been presented and the air monitoring stations of the study area have been shown. The study area includes five monitoring stations.

The study area encompasses a total of 6,081.21 square kilometers and has a population of nearly 60 million, which represents approximately one-third of Bangladesh's total population (Zaman et al., 2010). The average temperature in this area is 27.51 degrees Celsius, and the average rainfall measures 18.45 mm (Bhuyan et al., 2018). Given that Dhaka serves as the social, economic, political, and cultural hub of Bangladesh, urban growth is accelerating rapidly, with many people residing in Dhaka in pursuit of a better quality of life (Zaman et al., 2010). This research will use five continuous air quality monitoring stations, all overseen by the "Department of the Environment (DOE)". The stations are located as follows: Station-1 at Sangshad Bhaban in Sher-e-Bangla Nagar, Station-2 at Firmgate, Station-3 at Darus Salam, Station-4 in Gazipur, and Station-5 in Narayanganj. Three of these stations are within Dhaka City: Station-1, Station-2, and Station-3, which are all in close proximity to each other. Station-4 is situated in Gazipur and Station-5 in Narayanganj, both on the urban outskirts of Dhaka City. Although all stations are in densely populated areas, Stations 1, 2, and 3 are in mixed-use areas encompassing

commercial, industrial, and residential zones. In contrast, Stations 4 and 5 are primarily located in industrial zones.

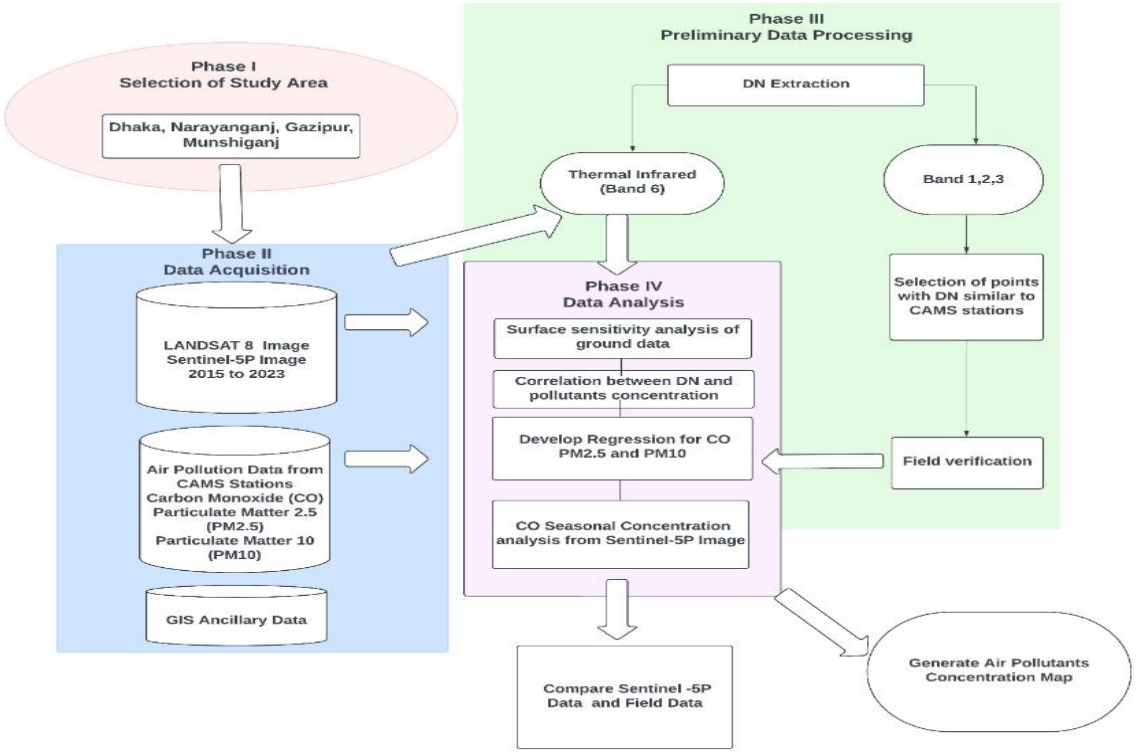

Fig. 1. Research methodology

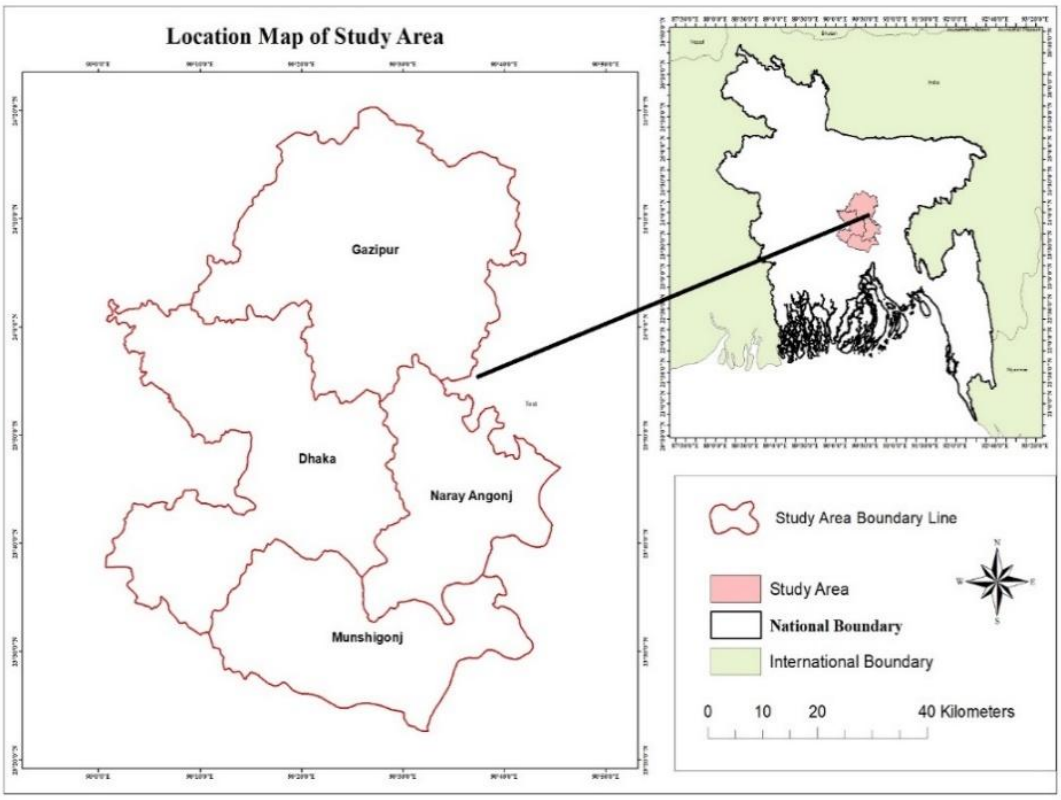

Fig. 2. Map of the study area

The Air Quality Division of the Department of Environment (DOE) provided data for this study from 2015 to 2022 at the selected continuous air quality monitoring stations in this study area. Besides, Sentinel-5 data has been used for spatial analysis of CO. The air quality dataset contains three variables: particulate matter with a diameter of less than 10 m (PM_{10}), particulate matter with a diameter of less than 2.5 m ($PM_{2.5}$), carbon monoxide (CO). Table 1 has been presented the location of five air monitoring stations, monitoring capacity and the name of existed districts of the research area.

Table 1: Air quality monitoring stations

City	ID	Location	Lat/Lon	Monitoring Particles for this research
Dhaka	CAMS-1	Sangshad Bhaban, Sher-e-Bangla Nagar	23.76 N 90.39 E	PM_{10}, $PM_{2.5}$, CO
	CAMS-2	Firmgate	23.77 N 90.38 E	PM_{10}, $PM_{2.5}$, CO
	CAMS-3	Darus-Salam	23.78 N 90.36 E	PM_{10}, $PM_{2.5}$, CO
Gazipur	CAMS-4	Gazipur	23.99 N 90.42 E	PM_{10}, $PM_{2.5}$, CO
Narayanganj	CAMS-5	Narayanganj	23.63 N 90.51 E	PM_{10}, $PM_{2.5}$, CO

This research also utilizes Landsat 8 satellite imagery to gather air pollutant data from the monitoring stations and ancillary data. The study uses datasets from Landsat 8 satellite images spanning 2015 to 2022. The air quality data includes three pollutants: CO, $PM_{2.5}$, and PM_{10}. Ancillary data for the research consists of GIS datasets, which include topographic maps. A key step in the preliminary data processing involves extracting Digital Numbers (DN) from several bands for the air monitoring stations. This step helps in obtaining the DN combinations of the stations and identifying other points with similar DN values. The DN from Landsat 8, including the thermal infrared band and bands 1, 2, and 3, is extracted based on the pixel locations of the stations. To extract DN for the five stations, the images are overlaid onto the GIS layer of the study area. Following DN extraction, map query analysis in ArcGIS 10.8 is used to complete the task.

Results and Discussion

The analysis has been completed in three steps; A. Regression analysis, B. Compare to CO Sentinel-5P data with ground data, C. Production of air quality maps of the study areas. Based on the results in Table 2, there is a stronger correlation between DN and $PM_{2.5}$ as well as DN and PM_{10} compared to the correlation between DN and CO. A significant correlation is evident between the DN of the thermal IR band from Landsat 8 and the pollutants (CO, $PM_{2.5}$ and PM_{10}).

The relationship between DN and air pollutants has been presented in Table 2. Though the average relationship value between DN numbers and CO is 0.59, the values are high for 2019 to 2021(0.665, 0.941, 0.741). The highest average value of $PM_{2.5}$ and DN number is 0.60 for 8 years. The relationship values between DN Numbers and $PM_{2.5}$ are 0.563, 0.893, 0.783, 0.482,0 .472, 0.596, 0.663, 0.317 from 2015 to 2022. For PM_{10}, the average value is 0.54 for 8 years. Besides, the values are 0.79,0.346,0.36,0.329,0.489,0.325,0.858,0.814 of PM_{10} from 2015 to 2022.

Table 2: Relationship between DN and air pollutants for 2015 to 2022

Particle	2015	2016	2017	2018	2019	2020	2021	2022	Average
CO	0.598	0.476	0.487	0.446	0.665	0.941	0.741	0.379	0.59
$PM_{2.5}$	0.563	0.893	0.783	0.482	0.472	0.596	0.663	0.317	0.60
PM_{10}	0.79	0.346	0.36	0.329	0.489	0.325	0.858	0.814	0.54

Fig. 3 to 5 illustrate the regression analysis between DN and air pollutants concentrations based on the obtained data from five continuous air quality monitoring stations. The regression analysis of DN from the Landsat thermal infrared band against the three pollutants (CO, $PM_{2.5}$ and PM_{10}) concentrations indicates a positive correlation.

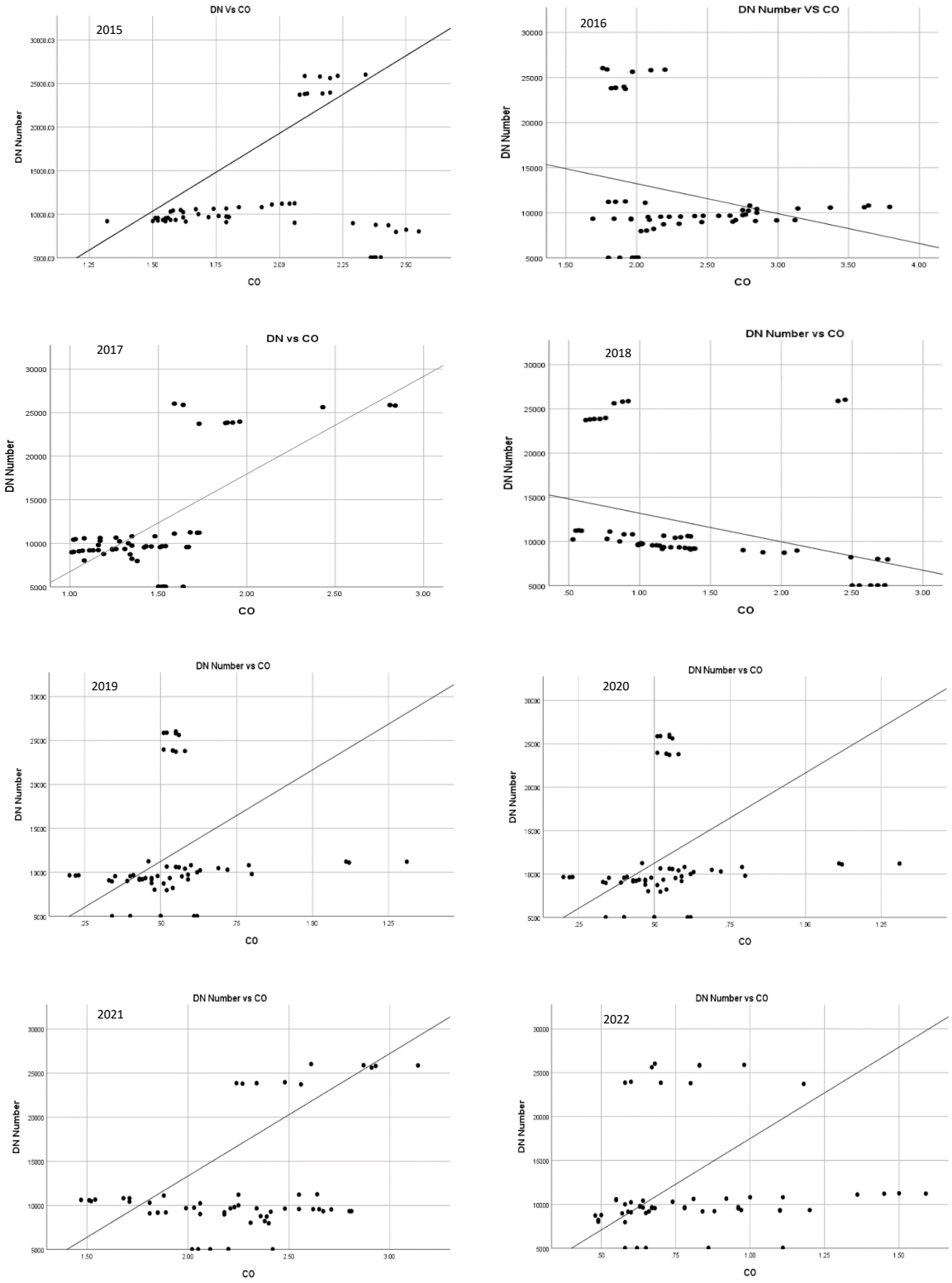

Fig. 3. Relationship between DN and air quality parameter (CO) from 2015-2022.

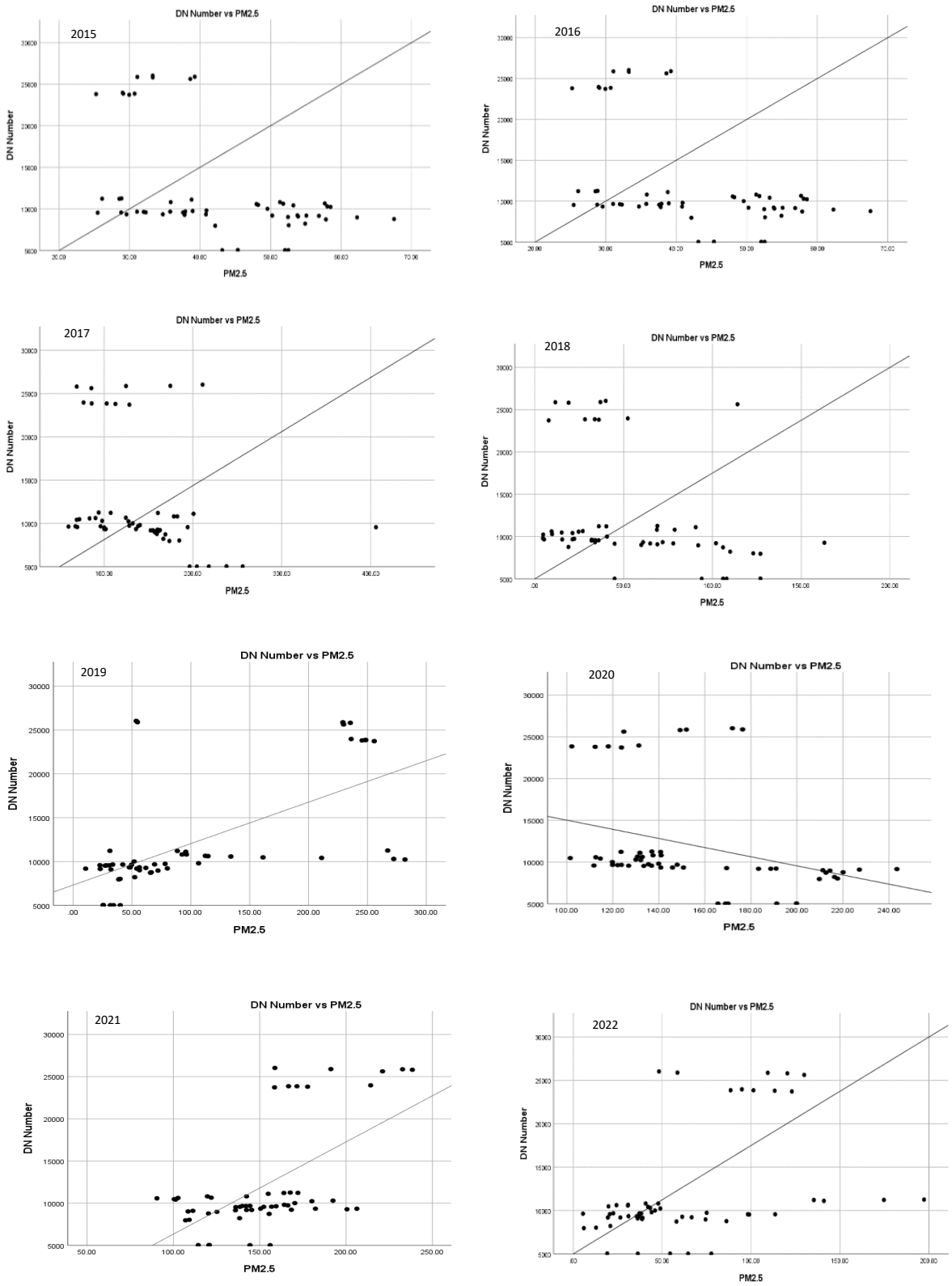

Fig. 4. Relationship between DN and air quality parameter ($PM_{2.5}$) from 2015-2022.

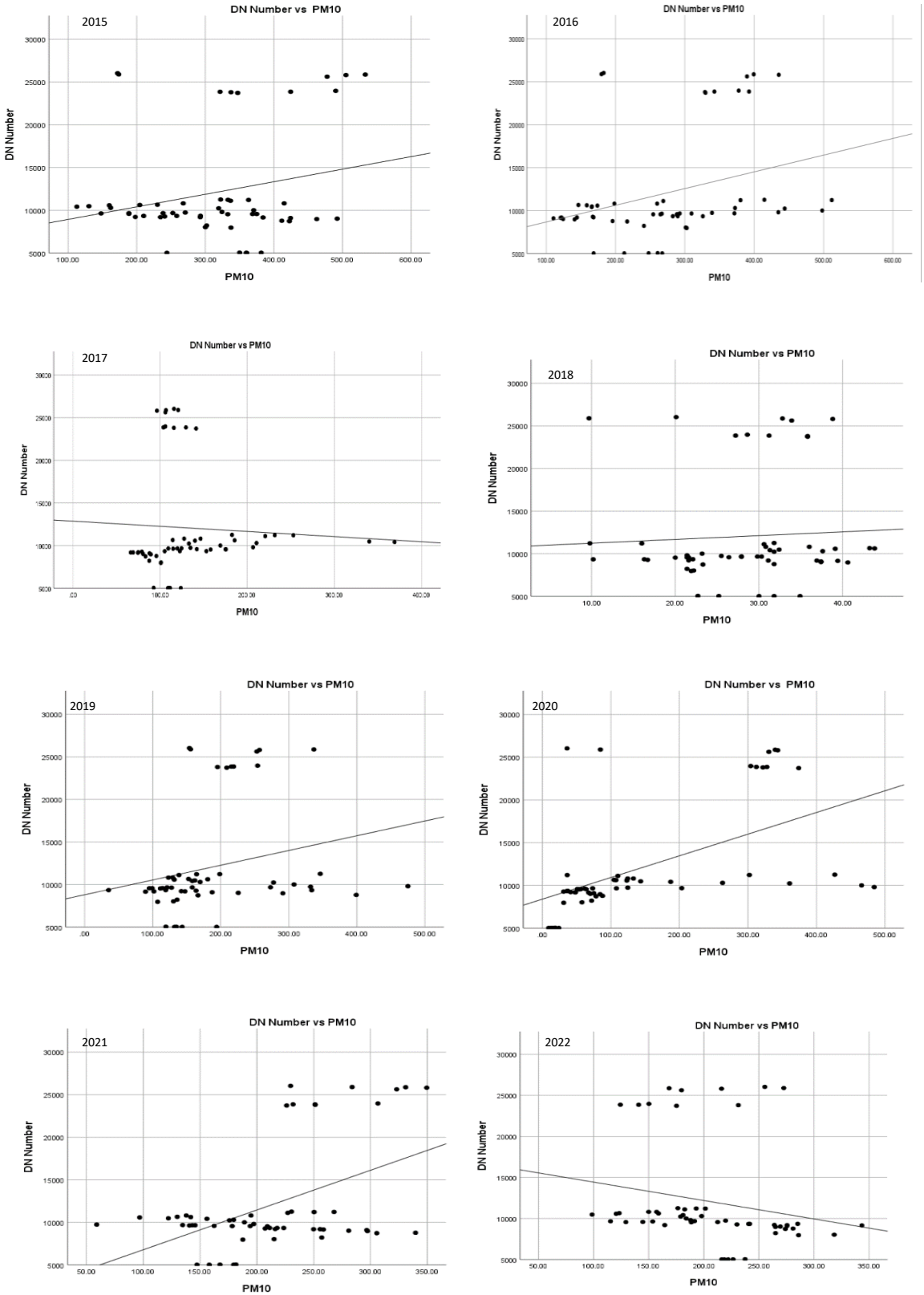

Fig. 5. Relationship between DN and Air Quality Parameter (PM_{10}) from 2015-2022.

In Fig. 6 and 7, the concentrations of $PM_{2.5}$ across various surfaces is illustrated. The surfaces are categorized into seven distinct areas: sensitive areas, residential areas, mixed-use areas, commercial areas, road intersections, industrial zones, and village areas.

Fig. 6(a) presents the $PM_{2.5}$ concentrations in the Dhaka area, where commercial zones provide the highest concentration at 309 µg/m³, followed by residential areas at 281 µg/m³. Narayanganj has the maximum $PM_{2.5}$ concentrations of 292 µg/m³ at industrial zones, while the lowest concentration is 188 µg/m³, as shown in Fig. 6(b). Fig. 6(c) highlights that $PM_{2.5}$ concentrations are extremely high across all surface categories in Gazipur, with industrial areas having the highest level at 298.25 µg/m³. Conversely, Munshiganj shows comparatively lower $PM_{2.5}$ values, with a maximum concentration of 112.46 µg/m³, as depicted in Fig. 6(d).

Fig. 7 further emphasizes that Dhaka, Narayanganj, and Gazipur exhibit significantly higher PM_{10} concentrations across most surface types. So, air quality is a concern for these areas.

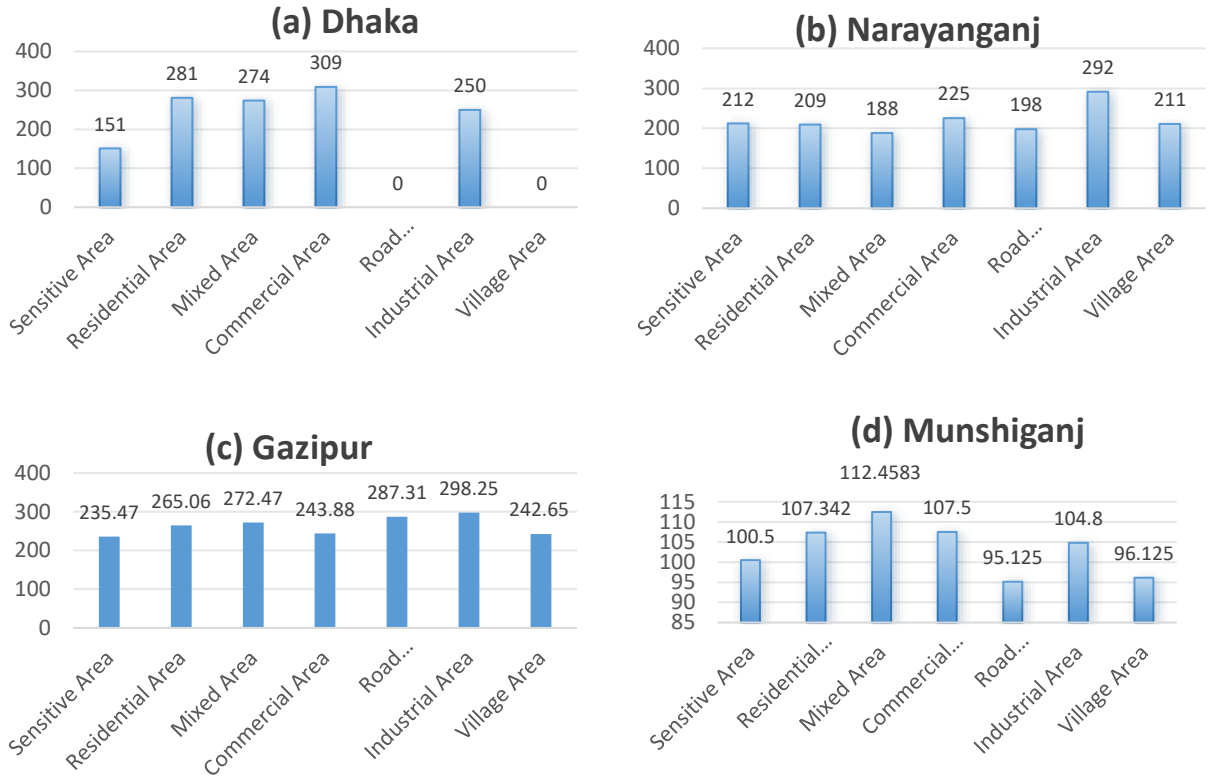

Fig. 6: Concentrations of $PM_{2.5}$ (µg/m³) on different surfaces (a, b, c, d)

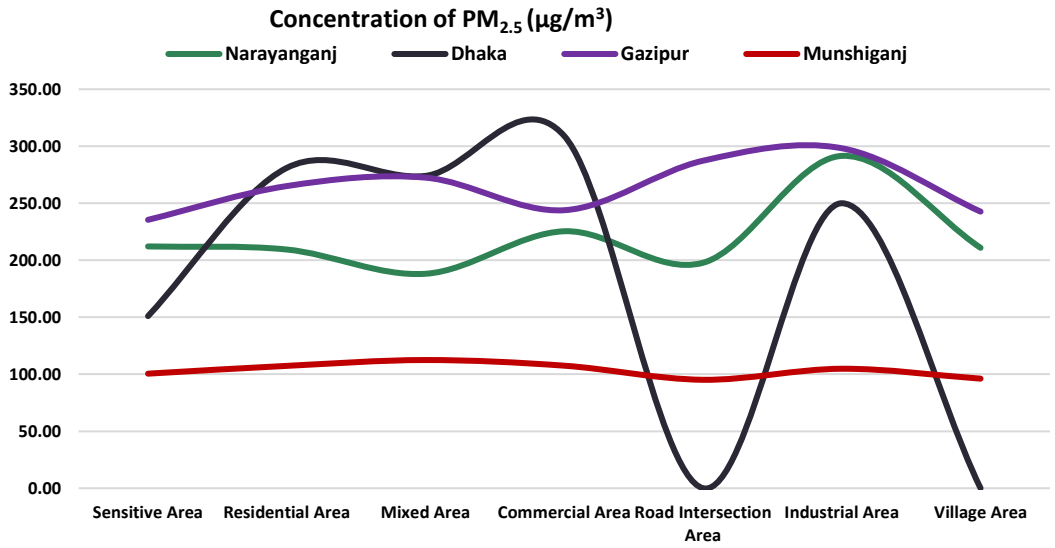

Fig. 7. Concentrations of $PM_{2.5}$ (µg/m^3) on land uses

Fig. 8 and 9 illustrate the concentration of PM_{10} across different surface types in various regions. The surfaces are categorized into seven types: sensitive areas, residential areas, mixed-use areas, commercial areas, road intersections, industrial areas, and village areas.

The PM_{10} concentrations for the Dhaka area are shown in Fig. 8(a), where commercial areas have the highest concentrations at 403 µg/m³, followed by residential areas at 360 µg/m³. As Fig. 8(b) shows, Narayanganj has its highest PM_{10} concentrations in industrial areas at 374 µg/m³, reflecting the overwhelming majority of industrial zones. The lowest concentration in Narayanganj is 242 µg/m³. In Gazipur, PM_{10} levels are higher across all surface types represented in Fig. 8(d). The highest concentrations are recorded at industrial areas of 377.82 µg/m³. Munshiganj, on the other hand, as shown in Fig. 8(c), has significantly lower PM_{10} concentrations, with a maximum value of 145.41 µg/m³.

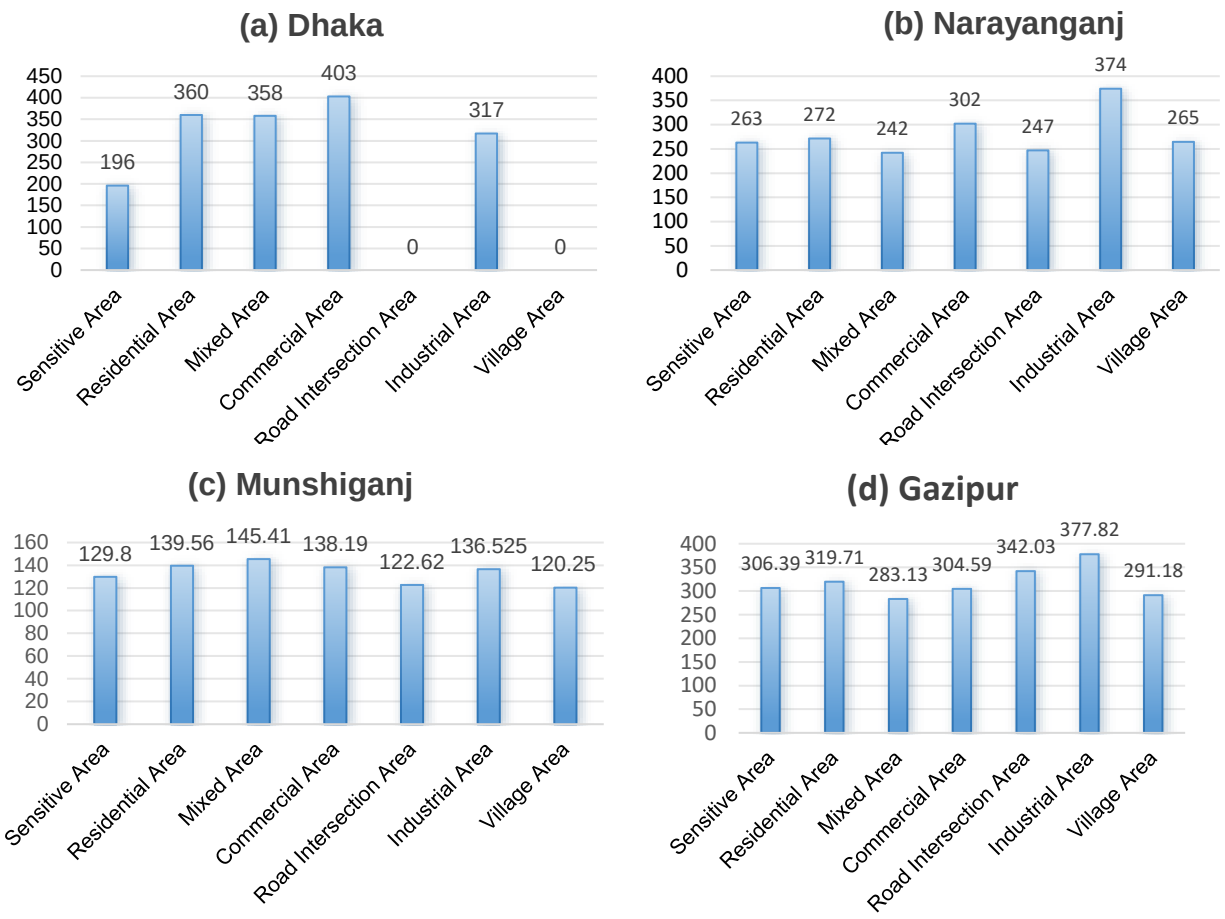

Fig. 8. Concentrations of PM_{10} (µg/m^3) on different surfaces (a, b, c, d)

Fig. 9 further indicates that Dhaka, Narayanganj, and Gazipur exhibit significantly higher PM_{10} concentrations across most surface types, while Munshiganj shows lower values, highlighting its relatively lower pollution levels compared to the other areas.

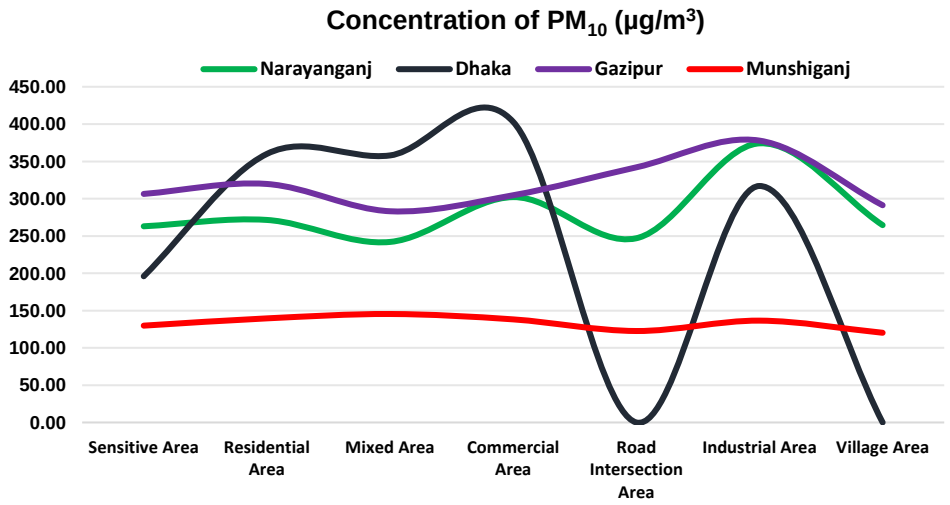

Fig. 9. Concentrations of PM_{10} (µg/m^3) on land uses

Fig. 10 (a, b, c, d, e) depicts the carbon monoxide (CO) concentrations in the study area from 2019 to 2022 using data from Sentinel-5P. These maps represent the CO concentrations for the months of December, January, February, April, and May. A clear seasonal variation between winter and summer are observed in analyzing the CO (carbon monoxide) concentration maps for the months of December, January, February, April, and May. Basically, higher concentrations of CO are noted during the winter months (December, January, and February) compared to the summer months (April and May). The main cause behind this pattern is the in the rise in heating activities that occur during the colder months such as the burning of fossil fuels and biomass for heat. Moreover, lower temperatures during winter often result in atmospheric inversions, which stop pollutant like CO dispersing from outer atmosphere. This leads to an accumulation of CO near the ground. So, its concentration level increases.

Conversely, during the summer months, the intensity of solar radiation increases. That causes to greater atmospheric mixing and more effective pollutant dispersion. Consequently, CO concentrations are generally lower in summer. Furthermore, the increase in photochemical reactions in summer months results in the transformation of pollutants into other compounds, which may reduce CO levels. This seasonal variation signifies the role of both human activities and meteorological conditions in determining the concentration of atmospheric pollutants like CO throughout the year. Dhaka is the most affected by CO particles over the periods. Moreover, the concentration of CO is also high for Narayanganj in winter season. On the contrary, CO is abundant for Gazipur in summer months.

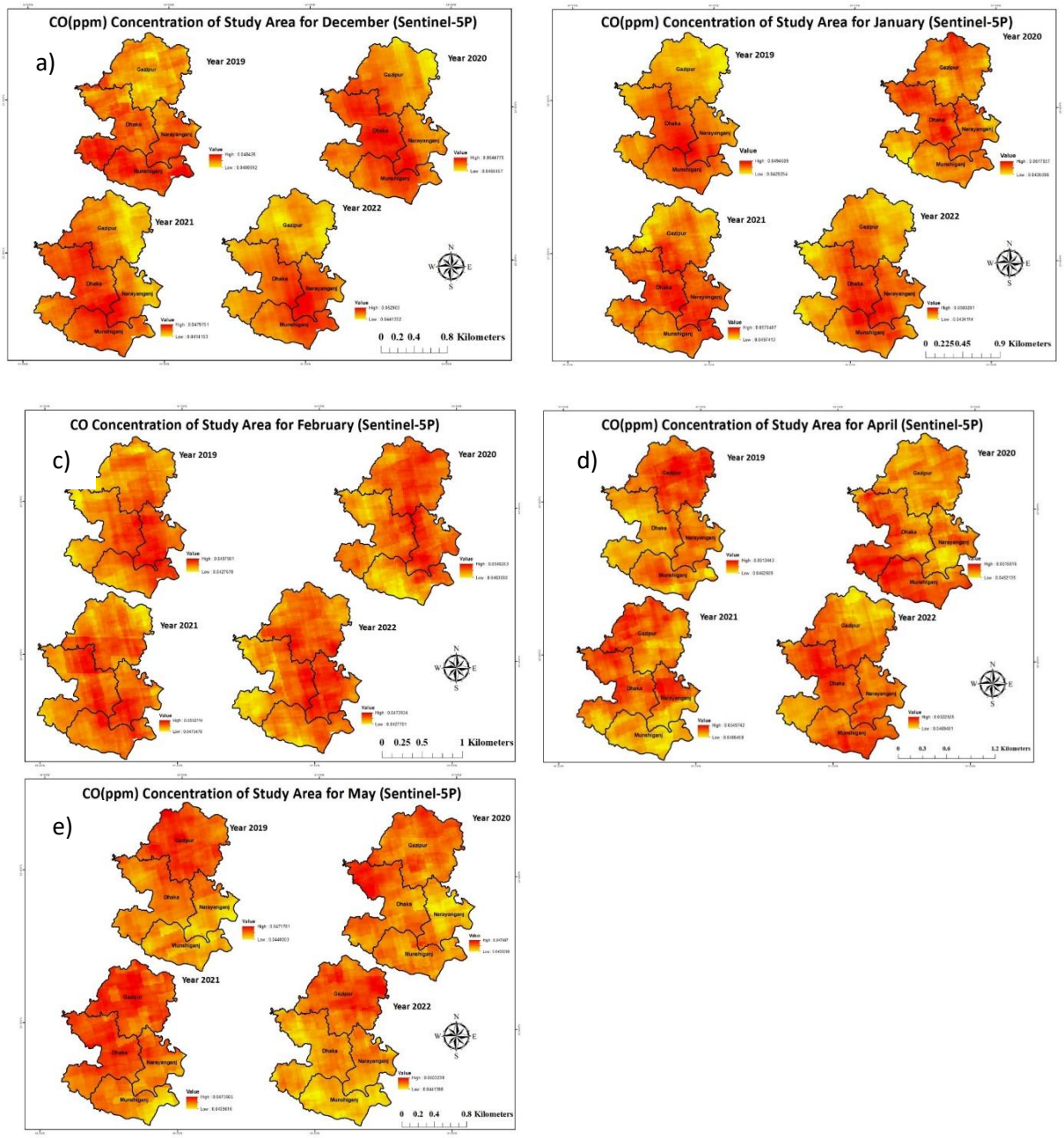

Fig. 10. Seasonal variation of CO from 2019 to 2022, a) December, b) January, c) February, d) April, and e) May

Besides, the CO concentration of the area for 2015 to 2022 has shown in Fig. 11 and the maps are generated according to ground data. Fig. 12 is the analysis of CO Concentration for 8 years of the study area.

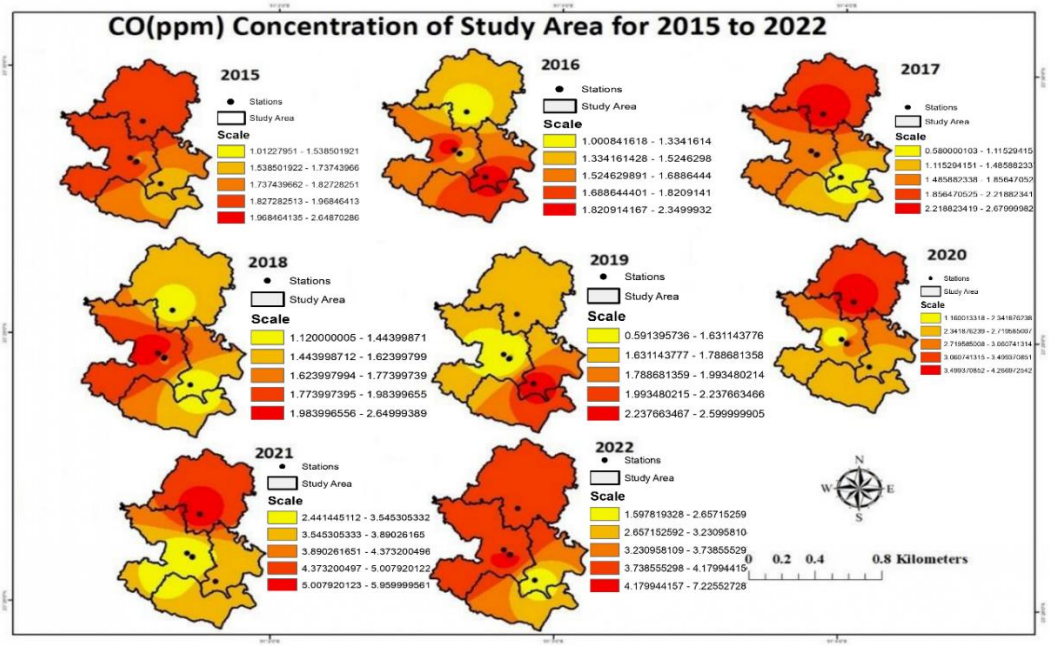

Fig. 11. Concentration of CO from ground data (2015 to 2022)

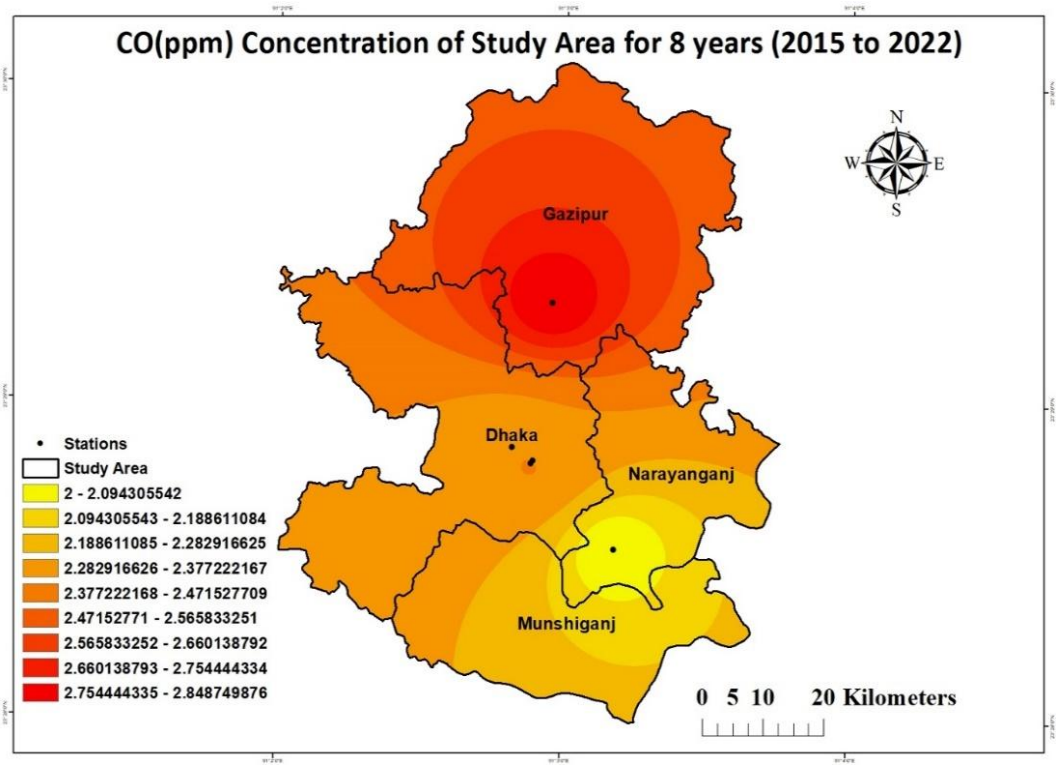

Fig. 12. Concentration of CO from ground data for 8 years

From 2015 to 2022 years $PM_{2.5}$ Concentration has been shown in Fig. 13, where the value is increased day by day. Besides, in Fig. 14, 8 years of $PM_{2.5}$ concentrations has presented.

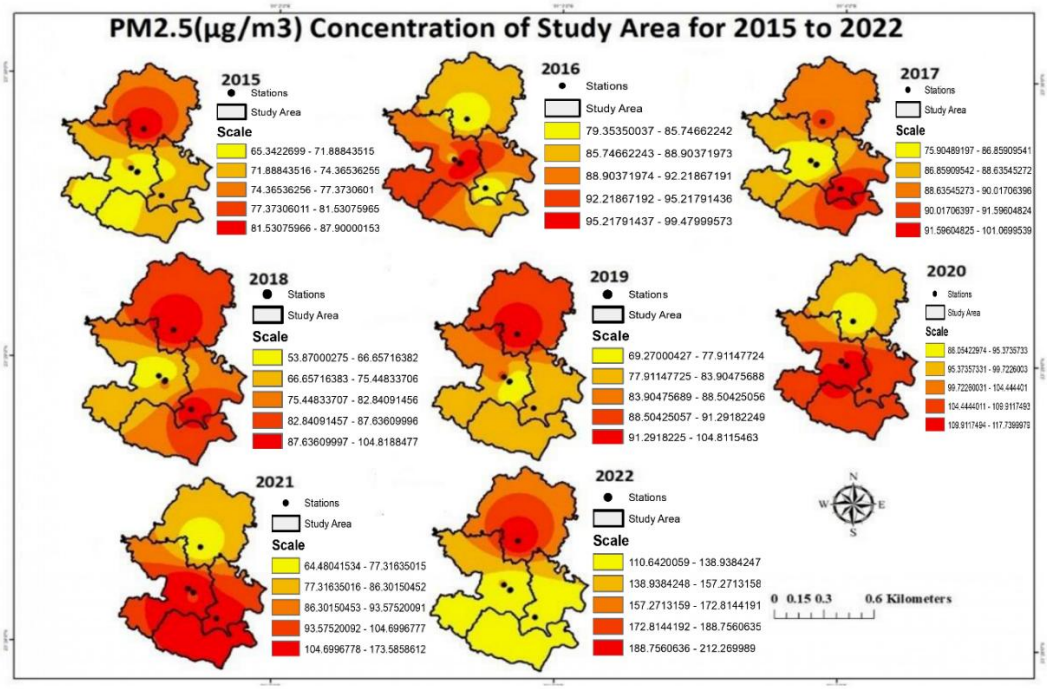

Fig. 13. Concentration of $PM_{2.5}$ from ground data (2015 to 2022)

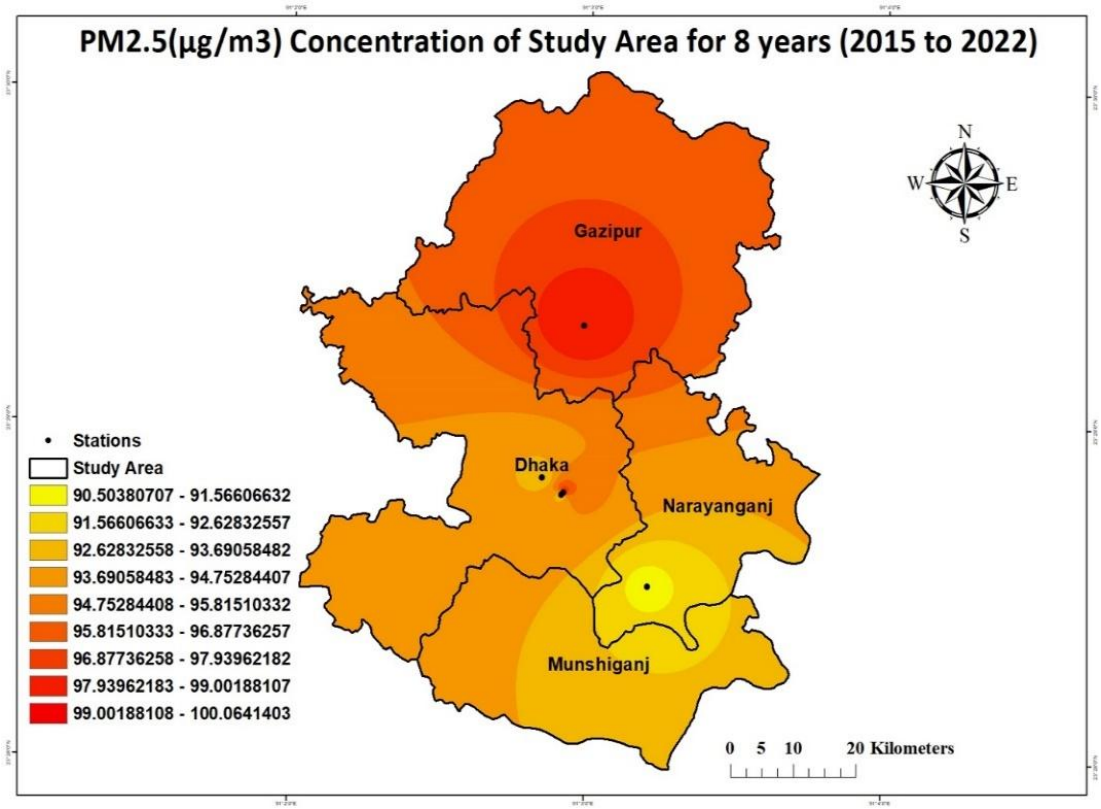

Fig. 14. Concentration of $PM_{2.5}$ from ground data for 8 years

In the Fig. 15, PM_{10} concentration has shown for 2015 to 2022 and in Fig. 16, PM_{10} concentration has presented for 8 years of study area.

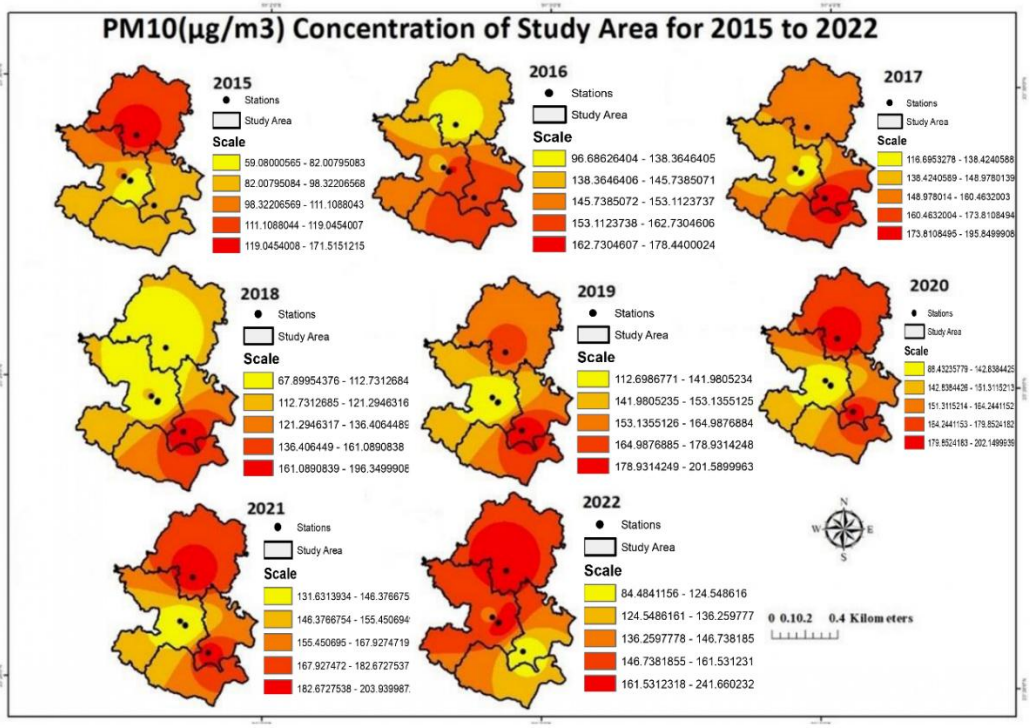

Fig. 15. Concentration of PM_{10} from ground data (2015 to 2022)

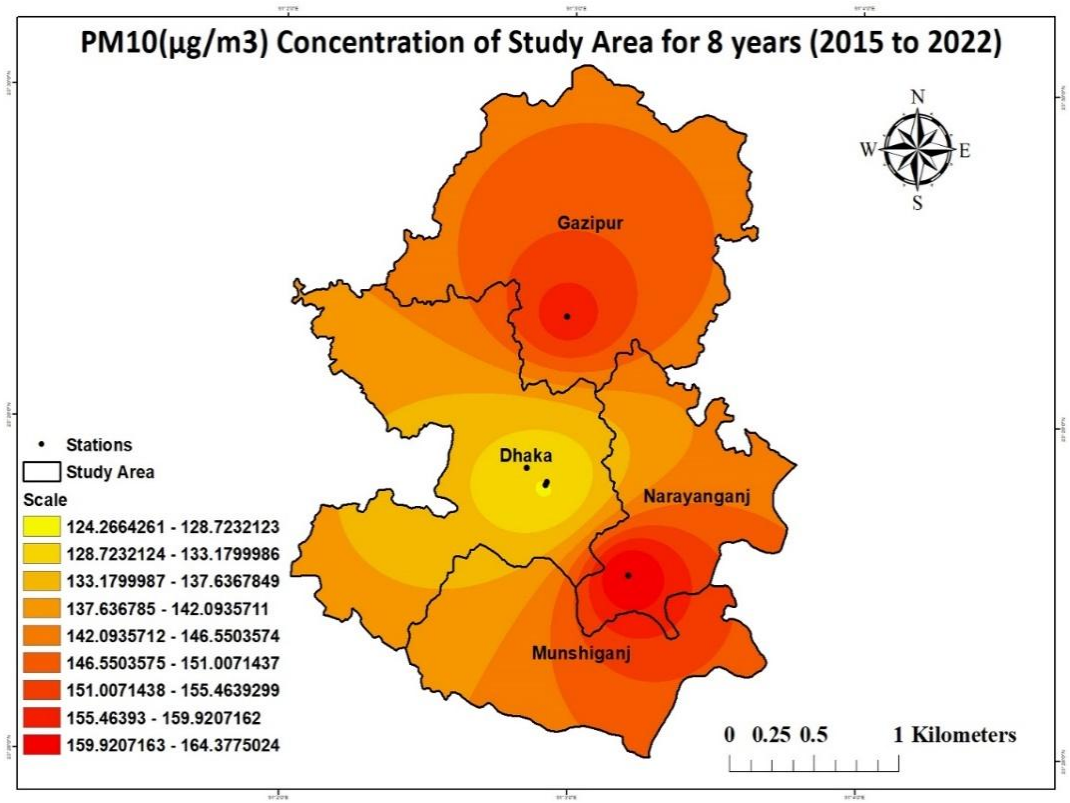

Fig. 16. Concentration of PM_{10} from ground data for 8 years

Conclusions

Overall, the research demonstrates that integrating remote sensing technology with GIS techniques, specifically the kriging interpolation method, can effectively monitor air pollutant concentrations. Satellite-based imagery offers a cost-effective approach to producing air quality maps, particularly at a micro-scale level. The strong correlation between Digital Numbers (DN) and pollutants suggests that the thermal infrared band of Landsat 8 can be used to determine the relationship between satellite measurements and air quality parameters. The findings from this project indicate that satellite remote sensing and GIS methods can be valuable tools for environmental managers and local authorities to continuously monitor urban air quality at a micro-scale level.

Acknowledgements

I would like to show my deep gratitude to the Honorable Chairman of SPARRSO for his continuous support and guidance in this research. I would like to thank the Director General of the Department of Environment for providing air concentration data for this study.

References

Abdullah, S., Ismail, M., & Ahmed, A. N. (2018). Identification of air pollution potential sources through Principal component analysis (PCA). *International Journal of Civil Engineering and Technology, 9(7),* 1435–1442*.*

Bhuyan, Md. D. I., Islam, Md. M., & Bhuiyan, Md. E. K. (2018). A trend analysis of temperature and rainfall to predict climate change for Northwestern region of Bangladesh. *American Journal of Climate Change, 07(02),* 115–134*.* https://doi.org/10.4236/ajcc.2018.72009

Brunekreef, B., & Holgate, S. T. (2002). Air pollution and health. *Lancet,* 360(9341), 1233–1242. https://doi.org/10.1016/S0140-6736(02)11274-8

Gurjar, B. R., Jain, A., Sharma, A., Agarwal, A., Gupta, P., Nagpure, A. S., & Lelieveld, J. (2010). Human health risks in megacities due to air pollution. *Atmospheric Environment, 44(36),* 4606–4613*.* https://doi.org/10.1016/j.atmosenv.2010.08.011

Halim, N. D. A., Latif, M. T., Mohamed, A. F., Maulud, K. N. A., Idrus, S., Azhari, A., Othman, M., & Sofwan, N. M. (2020). Spatial assessment of land use impact on air quality in mega urban regions, Malaysia.

Sustainable Cities and Society, 63 (January), 102436. https://doi.org/10.1016/j.scs.2020.102436

Heald, C. L., & Spracklen, D. V. (2015). Land Use Change Impacts on Air Quality and Climate. *Chemical Reviews,* 115(10), 4476–4496. https://doi.org/10.1021/cr500446g

Hossain, S., Labib, S. M., Bhowmik, A. K., & Khan, S.M. (2016). Stakeholder Debate in Policy Implementation: An Evaluation of Bangladesh Leather Processing Industry Relocation Policy. *Bangladesh e-Journal of Sociology,* 13(1). http://ssrn.com/abstract=2612306https://ssrn.com.

Huang, Y. K., Luvsan, M. E., Gombojav, E., Ochir, C., Bulgan, J., & Chan, C. C. (2013). Land use patterns and SO2 and NO2 pollution in Ulaanbaatar, Mongolia. *Environmental Research,* 124(2), 1–6. https://doi.org/10.1016/j.envres.2013.02.006

Huang, Z., & Du, X. (2018). Urban Land Expansion and Air Pollution: Evidence from China. *Journal of Urban Planning and Development,* 144(4), 05018017. https://doi.org/10.1061/(ASCE)UP.1943-5444.0000476

Irga, P. J., Burchett, M. D., & Torpy, F. R. (2015). Does urban forestry have a quantitative effect on ambient air quality in an urban environment? *Atmospheric Environment,* 120, 173–181. https://doi.org/10.1016/j.atmosenv.2015.08.050

Khaled Ahmad Ali Abdulla Al Koas, A.A.A.A.K (2010). GIS-based Mapping and Statistical Analysis of Air Pollution and Mortality in Brisbane, Australia. School of Built Environment and Engineering Research, Queensland University of Technology, Australia.

Li, S., Wang, H., Hu, H., Wu, Z., Chen, K., & Mao, Z. (2019). Effect of ambient air pollution on premature SGA in Changzhou city, 2013-2016: A retrospective study. *BMC Public Health,* 19(1), 1–10. https://doi.org/10.1186/s12889-019-7055-z

Li, Y., Wang, J., Chen, C., Chen, Y., & Li, J. (2016). Estimating PM2.5 in the Beijing-Tianjin-Hebei region using MODIS AOD products from 2014 to 2015. *International Archives of the Photogrammetry, Remote Sensing and Spatial Information Sciences - ISPRS Archives,* 41, 721–727.

Pereira, M. C., Santos, R. C., & Alvim-Ferraz, M. C. M. (2007). Air quality improvements using European environment policies: A case study of

SO2 in a coastal region in Portugal. *Journal of Toxicology and Environmental Health - Part A: Current Issues,* 70(3–4), 347–351. https://doi.org/10.1080/15287390600884990

Sun, L., Wei, J., Duan, D. H., Guo, Y. M., Yang, D. X., Jia, C., & Mi, X. T. (2016). Impact of Land-Use and Land-Cover Change on urban air quality in representative cities of China. *Journal of Atmospheric and Solar-Terrestrial Physics,* 142, 43–54.

Suzuki, H., Dastur, A., Moffatt, S., Yabuki, N., & Maruyama, H. (2010). *Eco2 Cities: Ecological cities as economic cities.* https://books.google.com.

United Nations Department of Economic and Social Affairs (UNDESA) (2014). World urbanization prospects: *The 2014 revision.* https://www.un.org/en/development/desa/publications/2014-revision-world-urbanization-prospects.html (Accessed on July, 2024)

Wang, S., Zeng, J., Huang, Y., Shi, C., & Zhan, P. (2018). The effects of urbanization on CO2 emissions in the Pearl River Delta: A comprehensive assessment and panel data analysis*. Applied Energy*, 228(June), 1693–1706. https://doi.org/ 10.1016/j.apenergy.2018.06.155

World Health Organization (WHO). (2020). https://www.who.int/health-topics/air-pollution. tab=tab_1

Xu, G., Jiao, L., Zhao, S., Yuan, M., Li, X., Han, Y., Zhang, B., & Dong, T. (2016). Examining the impacts of land use on air quality from a spatio-temporal perspective in Wuhan, China. *Atmosphere, 7(5),* 1–18. https://doi.org/10.3390/atmos7050062

Zahari, M. A. Z., Majid, M. R., Ho, C. S., Kurata, G., Nadhirah, N., & Irina, S. Z. (2016). Relationship between land use composition and PM_{10} concentrations in Iskandar Malaysia. *Clean Technologies and Environmental Policy,* 18(8), 2429–2439. https://doi.org/10.1007/s10098-016-1263-3

Zaman, U.H, Khan T. M., & Islam, J. M. (2010). Urbanization in Bangladesh: Present Status and Policy Implications. *In ASA University Review,* 4 (2).

Zhang, K., & Batterman, S. (2013). Air pollution and health risks due to vehicle traffic. *Science of the Total Environment,* 450–451, 307–316. https://doi.org/10.1016/j.scitotenv.2013.

Flash Flood Monitoring in Tanguar Haor: a Hydro-Meteorological Approach

Mohammad Imrul Islam*, Md. Mahmudur Rahman, Md. Abdur Rahman-Al-Mamun, Md. Ariful Islam, Zebunnesa Khatun

Bangladesh Space Research and Remote Sensing Organization (SPARRSO), Agargaon, Sher-e-Bangla Nagar, Dhaka-1207, Bangladesh.
**Corresponding author E-mail: imrul_islam@sparrso.gov.bd*

Abstract

Flash floods pose a major threat to Tanguar Haor, impacting agriculture, livelihoods, and the ecosystem. This study examines flash flood occurrences and their relationship with precipitation variability over the Meghalaya-Tanguar basin from 2015 to 2023. Using remote sensing datasets (Sentinel-1 SAR, SRTM, CHIRPS, GPM, GSMaP) and ground-based rainfall measurements via Google Earth Engine (GEE), the study analyzes water extent variations and precipitation patterns. Findings reveal that water extent peaks in the pre-monsoon and monsoon seasons, with severe flooding in 2016, 2017, 2019, and 2022. GSMaP data indicates significant rainfall variability, with early monsoon rains triggering flash floods, particularly in the pre-monsoon period. Flash floods have severely impacted Boro rice phenology, disrupting crop growth stages. The 2017 event was particularly devastating despite lower cumulative rainfall, highlighting the role of rainfall distribution. Additionally, sedimentation in rivers and canals worsens flooding by restricting water flow. These insights emphasize the need for targeted interventions to enhance water management. Understanding rainfall-induced flash floods is crucial for developing effective mitigation strategies to protect agriculture, livelihoods, and the ecosystem.

Keywords: Flash flood, Rainfall, Google Earth Engine, Pre-monsoon, Rice Phenology.

Introduction

Disasters, both natural and human-made, are a global issue (Adjei-Darko, 2017). Climate and land-use changes are key drivers of increased weather extremes, disproportionately impacting vulnerable nations (Chowdhury, 2024; Talukdar et al., 2022). Meteorological hazards account for 78% of global financial losses and 38% of disaster-related deaths, with their frequency rising threefold over the past 35 years due to climate change (Hoeppe, 2015). These hazards impact poor populations more severely, particularly in developing countries like Bangladesh, where over one billion people reside in flood-prone areas, a number expected to double by 2050 (UNU, 2018).

Tanguar Haor, one of the largest freshwater wetlands, is particularly vulnerable. Flash floods not only damage agriculture but also disrupt the

ecosystem (Carreno & De Marta, 2019). Such floods are influenced by precipitation, topography, and soil characteristics (Dey et al., 2021). Human activities such as deforestation, unplanned infrastructure, and the effects of climate change have intensified these floods in recent years (Dey et al., 2021).

Understanding the causes of flash floods and the interplay between land use and hydro-meteorological patterns is essential for mitigation. Remote sensing (RS) technology, which monitors earth dynamics at various scales, is a powerful tool for disaster management (Uddin et al., 2019). Several studies have used RS to assess flood impacts on agriculture, particularly Boro rice, in Bangladesh (Ahmed et al., 2017; Uddin et al., 2019). Socio-economic factors, riverbed siltation, and infrastructure also affect rice production in these areas (Akter et al., 2023).

The study aims to monitor flash floods in Tanguar Haor. Specific objectives are to a) identify flash flood events using Sentinel-1 SAR data from 2015 to 2023, b) analyze the hydro-meteorological patterns in the Meghalaya-Tanguar Haor watershed from 2015 to 2023, and c) examine the link between flash floods, hydro-meteorological patterns, and agricultural impacts.

Materials and methods

Study Area

Tanguar Haor is one of the biggest palustrine wetland ecosystems in Bangladesh. This haor is located in the North-East part of Bangladesh sharing a border of about 17 km with Nongstoin (Meghalaya), India in its north. Administratively, one third of Tanguar Haor lies in the Tahirpur Upazilla and the remainder in Dharmapasha Upazilla, both within the Sunamganj District of the Sylhet Division (Fig. 1). Tanguar Haor, covering an area of 11,700 hectares consists of 120 beels, is part of a wetland/floodplain complex of the Surma-Kushiyara river basin. These two rivers are among the main tributaries of the Meghna river and also connected with Dhanu, Baulai and Jadukata river through the extended floodplain of Tanguar Haor. The haor is located at an altitude of only 2.5–5.5 m above mean sea level. The landscape topography of Tanguar Haor is uneven. Because of its bowl shape nature, it acts like a natural reservoir. About 50% of the area of Tanguar Haor is water bodies, followed by 31% crop land.

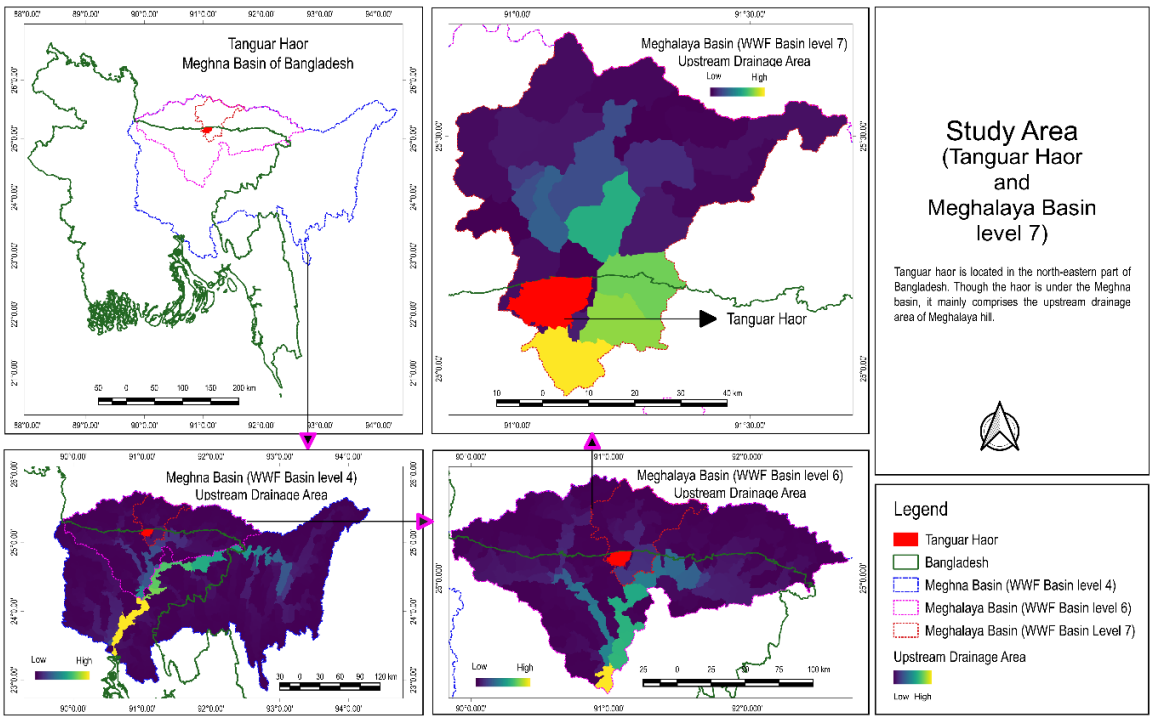

Fig. 1. Study area.

Research Materials

- Shuttle Radar Topography Mission (SRTM)
- Sentinel-1 SAR
- Raingauge Rainfall
- Climate Hazards Group InfraRed Precipitation with Station data (CHIRPS)
- Global Precipitation Measurement (GPM)
- Global Satellite Mapping of Precipitation (GSMaP)

Methodology

The present research integrates remote sensing (RS)–geographic information system (GIS) technology with ground observations to comprehensively monitor the flash floods in Tanguar Haor, providing valuable insights for flood management and agricultural planning.

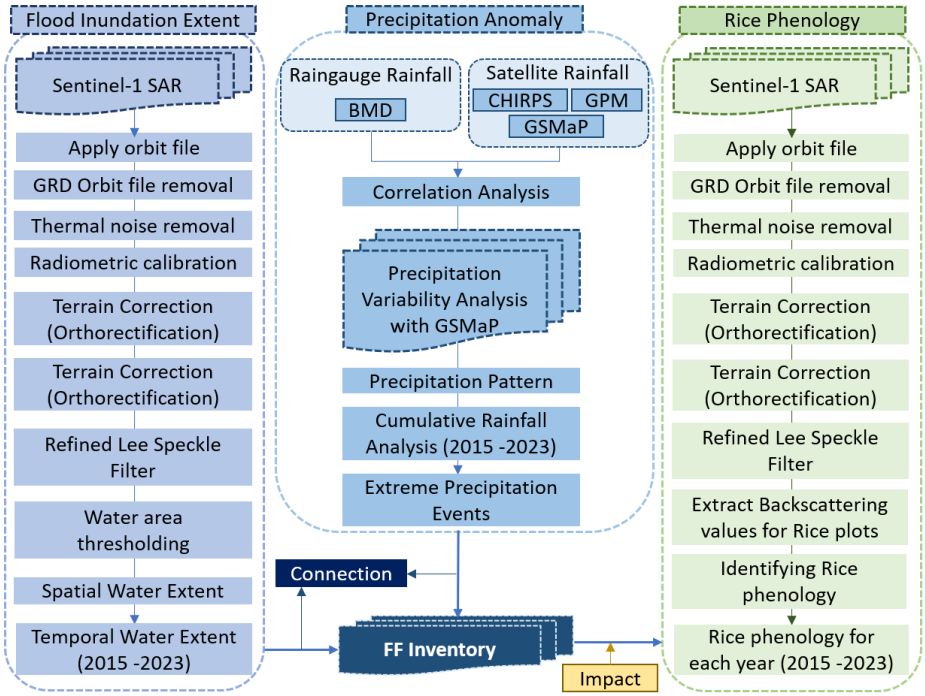

Fig. 2. Methodological flowchart.

The study focuses on identifying the events of flash floods in Tanguar Haor using Synthetic Aperture Radar (SAR) data. Flash flood events identification comprises the utilization of multitemporal Sentinel-1 satellite data of European Space Agency (ESA). To identify the hydro-meteorological pattern in Meghalaya-Tanguar Haor basin, this study deploys satellite-based rainfall verified with raingauge rainfall data. Sentinel-1 satellite data are also utilized to study the phenology of Boro rice in Tanguar Haor. The connection between flood inundation extent, precipitation anomalies, and rice phenology is analyzed to understand the impact of rainfall on flash floods and agricultural practices in Tanguar Haor.

The study focuses on identifying the events of flash floods in Tanguar Haor using Synthetic Aperture Radar (SAR) data. Flash flood events identification comprises the utilization of multitemporal Sentinel-1 satellite data of European Space Agency (ESA). To identify the hydro-meteorological pattern in Meghalaya-Tanguar Haor basin, this study deploys satellite-based rainfall verified with raingauge rainfall data. Sentinel-1 satellite data are also utilized to study the phenology of Boro rice in Tanguar Haor. The connection between flood inundation extent, precipitation anomalies, and rice phenology is analyzed to understand the impact of rainfall on flash floods and agricultural practices in Tanguar

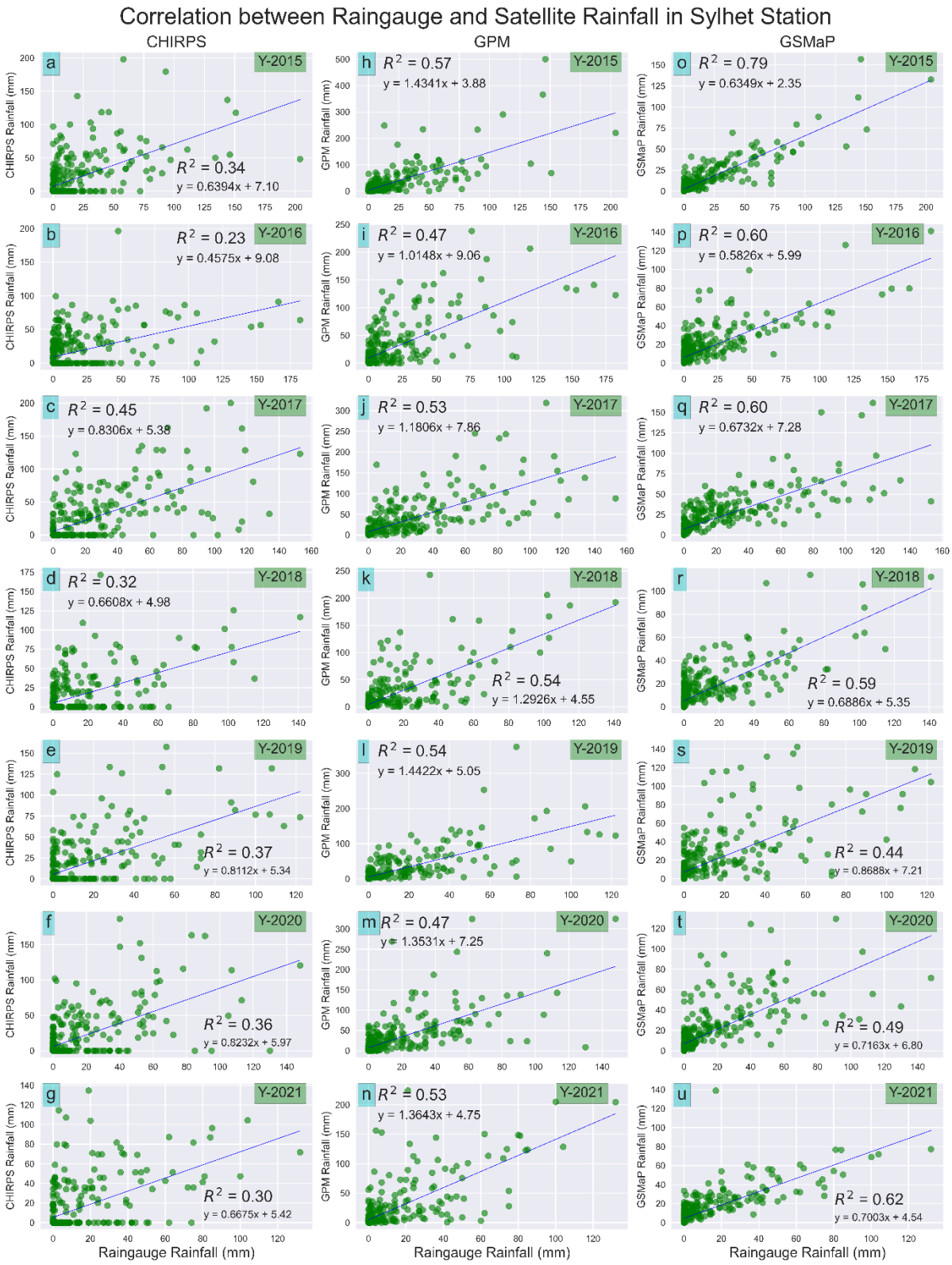

Fig. 3: Temporal rainfall of rain gauge in Sylhet station and satellite data in 2022.

Above figure shows the correlation between raingauge measurements and three different satellite rainfall datasets (CHIRPS, GPM, and GSMaP) at the Sylhet station, analyzed annually from 2015 to 2021 (Fig. 3).

Results and discussion

Identifying flash floods in Tanguar Haor involves detecting rapid and intense flooding events in the area. This involves analyzing the variation of water extent in response to heavy precipitation events throughout the year, particularly during the pre-monsoon and monsoon season. To determine variations in water extent, the present study analyzes Sentinel-1 SAR image collections from 2015 to 2023 exploiting Google Earth Engine (GEE) cloud computing platform. The graph demonstrates the variations in water extent in Tanguar Haor, highlighting differences and trends over the years (Fig. 4). The water extent tends to increase rapidly during pre-monsoon and reaches a peak during monsoon season. After peaking, the water extent usually declines gradually towards the end of the year.

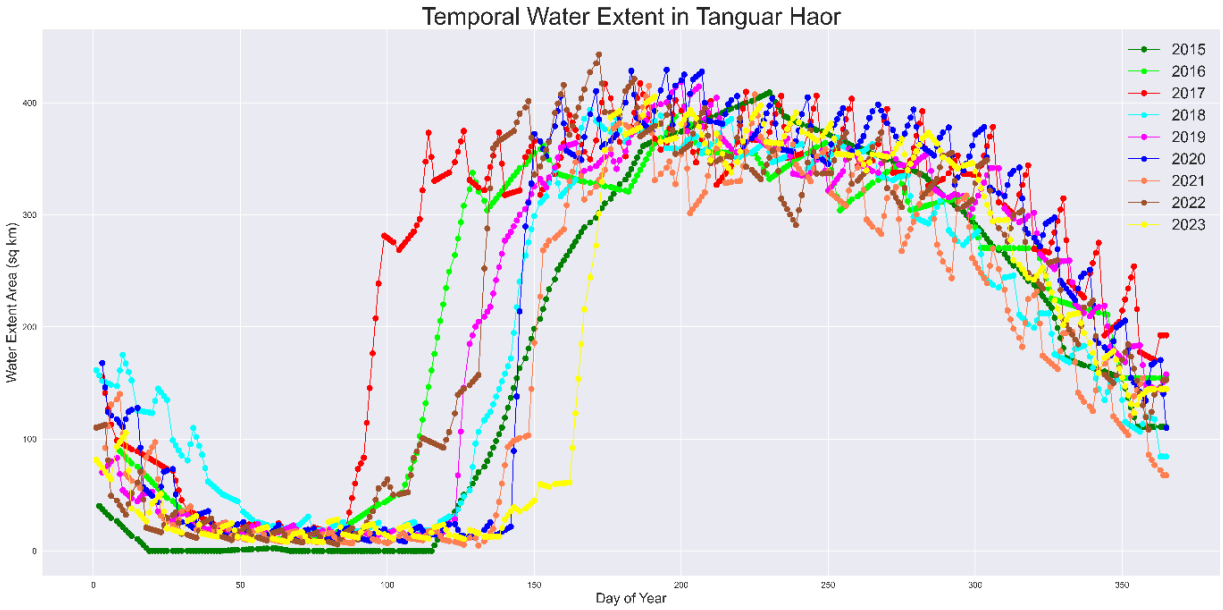

Fig. 4. Variation of water extent in each year from 2015 to 2023 in Tanguar Haor.

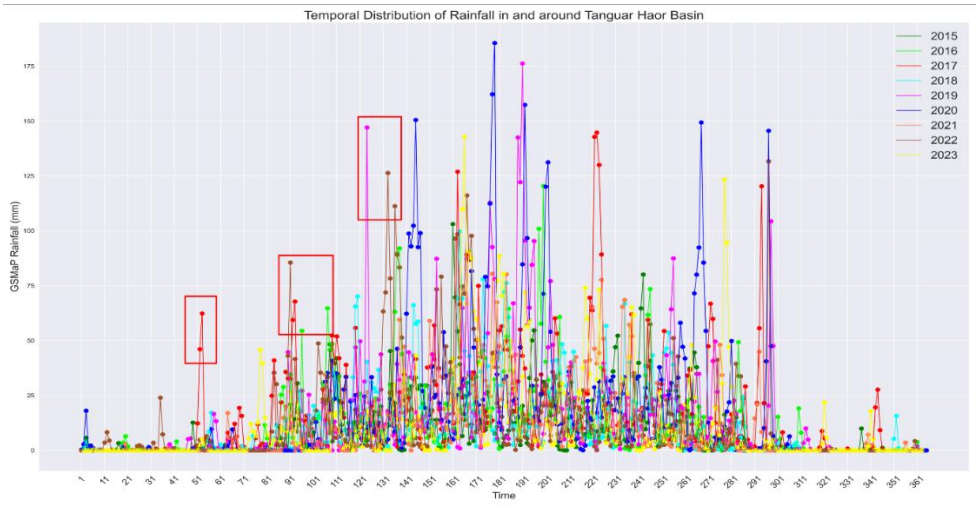

Fig. 5. Temporal variability of daily rainfall in the Meghalaya-Tanguar basin from 2015 to 2023.

The Fig. 5 shows the temporal distribution of rainfall in the Meghalaya-Tanguar basin over several years (2015-2023). There is a clear seasonality in the rainfall pattern, with the majority of rainfall occurring during the monsoon season (middle of the year), causing inundation in the haor basin every year. Rainfall tapers off towards the post-monsoon season (October to December), returning to lower values.

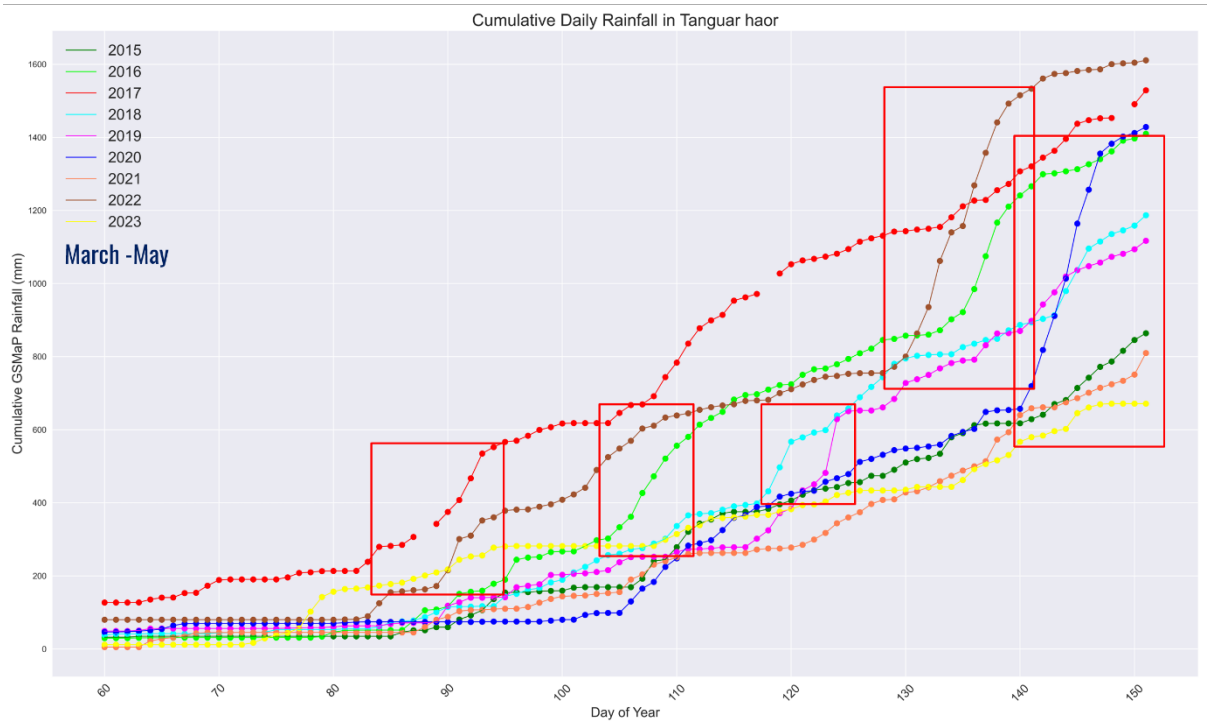

Fig. 6. Cumulative daily rainfall of GSMaP in the Meghalaya-Tanguar basin during pre-monsoon.

Fig. 6 focuses on the seasonal variability and irregular patterns of pre-monsoon rainfall. Notably, there are some unusual increases of cumulative rainfall in 2016, 2017, 2019, and 2020. In 2017, the red line indicates sudden rises in cumulative rainfall shortly after day 90 and day 107, which are unusual and harmful, as the boro rice in the haor basin is still in its growth stages. In 2022, there are two notable increases in cumulative rainfall just after day 100 and day 128. Similarly, in 2020, the blue line shows a sharp rise from day 140. Additionally, there are two increases in cumulative rainfall between days 115 and 125 for the years 2018 and 2019.

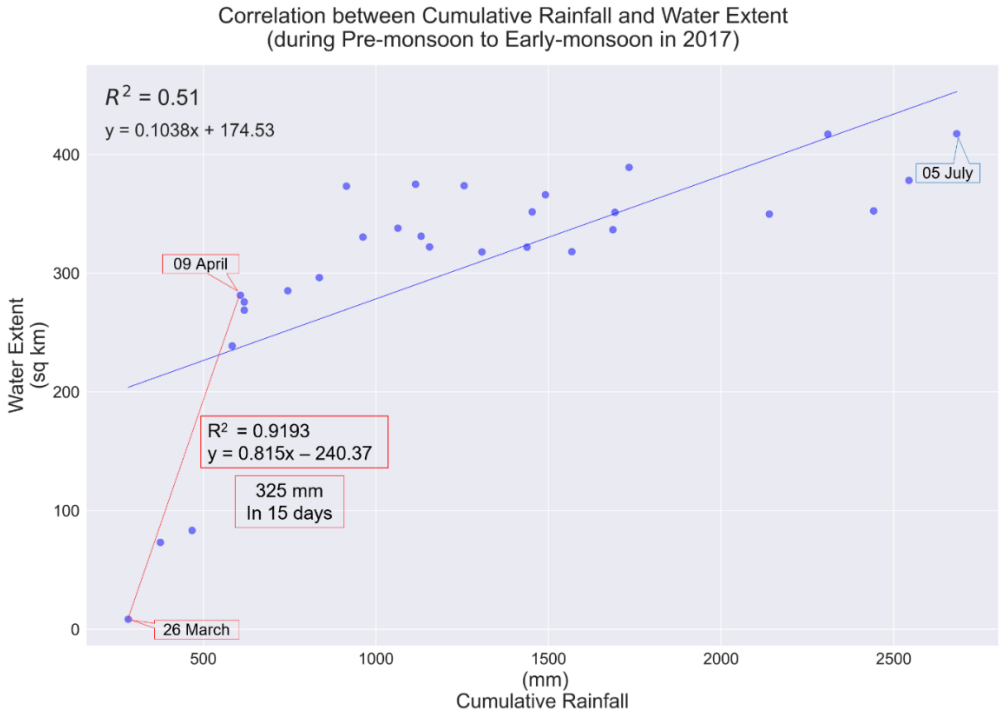

Fig. 7. Correlation between cumulative rainfall and water extent in Tanguar Haor during the pre-monsoon to early-monsoon season of 2017.

The scatter plot illustrates the relationship between cumulative rainfall and water extent in Tanguar Haor during the pre-monsoon to early-monsoon season of 2017, showing both the overall trend and specific period of rapid change (Fig. 7). The general trend shows that as cumulative rainfall increases, the water extent also increases. The highlighted period from March 26 to April 9 shows a particularly strong correlation between rainfall and water extent, where the cumulative rainfall increased by 325 mm in 15 days, resulting in a rapid rise in water extent.

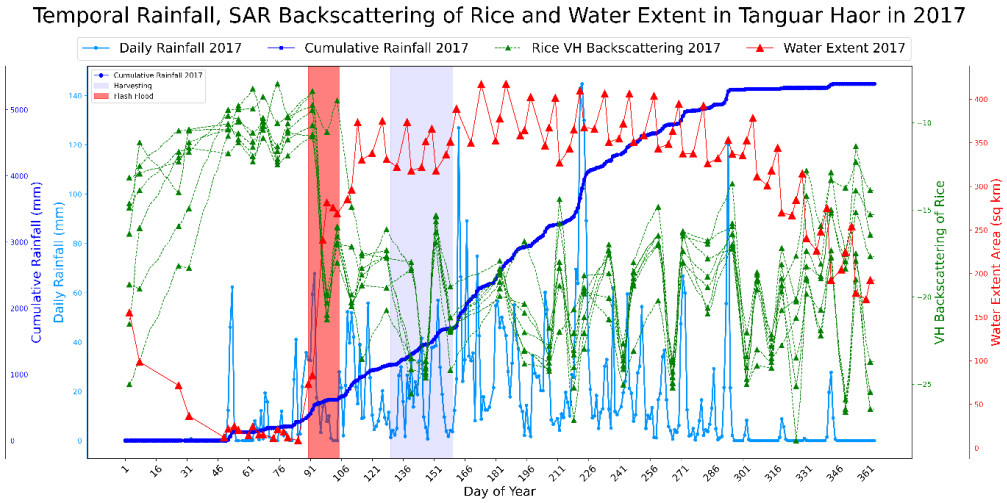

Fig. 8. Temporal rainfall, SAR backscattering of rice and water extent in Tanguar Haor in 2017.

Daily rainfall shows peaks and troughs, with significant rainfall events contributing to the cumulative total. The graph highlights specific periods where rainfall peaks coincide with increases in water extent, indicating flood events. The light blue shaded areas denote the boro rice harvesting periods, while the red shaded areas likely represent significant flash flood events, marked by sudden spikes in daily rainfall and rises in cumulative rainfall and water extent. In the red shaded areas, the VH backscattering values of boro rice sharply decreased, reflecting the impact of flash floods on rice growth stages, which were expected to decline during the harvesting period shown in the light blue shaded areas (Fig. 8).

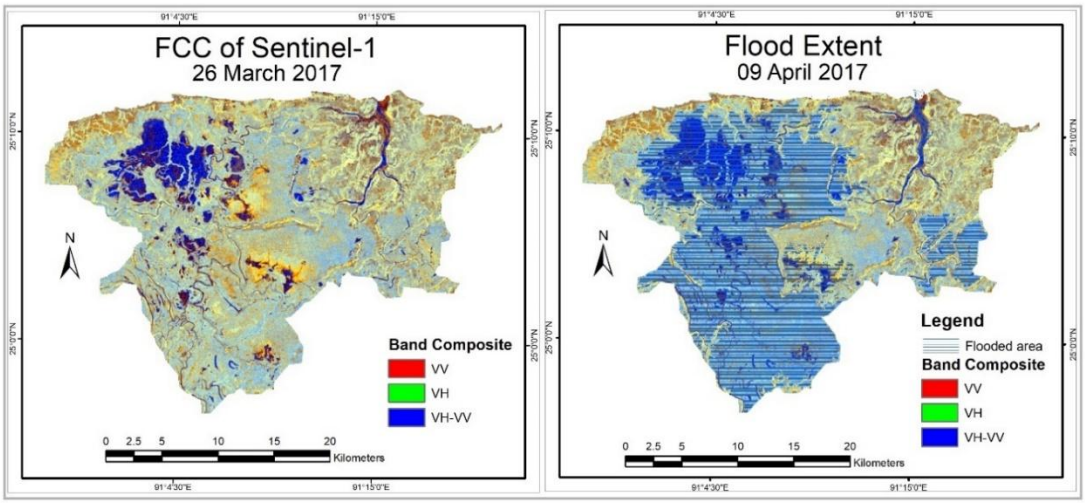

Fig. 9. Flash flooding over the Tanguar basin dominated with boro cultivation in 2017.

In 2017, farmers experienced a dangerous flash flood during late March to early May. The flood extent map shows comparatively lower flooded area on 09 April 2017 (Fig. 9) but it was the most harmful flash flood in recent years since the Boro rice didn't reach its ripening / harvesting phase.

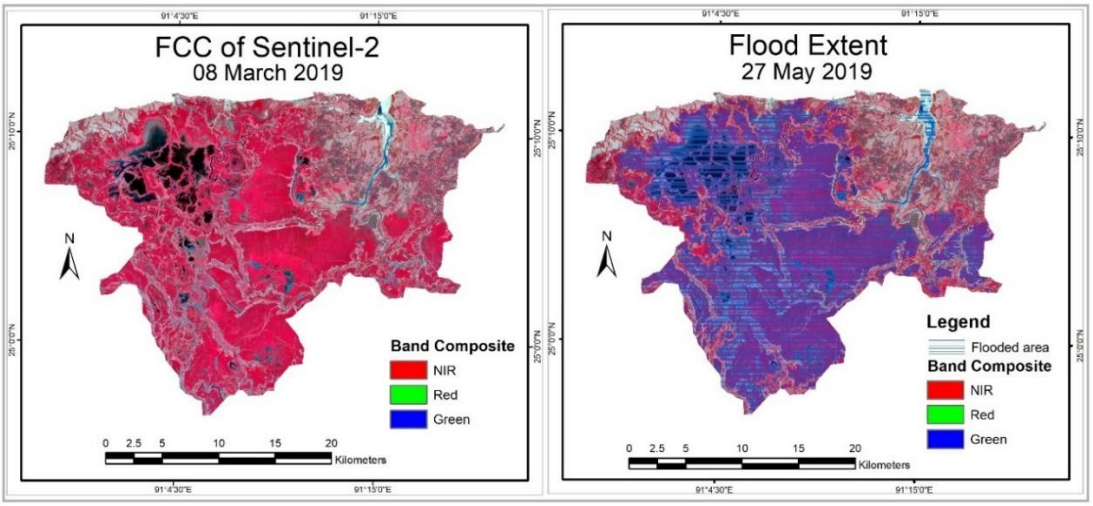

Fig. 10. Flash flooding over the Tanguar basin dominated with boro cultivation in 2019.

This FFC (False Color Composite) image from Sentinel-2, taken on March 8, 2019, shows a dominant bright red color, which represents boro rice with high biomass (Fig. 10). Red likely represents vegetation, as healthy vegetation reflects near-infrared light which is displayed in red in a false-color image. This Boro rice used to be harvested at the end of May.

This study sheds light on the intricate spatiotemporal dynamics of flash floods in Tanguar Haor, and their strong correlation with precipitation variability from 2015 to 2023. The analysis of this study reveals that water extent in Tanguar Haor experiences rapid increases during the pre-monsoon season, peaks in the monsoon, and declines towards the year's end utilizing Sentinel-1 SAR imagery in the Google Earth Engine (GEE) platform. The exceptional rainfall patterns detected by the Global Satellite Mapping of Precipitation (GSMaP) data, particularly over the Meghalaya-Tanguar basin, underscore the erratic nature of rainfall distributions, with early monsoon rains in some years triggering flash floods. Notably, early pre-monsoon peaks in water extent induced by erratic rainfall over Meghalaya-Tanguar basin, observed in years like 2016, 2017, 2019, and 2022, resulted in severe agricultural damage. For instance, in 2017, a rapid rise in water extent was linked to a 325 mm increase in cumulative rainfall within 15 days which particularly destroys the Boro cultivation.

Conclusions

In conclusion, this study sheds light on the intricate spatiotemporal dynamics of flash floods in Tanguar Haor, and their strong correlation with precipitation variability from 2015 to 2023. The analysis of this study reveals that water extent in Tanguar Haor experiences rapid increases during the pre-monsoon season, peaks in the monsoon, and declines towards the year's end utilizing Sentinel-1 SAR imagery in Google Earth Engine (GEE) platform. The exceptional rainfall patterns detected by the Global Satellite Mapping of Precipitation (GSMaP) data, particularly over the Meghalaya-Tanguar basin, underscore the erratic nature of rainfall distributions, with early monsoon rains in some years triggering flash floods. Notably, early pre-monsoon peaks in water extent induced by erratic rainfall over Meghalaya-Tanguar basin, observed in years like 2016, 2017, 2019, and 2022, resulted in severe agricultural damage. For instance, in 2017, a rapid rise in water extent was linked to a 325 mm increase in cumulative rainfall within 15 days, which particularly destroys Boro cultivation.

Acknowledgements

This research is supported by the Bangladesh Space Research and Remote Sensing Organization (SPARRSO).

References

Adjei-Darko, P. (2017). Remote sensing and geographic information systems for flood risk mapping and near real-time flooding extent assessment in the greater Accra metropolitan area. KTH Royal Institute of Technology, School of Architecture and the Built Environment, Stockholm, Sweden.

Ahmed, M. R., Rahaman, K. R., Kok, A., & Hassan, Q. K. (2017). Remote sensing-based quantification of the impact of flash flooding on the rice production: A case study over Northeastern Bangladesh. *Sensors*, 17(10), 2347. https://doi.org/10.3390/s17102347

Akter, N., Islam, M. R., Karim, M. A., Miah, M. G., & Rahman, M. M. (2023). Spatiotemporal rainfall variability and its relationship to flash flood risk in Northeastern Sylhet Haor of Bangladesh. *Journal of Water and Climate Change*, 14(11), 3985-3999. https://doi.org/10.2166/wcc.2023.165

Carreño Conde, F., & De Mata Muñoz, M. (2019). Flood monitoring based on the study of Sentinel-1 SAR images: The Ebro River case study.

Water, 11(12), 2454. https://doi.org/10.3390/w11122454

Chowdhury, M. S. (2024). Flash flood susceptibility mapping of north-east depression of Bangladesh 2 using different GIS based bivariate statistical models. *Watershed Ecology and the Environment*, 6, 26-40. https://doi.org/10.1016/j.wsee.2023.12.002

Dey, N. C., Parvez, M., & Islam, M. R. (2021). A study on the impact of the 2017 early monsoon flash flood: potential measures to safeguard livelihoods from extreme climate events in the haor area of Bangladesh. *International Journal of Disaster Risk Reduction*, 59, 102247. http://dx.doi.org/10.1016/j.ijdrr.2021.102247

Hoeppe, P. (2015). Trends in weather related disasters – Consequences for insurers and society. *Weather Clim. Extrem.* 11, 70–79, https://doi.org/10.1016/j.wace.2015.10.002.

Talukdar, S., Ghose, B., Shahfahad, Salam, R., Mahato, S., Pham, Q. B., & Avand, M. (2020). Flood susceptibility modeling in Teesta River basin, Bangladesh using novel ensembles of bagging algorithms. *Stochastic Environmental Research and Risk Assessment*, 34, 2277-2300. https://doi.org/10.1007/s00477-020-01862-5

Uddin, K., Matin, M. A., & Meyer, F. J. (2019). Operational flood mapping using multi-temporal Sentinel-1 SAR images: A case study from Bangladesh. *Remote Sensing*, 11(13), 1581. https://doi.org/10.3390/rs11131581

UNU, (2018). UNU Update: Two billion face flood danger soon. accessed 7.12.22. http://archive.unu.edu/update/archive/issue32_2.htm.

Bankline Shifting and Sand Bar Dynamics of the Teesta River Using Multi-Temporal Satellite Images

S M Ahsan Habib*, Md. Sazedur Rahman, Md. Jahidul Ashik, Md. Nur Hossain Sharifee

Bangladesh Space Research and Remote Sensing Organization (SPARRSO), Agargaon, Sher-e-Bangla Nagar, Dhaka-1207, Bangladesh.
**Corresponding author E-mail: ahsan@sparrso.gov.bd*

Abstract

Teesta is one of the strongest rivers that has caused floods almost every year during the rainy season in the northern part of Bangladesh in recent decades. This mighty river deals with low flow during the dry season, which might be due to combined natural and man-made causes. This river is well known to make people homeless and damage crops by the flooding and eroding nature of the river bank. Thus, the present study aims to reveal the changing pattern of the river bank and the sandbars and find out the dynamic and stable part of the river bank. Landsat MSS and TM data for the period of 1996 to 2023 with a four-year interval have been analyzed to meet the purpose. The analysis divulged that the Teesta River is highly dynamic with bank line erosion and sandbar deposition. The present study found that erosion is dominating the accretion for the bank line, making the river wider, whereas accretion is dominating the erosion for sandbars, making the river more braided. Erosion in the left bank is much greater than the deposition, whereas deposition in the right bank is greater than the erosion. The present study also found that the river area and the sandbar area were modulated by the maximum discharge from May to October of the year. The present study has identified steadfast evidence on the dynamically eroding nature of Teesta River depicting an urge to the policymakers for taking appropriate initiatives on river bank management to reduce the suffering of the riverine people and attain sustainable development as well.

Keywords: Teesta River, Deposition, Erosion, Sandbars, Bankline shifting, LANDSAT.

Introduction

Bangladesh is the second biggest deltaic floodplain in the world. It was primarily created by massive sediment deposition from the Ganges-Padma, Brahmaputra-Jamuna, and Meghna River systems and other numerous tributaries and distributaries. There is a complex network of 907 rivers in the country, including 57 transboundary rivers (NRCC, 2023). Through these transboundary rivers, Bangladesh receives the majority of its water supplies from upstream nations. One of the main transboundary rivers, the Teesta flows through the five districts (Rangpur, Lalmonirhat, Nilphamari, Kurigram, and Gaibandha) of Bangladesh (Fig. 1). It is the

largest freshwater resource in the northern region. The Bangladesh Water Development Board (BWDB) built Teesta Barrage between 1979 and 1998 to supply water for agriculture during the dry season and enable supplemental irrigation during the monsoon season. Since then, agricultural productivity in the northern region of Bangladesh has increased. India also built a barrage at "Gagoldoba," a few kilometers upstream of the Bangladesh border, to meet the demand for agricultural water during the dry season. For the last few decades, Teesta experienced extremely low flow during the dry season and unusual erosion-deposition events in several areas of its stream.

Teesta and its floodplain inundates almost every year during the rainy season and severely damage the properties of the riverine people. The river's ability to meet the demands of aquaculture and irrigation is compromised by this variation in peak and lowest flow, which also presents a serious risk to river management (Tarannum et al., 2018). The most significant and unpredictable disaster is riverbank erosion, which considers factors such as soil structure, rainfall quantity, river morphology, terrain of the river and surrounding areas, and flood effects. Teesta is not an exception to the alluvial river's difficulties with sediment erosion and deposition, which make the Brahmaputra basin's issues with flooding, erosion, and drainage congestion particularly serious (Sarkar et al., 2012). The short- and long-term channel adjustment, meander and sandbar development, sediment dynamics of the river catchment, riparian land loss, and downstream sedimentation issues are all significantly impacted by riverbank erosion (Lawler et al., 1997). Due to alluvial origins, rivers' floodplains are primarily made of sediments carried by floods, as the majority of the materials on their banks are cohesive sediments with fine grains (Azuma et al., 2007). Whereas development works such as bank protection measures like embankment, dams, and bridge may also cause local morphological changes of the river, affecting the ultimate sediment balance of the river. Thus, fluvial channel form and its dynamics over the period have been a major interest of study in fluvial geomorphology (Nabi et al., 2016). Therefore, for efficient planning and management of the alluvial settings, a greater understanding of the morphological changes of alluvial rivers, notably bank shifting, channel migration owing to erosion and accretion processes, sandbar dynamics as well as approaches to detect resulting patterns, would be helpful.

Upholding the remote sensing technique in the study of river morphology, temporal satellite remote sensing data of a river with unstable banks can be studied in Geographic Information System (GIS) for

identification of river bank erosion as well as sandbar dynamics (Pal et al., 2017). Several studies have been done on the river bank migration using remote sensing satellite data since the availability of such dataset (Bhakal et al., 2005; Takagi et al., 2007; Baki & Gan, 2012). Teesta is one of the major tributaries of the Brahmaputra River which is now in the scientific attraction due to the impacts of climate change and human intervention on its flow. Several studies have been carried out on the planform pattern and spatio-temporal changes of the channel morphology of the Teesta River (Afrose, 2012; Ghosh, 2014; Akhter et al., 2019). Besides, there is a study (Das et al., 2022) which studied the climate change impact on the water availability in the Teesta River for different climate change scenarios. Despite this research it is still important to reveal a clear picture of the bank line and sand bar shifting pattern with a short-term interval for a long time to support an adequate erosion management plan, which reduces loss of property and assets. So, the present study attempts to investigate bank line shifting and sand bar dynamics for the last few decades, taking a short interval of time. The present study also identifies the erosion-prone areas of the Teesta River, which could support current bank protection measures and contribute to development projects.

Materials and methods

Study Area

The fourth main river system in Bangladesh and the most energetic river, Teesta, is situated in the northern part of Bangladesh (Fig. 1). It is also regarded as Bangladesh's lifeline in the north. Roughly 14 percent of Bangladesh's total cultivated area is covered by rivers, which provide livelihood opportunities for 7.3 percent of the country's population and over 21 million people who are directly or indirectly dependent on them (BBS, 2016).

Table 1: Physical descriptions of river Teesta as per Rivers of Bangladesh (BWDB, 2011)

Features	Description
Length	129 km (in Bangladesh)
Width	0.7km (minimum), 5.5km (maximum), 3km (average)
Bank Level (upstream to downstream)	Left: 57.10m to 18.37m Right: 56.18m to 19.00m
Bed Level (upstream to downstream)	54.00 m to 16.74m

It passes through the five districts that make up the Rangpur Division in Bangladesh: Gaibandha, Kurigram, Lalmonirhat, Nilphamari, and Rangpur districts (BBS, 2016). The Teesta and a few other small and medium-sized rivers comprise the region's floodplain. Every year during the flood season, this river dumps sediments that make the plain fertile and conducive to cultivation (Mandal & Chakrabarty, 2016). The total Teesta River is about 414 km long and originates in the Pauhunri Mountain in the eastern Himalayas, till it meets the Brahmaputra River in Bangladesh and flows through. For our study purpose, the selected reach is about 112km long part in Bangladesh that starts from Khoga Khoribari, Dimla Upazila, Nilphamari District, and ends at Haripur Ghat, Sundarganj Upazila, Gaibandha District. For precise analysis, the total area is divided into 4 parts (Fig. 1) according to the bend.

Data

In order to do the analysis, Landsat satellite pictures of the Teesta are collected from 1996 to 2023 for November to December, when the cloud coverage is low, having dry season. Hydrological (monthly maximum and minimum discharge and water level) data were collected from BWDB of Dalia and Kaunia point (Fig. 1). Landsat satellite images have been used for the generation of bank line and sand bar data due to their long and available records which cover the study period.

Table 2: Landsat satellite images used in the present study

Year	Version	Bands	Acquired Date	Acquired time (GMT)
1996	Landsat-5		11/30/1996	3:51:42
1999	Landsat-5	Band 1-Blue, Band 2-	12/25/1999	4:05:17
2003	Landsat-5	Green, Band 3- Red and	11/18/2003	4:08:32
2007	Landsat-7	Band 4-Near-Infrared	11/05/2007	4:20:13
2011	Landsat-5		11/08/2011	4:17:52
2015	Landsat-8	Band 2 – Blue, Band 3 –	11/19/2015	4:30:20
2019	Landsat-8	Green, Band 4 - Red,	11/14/2019	4:30:33
2023	Landsat-8	Band 5- Near-Infrared	11/09/2023	4:30:20

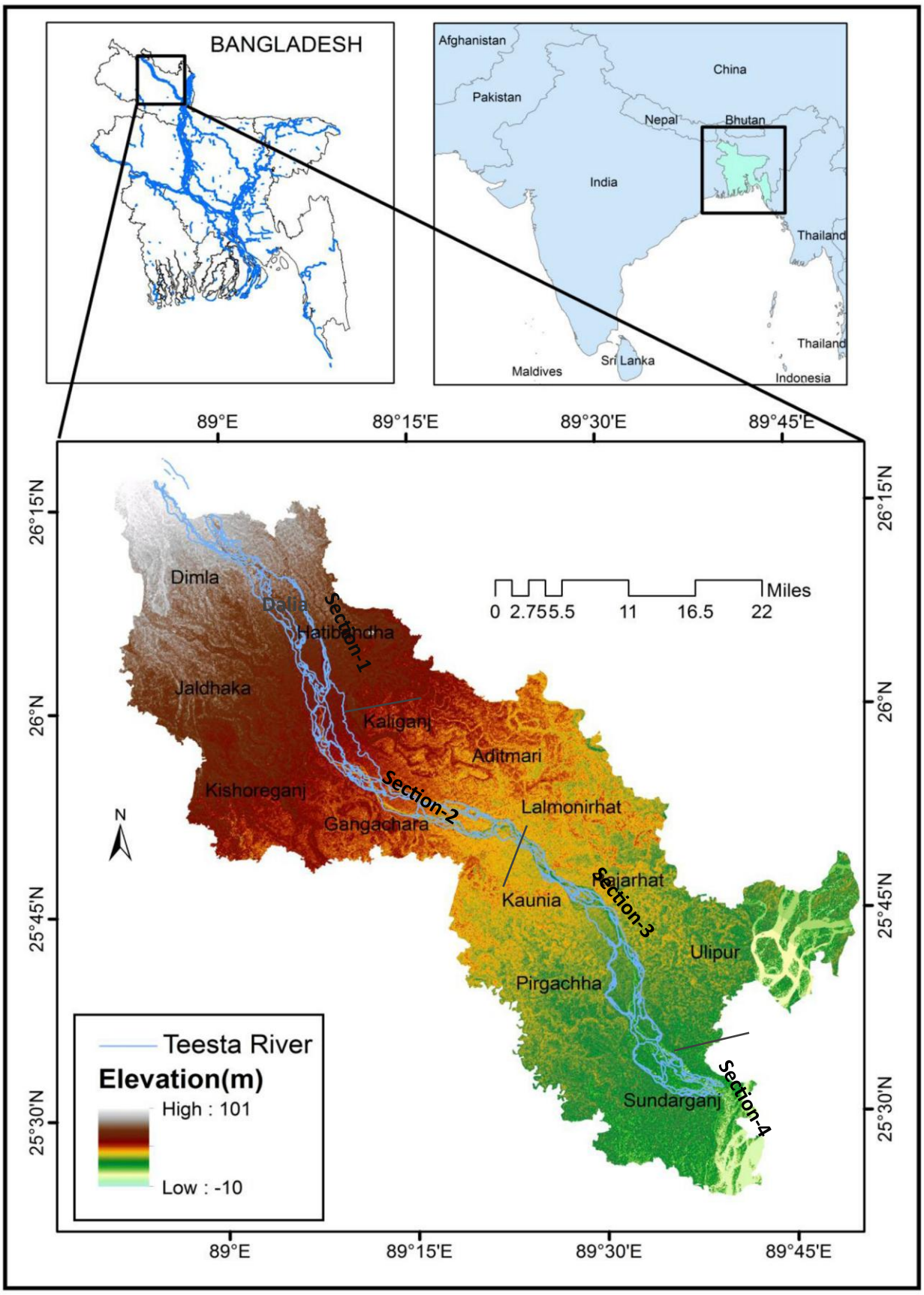

Fig. 1. Map of the study area.

Methodology

Raster Data Processing

Landsat images were geo-referenced from 1996 to 2023 to investigate riverbank and sandbar dynamics along the Teesta River. ArcGIS (v10.8.2) software was used for image processing and data generation. The study area, spanning from Khoga Khoribari, Dimla Upazila, to Haripur Ghat, Sundarganj Upazila, was divided into four strips based on meandering bends, with cross-sections drawn to track morphological changes. Unsupervised classification techniques identified three land cover classes: water, sand, and cultivated/vegetated land. Digitized maps of riverbanks, sandbars, and land use changes were created and projected to ensure accuracy in area calculations. The analysis quantified morphological changes for number of years (1996, 1999, 2003, 2006, 2011, 2015, and 2023), providing insights into the spatial and temporal dynamics of the river (Planning, 2002). All the processes were in the following flowchart.

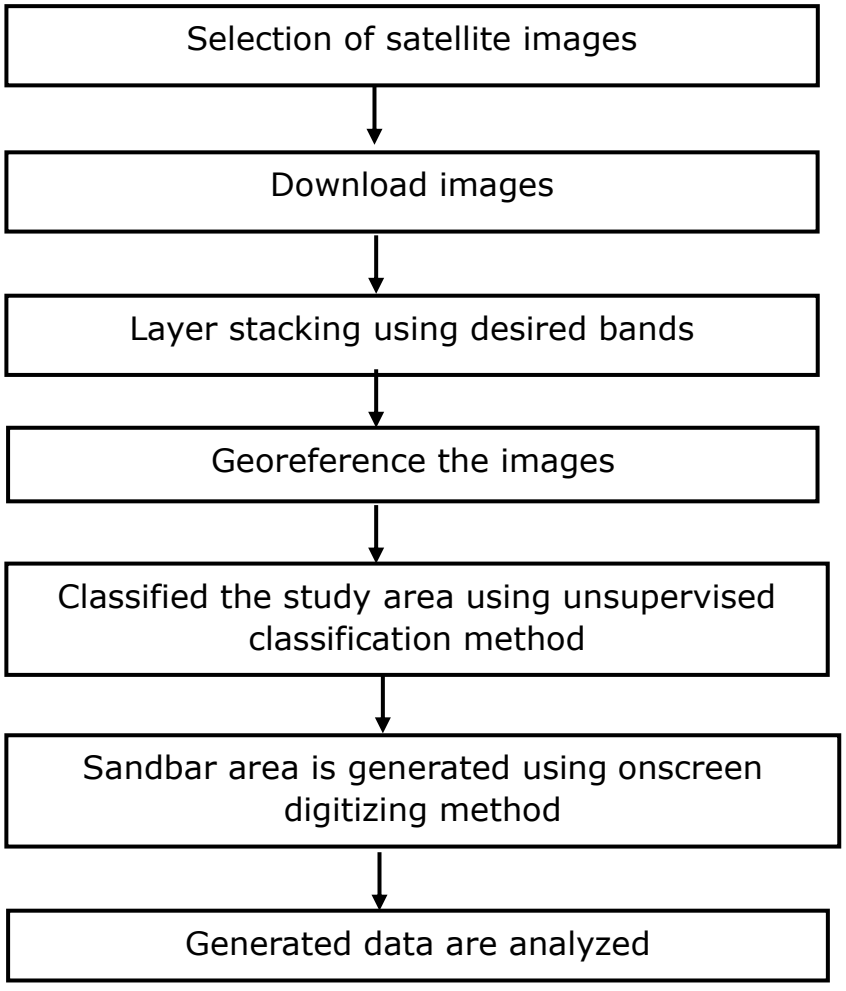

Fig. 2. Workflow of raster data processing

Erosional and depositional data extraction and analysis

Erosion and deposition area has been estimated from the projected maps through area estimation using GIS software tools for polygon areas with the shifting bank-lines and sandbars in study period. In that case union tool was used to identify the erosion and deposition in GIS platform for maps of two adjacent years. Thus, the eroded and deposited area calculated according to the field id.

Shifting rates of the bank line and sandbars along the river section are calculated during a period from the following Eq. (1).

$$r = \frac{A_1 - A_2}{Y} \quad \text{.....(1)}$$

Here r (km^2/year) is the erosional shifting rate, A_1 (km^2) represents the total deposition between two adjacent years, A_2 (km^2) represents the total erosion between two adjacent years. Hence $A_1 - A_2$ represents the net deposition for positive value and erosion for negative value. Y (years) is the interval between two adjacent years.

Relation between extracted hydraulic and hydrologic data

To get the fundamental of the analysis and relevancy of management of water resources the correlation between the hydraulic and hydrologic data was calculated of the collected and extracted data for the whole study periods using Eq. (2). Hydrologic data provided essential inputs for hydraulic models, allowed accurate predictions of water movement through natural channel (Malcolm et al., 2012).

$$r = Correl(X, Y) = \frac{\sum(x-\bar{x})(y-\bar{y})}{\sqrt{\sum(x-\bar{x})^2 \sum(y-\bar{y})^2}} \quad \text{.....(2)}$$

Here r is the correlation value, x is the hydraulic data (erosion and deposition) for different analysis and $\bar{x}$ is the average of x. Here, y is the hydrologic data (water level and discharge of Dalia and Kaunia point) for different analysis.

Results

Analysis of the deposition and erosion of Teesta River

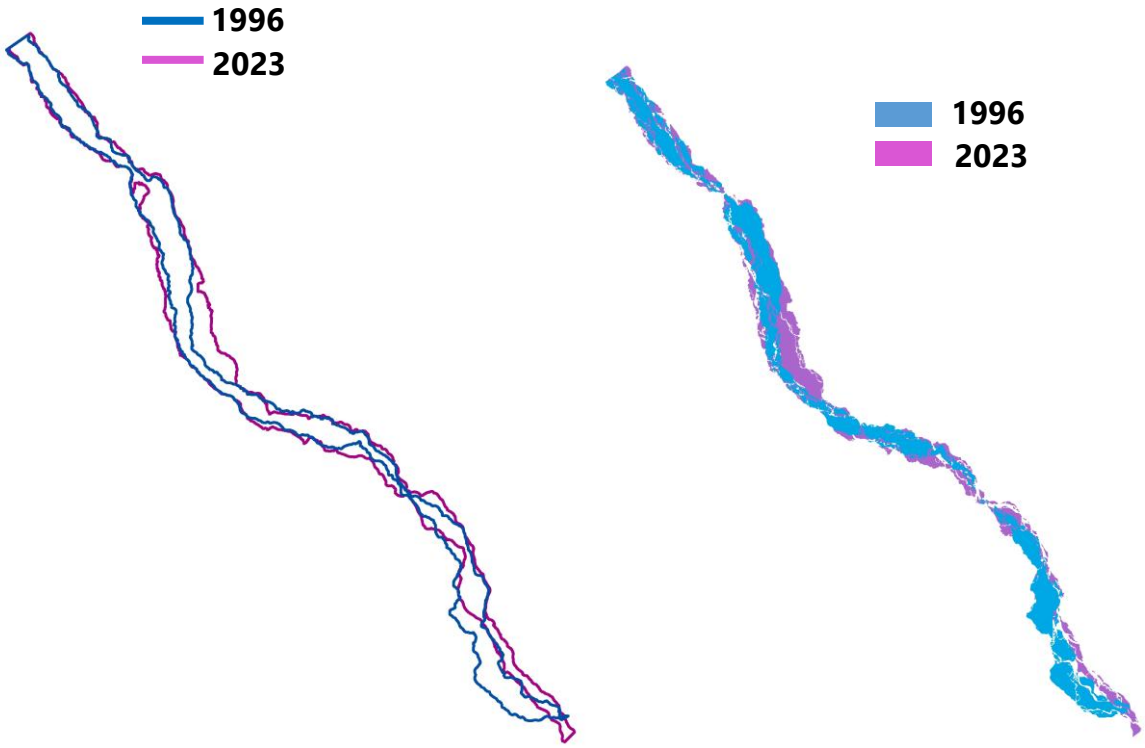

Fig. 3: Bank line (Left) and sand bars (Right) of the Teesta River since 1996 to 2023.

Bank line and sand bar area was generated from the Landsat satellite images shown in Fig. 3. Deposition and erosion of the Teesta River was calculated using equation 1. Here, permanent sand bar was defined based on the signature of the vegetation cover and settlement, and temporary sand bar are identified on the basis of the signature of bare land within the river area. During the study period, it has been found that deposition is large in the temporary sand bar and erosion is dominant in the permanent sand bar (Fig. 4, left). Erosion is also dominant in the bank line of the Teesta River. Erosion and deposition of sediments is large in temporary sand bars compared to erosion and deposition in the permanent sand bars. Variation in the deposition and erosion of the temporary sand bar area regulates the all sand bar area of the Teesta river in inter-annual timescale (Fig. 4, right). It is also found that the temporary sand bar area ultimately modulates the Teesta River area (Fig. 4, right).

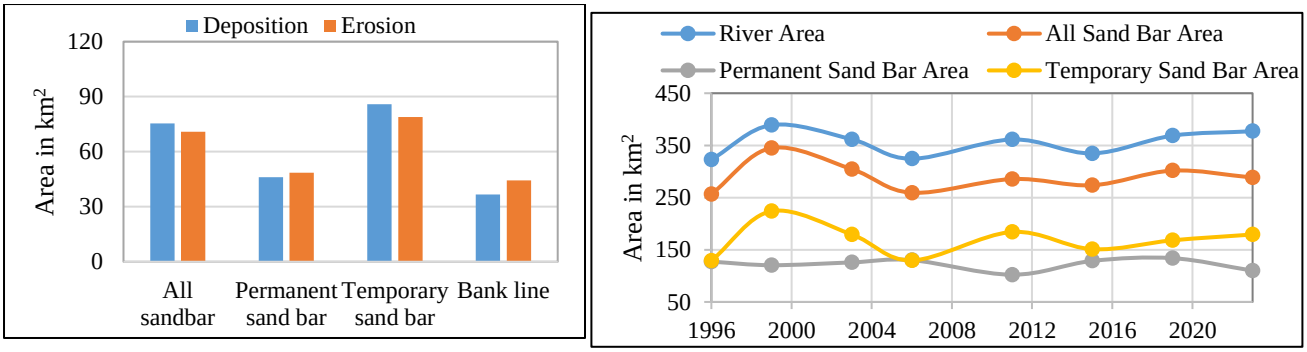

Fig. 4: Left, deposition and erosion statistics of the Teesta River during since 1996 to 2023. Right, Inter-annual variation of river area and sand bars during the study period.

Analysis of the sandbar dynamics

An island is any kind of landmass within a river that sits above water. Sand or other sediments can be built in a portion of the river by currents when the river level is high. During the dry season, these can be exposed above the surface. A branching in any river system occurs when a river is divided by islands (Schumm, 1985). The Teesta River is under the influence of small and large islands. The following figures represent the change of island area from 1996 to 2023. It is seen that the net island area is increasing for the study period and it is 1.67 km^2/year for all sandbars and 3.64 km^2/year for temporary sandbars of gross area, the maximum net erosional rate was -16.53 km^2/year for 2003-2006 and the net depositional rate was 31.71 km^2/year for 1996-1999 of the gross area of temporary sandbars and it was -15.06km^2/year for 2003-2006 and 29.36 km^2 for 1996-1999 of all sandbars (Fig. 5). From sectional analysis for all sandbars maximum net deposition was 8.98 km^2/year in section 2 for 1999-2003 and maximum erosion was -16.4km^2/year in section 4 of 1999-2003 for temporary sandbars was 11.47 km^2/year for in section-4 of 1996-1999 and -8.26 km^2/year in section-4 of 1999-2003. The following figures show that net erosional and depositional value and rate are highly dynamic for the 1996-1999 interval that was a major cause of Teesta barrage construction. The project was planned to be completed in two phases. The construction of the barrage started in 1979 and that of the irrigation canals in 1984 and was completed in 1997-98. Phase one was completed in 1998. Although the chart area at the river downstream has increased more than the upstream the change is lower than expected because of their quick transition as the new mainland. It's also evident that the trending curve is downward i.e. erosion is greater but still deposit is dominating the erosion that is happening as the deposition was huge during the construction of Teesta

Barrage on sandbars. Fig. 5 (bottom-right) represents the change in the permanent island area from 1996 to 2023. It is seen that the net island area is decreasing for the study period, and it is -0.47 km^2/year for the permanent sandbar of gross area. From the sectional analysis, the net maximum erosional rate was -8.15km^2/year for 1999-2003 of section 4 and the net depositional rate was 8.64 km^2/year for 1999-2003 of section 2, on the other hand, the gross area of permanent sandbars net maximum erosion was -6.05 km^2/year in 2019-2023 and net maximum deposition was 6.60 km^2/year of 2011-2015 for permanent sandbars.

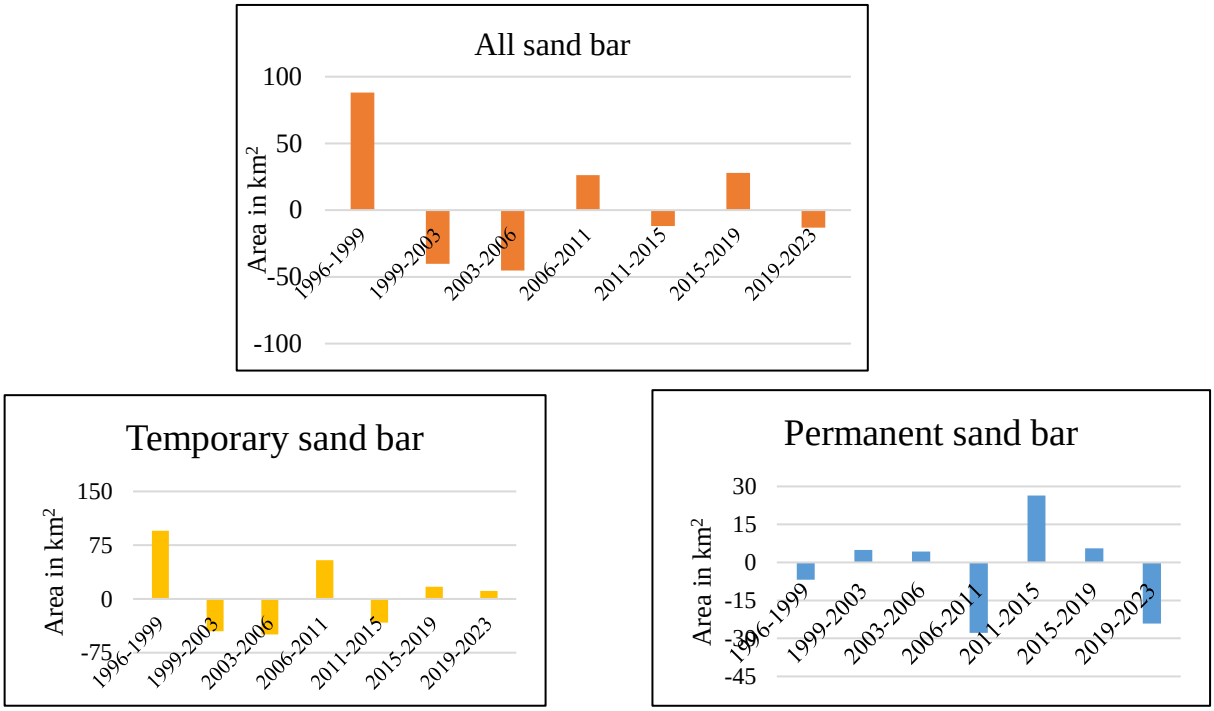

Fig. 5. Changes in all sandbar (top), temporary sandbar (bottom-left) and permanent sandbar (bottom-right).

Section wise changes of riverbank and sandbars during the study period

A higher standard deviation in bank line erosion and deposition values indicates a more dynamic river system. This reflects greater variability in erosion and deposition rates due to fluctuating flow conditions, seasonal changes, and human activities, leading to significant temporal and spatial changes in the river's morphology (USGS, 2024). From Fig. 6 it is evident that section 4 is highly dynamic and secondly, section 2 has a higher standard deviation value in section 4 than section 2. The lowest standard deviation value is for section 3. The present study identified locations affected by bank erosion accretion and bank line shifting and indicated the urgent need to protect the riverbanks by employing afforestation measures

and other strategies. Therefore, it is necessary to incorporate geomorphic changes in formulating flood management.

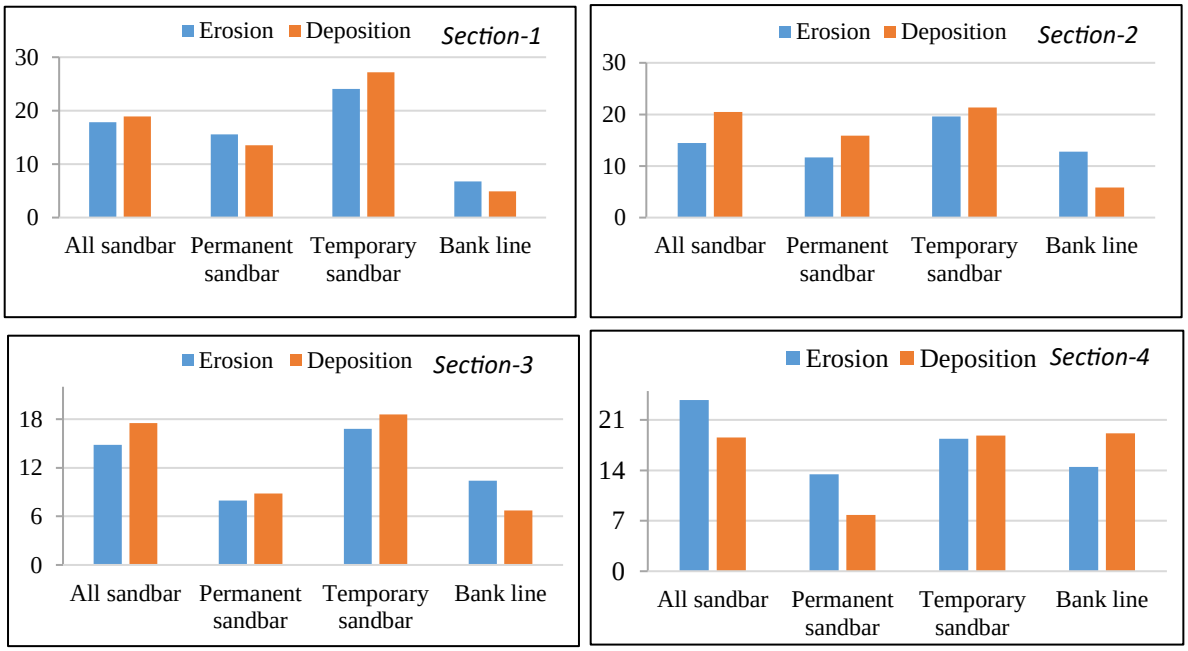

Fig. 6. Deposition and erosion statistics of four different sections of Teesta River.

Analysis of Bank Line Shifting of Teesta River

To get an overall picture of the erosion and accretion patterns of the bank line of Teesta River over seven time periods, 1996-1999, 1996-1999, 1999-2003, 2003-2006, 2006-2011, 2011-2015, 2015-2019 and 2019-2023, the maps of riverbank erosion and accretion are overlapped in Arc GIS. Next, the rates of bank movement as a function of the area along the river for both the left and the right banks for periods are plotted in the following figure. These figures show a considerable movement of the bank lines resulting from accretion indicating riverward movement of banks as well as erosion which depicts the landward movement of the banks for the periods. For the analysis between 1996 and 2023, bank line shifting rates varied from less than one km^2 per year to several km^2 per year. From 1996 to 2023 maximum net accretion and erosion rates in the left bank were 10.49 km^2/y in 2003-2006 and -11.25 km^2/y in 1996-1999 respectively, while the corresponding rates for the right bank were 17.39 km^2/y in 1999-2003 and -11.27 km^2/y in 1996-1999 respectively for the whole study area. On the whole, the left bank of the Teesta River has experienced more erosion rather than the right bank highlighting the existence of bank protection measures on the right bank. For the sectional analysis from 1996 to 2023, bank line shifting rates for maximum net erosion was -10.35 km^2/y in 1999-

2003 for section-2 and maximum net deposition was 5.34 km^2/y in 2003-2006 for section-2 for the left bank and for the right bank, it was -3.69 km^2/y in 1996-1999 for section-3 and 15.88 km^2/y in 1999-2003 for section-4 for Teesta River. From the overall analysis net left bank erosion is -2.60 km^2/year and right bank deposit is 1.02 km^2/year i.e. erosion is dominating the deposit by -1.58 km^2/y and the river area is increasing between two bank lines.

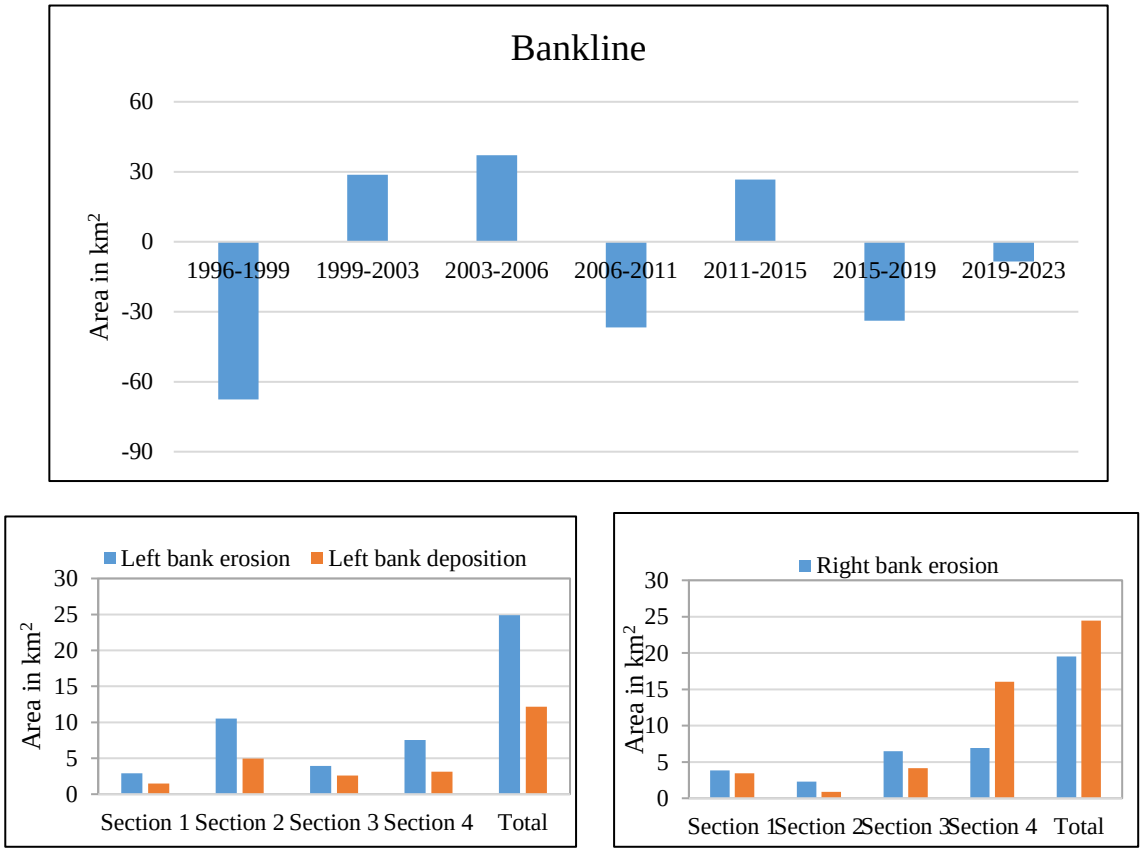

Fig. 7: Changes in the bank line for whole Teesta River (*top*), left bank (bottom-left), and right bank (bottom-right) of the Teesta River.

Relation between hydraulic and hydrologic data of the study area

Higher discharge levels increase the velocity and erosive power of a river. When the discharge is high, the river can carry more sediment and exert a greater force on its banks, leading to increased bank line erosion. Water level fluctuations can directly impact bank stability. High water levels can saturate bank soil, reducing its cohesion and making it more susceptible to erosion. Conversely, rapidly falling water levels can create a pressure difference between the bank and the river, further destabilizing the bank and accelerating erosion. The combination of high water levels and high discharge during flood events can cause severe banking erosion. The increased hydraulic pressure and flow velocity can lead to significant soil

loss and bank retreat (Darby & Simon, 1999; NWS, 2024). Fig. 8 represents the inter-annual changes of average monthly discharge during May to October for each year and Teesta River area. It is found that the maximum water discharge well correlated to the river area (r=0.52). Similarly, maximum water discharge well correlated to all sand bar area (r=0.53) (Fig. 9). Then, it can be said that maximum water discharge modulates the river area and all sand bar area of Teesta River. The correlation value between the Teesta River area and all sand bar area is 0.88, which indicates that erosion of the bank line increases the deposition in the sand bars and vice versa.

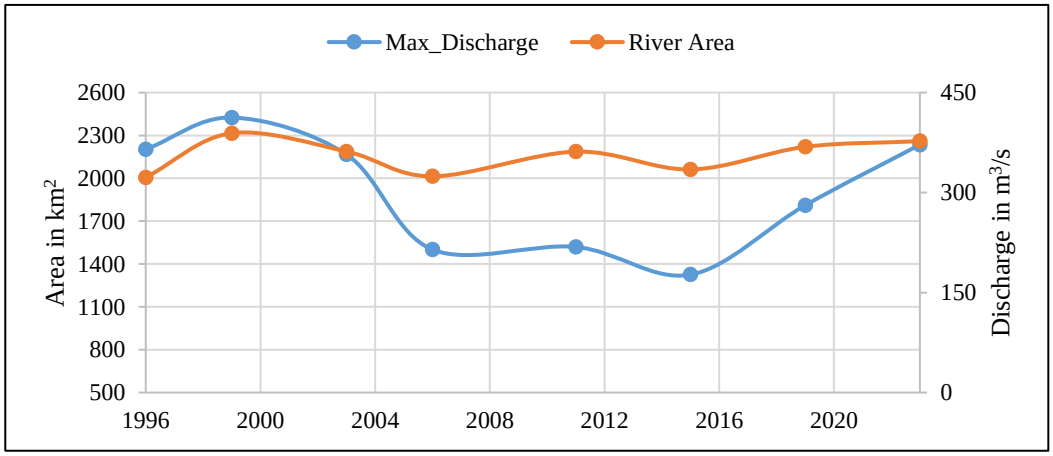

Fig. 8: Relation between discharge and river area between 1996 and 2023.

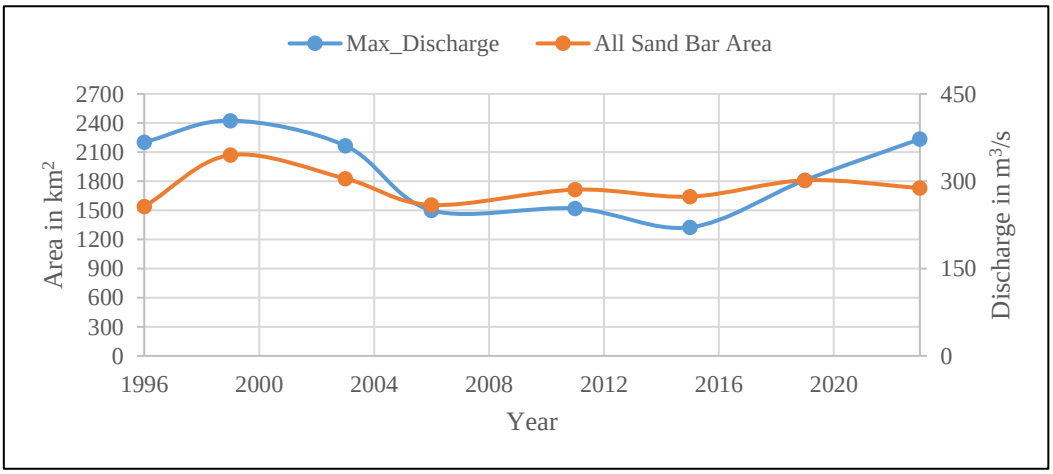

Fig. 9. Relation between discharge and sand bar area of the Teesta River between 1996 and 2023.

Discussion

The present work using remote sensing and GIS based approach with multi-date satellite data has revealed sharp changes in fluvial land form in recent

years resulting in considerable inhabited land loss. It is observed that in general the river has eroded both the banks throughout its course except at a few sites where banks are well defined as the river is constricted due to presence of dykes at some places on the right bank. River adjustment processes that affected fluvial system of the river Teesta include forcing functions like channel degradation and aggradations, lateral river migration, widening or narrowing, avulsion, changes in the quantity and character of the sediment load at spatial and temporal scale, intensely powerful monsoon regime, recurring earthquakes and adverse impact of anthropogenic factors. This study has proved the utility and application of satellite remote sensing which allows a retrospective, synoptic viewing of large regions and so provides the opportunity for a spatially and temporally detailed assessment of changes in river channel erosion/deposition. This study has further demonstrated how the use of GIS has been expedient in organization of geo-spatial databases and facilitation of channel position mapping and measurement. The Teesta is a meandering River with many oxbow bends. Over the years, under the combined impact of erosion, accretion, and human interventions, the Teesta River within Bangladesh has experienced significant hydro-morphological changes. Through the analysis of fifteen satellite images of Landsat MSS and TM collected between 1996 and 2023, below are the conclusions on the period riverbank migrations of Teesta River in Bangladesh. From the analysis, the mean erosion (negative value) and accretion rates estimated are -2.60 and 1.02 km^2/year on the left bank, and on the right bank of 7 interval. From the sectional analysis of left bank line net erosion was -0.39, -.80, -.36 and -1.05 km^2/year and for right bank it was -0.17, -0.42, -0.67 and 2.27 km^2/year of 4 sections of 7 interval. The migration results of both banks indicate a very dynamic form of erosion and accretion processes leading to channel shifting in the Teesta River. The left bank experienced erosion where the right bank experienced accretion but still bank line erosion is greater than deposition. The average sandbar net migration rate of all sand bar, temporary bar and permanent sandbar is 1.67, 3.64 and -0.47 km^2/year respectively for 7 intervals of 4 sections all sandbar and temporary sandbar is in deposition rate, but permanent sandbar is in erosion rate still total sandbar deposition is greater than sandbar erosion. The average net migration rate of 4 sections of 7 intervals estimated from Landsat images from 1996 to 2023 was 4.50, 2.38, 2.30, 2.03 and 3.75km^2/year for temporary sandbars, -0.29, 1.13, 0.26 and -1.56 km^2 for permanent sandbars and 0.40, 1.44, 0.78, -1.17 km^2 for all sandbars. From the dynamic behavior it is evident that section-4 is highly dynamic and secondly, section-2 as a higher standard deviation value section-4 than

section-2. The least standard deviation value is for section-3. The present study identified locations affected by bank erosion, accretion, and the bank line shifting and indicated the urgent need to protect the river banks employing afforestation measures and other strategies. Therefore, it is necessary to incorporate geomorphic changes in formulating flood management.

Conclusions

Multi-temporal satellite image was used to detect the change of bank line and sandbar in the Teesta River since 1996 with a four-year interval. The present study focused on the erosion and deposition pattern of Teesta River during the study period. The present study has used Landsat satellite image of 30x30m resolution with the application of GIS to identify the changes in the Teesta River over time. Hydrologic parameters at Dalia and Kaunia point of the river have been analyzed to find out the connection with the erosion and accretion pattern of the Teesta River. The present study revealed that the Teesta River is highly dynamic with bank line erosion and sandbar deposition. The present study found that erosion is dominating the accretion for the bank line, making the river wider, whereas accretion is dominating the erosion for sandbars, making the river more braided. Erosion in the left bank is much greater than the deposition, whereas deposition in the right bank is greater than the erosion. The present study also found that the river area and the sandbar area were modulated by the maximum discharge during May to October of the year. Accuracy of the research findings could be enhanced by using high resolution and multi-seasonal satellite data. The present study is critically important for decision-makers and policymakers. The outcome of the study could be used by the authorities for land management and proper river treatment work in the area. Also, the methodology can be implemented in different rivers of Bangladesh. It is important to note that change detection and measuring the rate using remote sensing is not a one-time endeavor, but rather an iterative process that requires periodic updates and refinement. Changes in land use, climate patterns, and other factors can influence, making it essential to regularly reassess and update river dynamics. So, further integration of the method in the future period is also necessary to keep the authorities up to date with the present situation.

Acknowledgments

This research is supported by the Bangladesh Space Research and Remote Sensing Organization (SPARRSO). This research acknowledges Bangladesh

Water Development Board (BWDB) for the hydrological data support to carry out the research.

References

Afrose, S, (2012). B. Sc. Engineering Thesis, Department of Water Resources Engineering, BUET, Dhaka, Bangladesh.

Akhter, S., Eibek, K. U., Islam, S., Islam, A. R. M. T., Chu, R., & Shuanghe, S. (2019). Predicting spatiotemporal changes of channel morphology in the reach of Teesta River, Bangladesh using GIS and ARIMA modeling. *Quaternary International*, 513, 80-94. https://doi.org/10.1016/j.quaint.2019.01.022

Azuma, R., Sekiguchi, H., & Ono, T. (2007). Studies of High-resolution Morphodynamics with special reference to river bank erosion. *Kyoto University Disaster Prevention Research Institute Annual Report.* C, 50(C), 199-209. http://hdl.handle.net/2433/73251

Baki, A. B. M., & Gan, T. Y. (2012). Riverbank migration and island dynamics of the braided Jamuna River of the Ganges–Brahmaputra basin using multi-temporal Landsat images. *Quaternary International*, 263, 148-161. https://doi.org/10.1016/j.quaint.2012.03.016

Bangladesh Bureau of Statistics (BBS). (2016). Statistical year book of Bangladesh, Bangladesh Bureau of Statistics, Dhaka, 2016.

Bhakal, L., Dubey, B., & Sarma, A. K. (2005). Estimation of bank erosion in the river Brahmaputra near Agyathuri by using geographic information system. *Journal of the Indian Society of Remote Sensing*, 33(1), 81-84. https://doi.org/10.1007/BF02989994

Darby, S. E., & Simon, A. (1999). The nature and significance of incised river channels. Incised river channels: processes, forms, engineering and management. *John Wiley & Sons*, Inc., New York, NY, 442.

Das, S., Datta, P., Sharma, D., & Goswami, K. (2022). Trends in temperature, precipitation, potential evapotranspiration, and water availability across the Teesta River basin under 1.5 and 2 °C temperature rise scenarios of CMIP6. *Atmosphere*, 13(6), 941. https://doi.org/10.3390/atmos13060941

Ghosh, K. (2014). Planform pattern of the lower Teesta River after the Gazaldoba barrage. *Indian Journal of Geography and Environment*, 13,

127-137. http://vidyasagar.ac.in/journal

Lawler, D. M., Couperthwaite, J., Bull, L. J., & Harris, N. M. (1997). Bank erosion events and processes in the Upper Severn basin. *Hydrology and Earth System Sciences*, 1(3), 523-534. https://doi.org/10.5194/hess-1-523-1997

Malcolm, I. A., Gibbins, C. N., Soulsby, C., Tetzlaff, D., & Moir, H. J. (2012). The influence of hydrology and hydraulics on salmonids between spawning and emergence: Implications for the management of flows in regulated rivers. *Fisheries Management and Ecology*, 19(6), 464-474. https://doi.org/10.1111/j.1365-2400.2011.00836.x

Mandal, S. P., & Chakrabarty, A. (2016). Flash flood risk assessment for upper Teesta river basin: using the hydrological modeling system (HEC-HMS) software. *Modeling earth systems and environment*, 2, 1-10. https://doi.org/10.1007/s40808-016-0110-1

Nabi, M. R., Rashid, M. S., & Hossain, M. I. (2016). Historical bankline shifting since 1760s: a GIS and remote sensing based case study of Meghna river plate of Rennell's atlas. *International Journal of Scientific and Research Publications*, 6(12), 473-483.

National Weather Service, (NWS), (2024). Flood discharge and water level correlation, National Weather Service.

NRCC (2023). Rivers of Bangladesh definition and numbers, Dhaka: National River Conservation Commission (NRCC). Available: https://en.prothomalo.com/environment/xyyqmcgwmo. [Accessed Aug 2024]

Pal, P. K., Rahman, A., & Yunus, A. (2017). Analysis on river bank erosion-accretion and bar dynamics using multi-temporal satellite images. *American Journal of Water Resources*, 5(4), 132-141. DOI:10.12691/ajwr-5-4-6

Planning, W. S. (2002). Developing and updating Empirical Methods for Predicting Morphological Changes of Jamuna River Information System, CEGIS, Dhaka.

Sarkar, A., Garg, R. D., & Sharma, N. (2012). RS-GIS based assessment of river dynamics of Brahmaputra River in India. *Journal of Water Resource and Protection*, 4, 63-72. https://doi.10.4236/jwarp.2012.42008

Schumm, S. A. (1985). Patterns of alluvial rivers. *Annual Review of Earth and Planetary Sciences*, 13, pp. 5. https://user.engineering.uiowa.edu/~cee_171/handouts/Schumm_1985.pdf

Takagi, T., Oguchi, T., Matsumoto, J., Grossman, M., Sarker, M., & Matin, M. (2007). Channel braiding and stability of the Brahmaputra River, Bangladesh, since 1967: GIS and remote sensing analyses. *Geomorphology*, 85(3-4), 294-305. https://doi.org/10.1016/j.geomorph.2006.03.028

Tarannum, T., Bhuyan, A., & Badhon, F. F. (2018). Morphological changes of river Teesta during the Last decade. In Proceedings of the 1st National Conference on Water Resources Engineering (NCWRE-2018) (Vol. 21, p. 22).

USGS, (2024). Streamflow and water level data., U.S. Geological Survey. https://waterdata.usgs.gov/nwis/rt

Inventory of Water Bodies for Fisheries Resources by Using High Resolution Satellite Sensor Data

Mohammad Imrul Islam*, Md. Abdur Rahman-Al-Mamun, Md. Mahmudur Rahman, Zebunnesa Khatun

Bangladesh Space Research and Remote Sensing Organization (SPARRSO)
Agargaon, Sher-e-Bangla Nagar, Dhaka – 1207.
**Corresponding author E-mail: imrul_islam@sparrso.gov.bd*

Abstract

Water coverage on land is a vital component of the water cycle, supporting transportation, irrigation, fisheries, and other human activities. Monitoring and mapping inland waterbodies using satellite imagery have significantly advanced with remote sensing technologies. This study aims to identify and map various types of inland waterbodies in Rupsa Upazila, Khulna, a region crucial for fisheries. High-resolution WorldView-3 satellite data and field observations were used to classify waterbodies, including rivers, canals, fish farms, ponds, and Beels. Findings reveal that rivers and canals are essential for water discharge and capture fisheries, while extensive fish farms dominate the former beel areas. Most ponds support aquaculture, though some near brickfields serve as sediment sources. Additionally, Khulna WASA reservoirs were identified as a distinct waterbody type. Field validation highlighted anomalies between remote sensing data and ground truth, emphasizing the need for continuous monitoring. The study underscores the importance of remote sensing for sustainable fisheries management. The generated waterbody map can aid policymakers in resource planning and conservation efforts. Further investigations are recommended to update and refine waterbody classifications, ensuring effective management strategies for enhancing fish production and maintaining aquatic biodiversity in the region.

Keywords: Waterbody, Fisheries, WorldView-3, Inventory.

Introduction

Water coverage in the land surface is a crucial part of the water cycle and mapping of waterbodies by interpreting satellite imagery has increased significantly. The surface water of earth planet is used for transportation, irrigation, fishing, and other human activities. Human intervention can alter the water level of the earth surface (Li et al., 2015). The monitoring of waterbodies plays a vital role in using water resources in a sustainable way. For this purpose, remote sensing is an excellent tool for surface water management as it has the capacity to identify and prepare surface water mapping (Deoli et al., 2021).

Remote sensing technique is significant for its real-time data and quick access to the land surface area and a perfect method for surface water body monitoring (Chen et al., 2004). Scientists have been using remote sensing techniques in the past decades to identify as well as distinguish water surface area. To produce thematic maps of land utilization or accentuation of water bodies, scientists have been using various satellite information that represents the changes on spatial, temporal, and ghastly aspects (Deoli et al., 2021). On the other hand, a number of techniques have been practiced extricating features by using satellite images (Masser, 2001, Peng et al., 2018). Mc Feeters proposed the normalized difference water index (NDWI) according to the analyses of the characteristics of water body (Shanlong et al., 2011) for the differentiation between surface water and vegetation. Four different water indices, namely WRI, NDWI, MNDWI and AWEI, to prepare map of natural water bodies (Jiang et al., 2014). Therefore, some challenges have been revealed between the results from remotely sensed data and the ground truth of the study area. (Deoli et al., 2021). Particular application method has its merit and demerits (Subramaniam et al., 2011; Li et al., 2013). The objectives of this study are to a) identify different types of inland waterbodies and b) map of different types of waterbodies.

Materials and methods

Study area

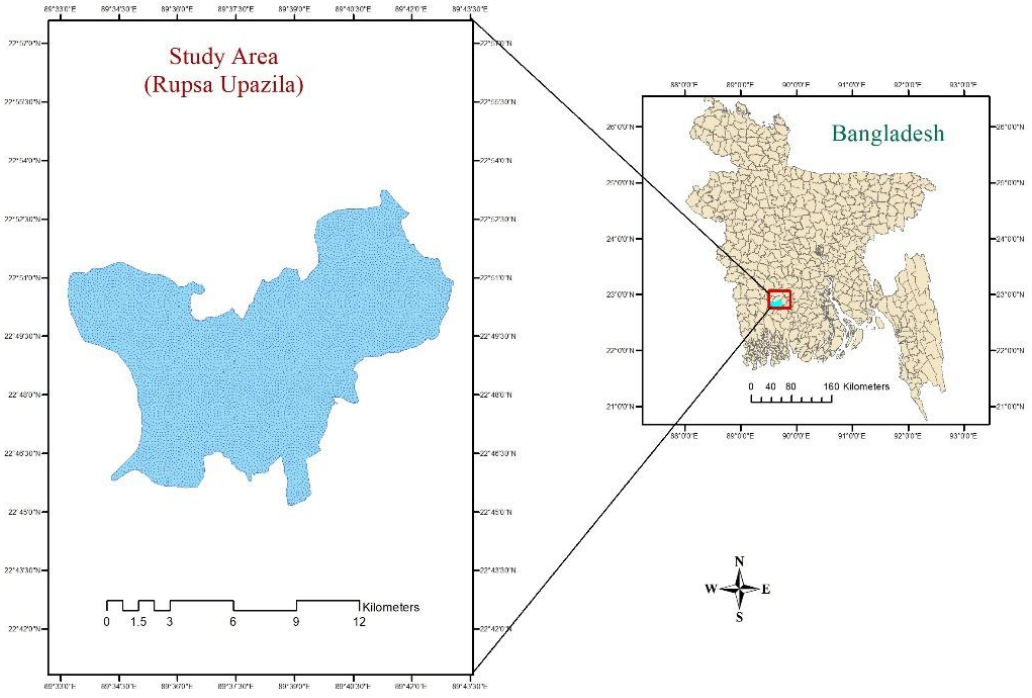

Fig. 1. Location of the study area.

Methodology

The selected study area is crucial for the fisheries sector as it covers both open and close water fisheries resources under aquaculture. In addition to this, the targeted area contains both freshwater and coastal water, which is the positive parameter of being rich in aquatic biodiversity and source of protein for Bangladeshi people. Considering the importance of fisheries resources, we selected this area as the area of interest for this study.

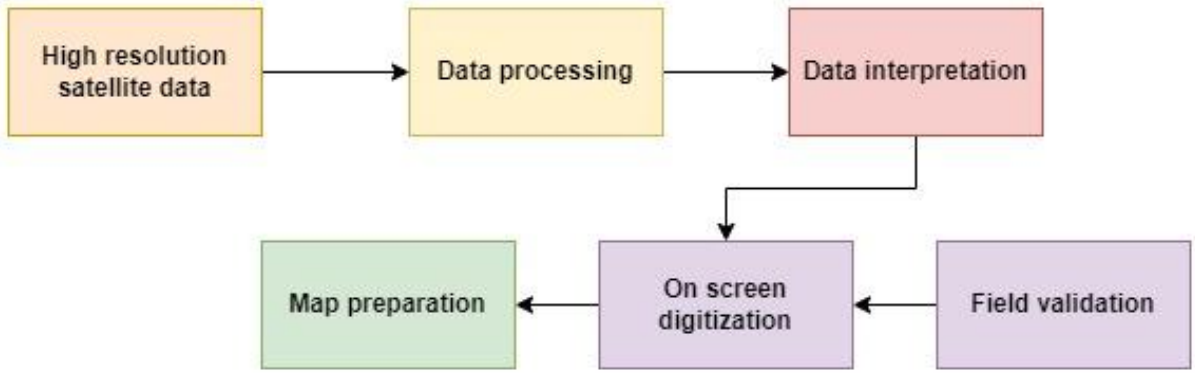

Fig. 2. Methodology of study.

To achieve the objectives of the study, high resolution satellite sensor data (world view-3) was used. On-screen digitization was done to identify all types of water bodies. The specification of the data is given in Table 1.

Table 1: Geospatial data used in this study

Spectral range	Band name	Spectral band	GSD (Ground Sample Distance)
Panchromatic Band (1)	450 – 800 nm		Nadir: 0.31 m, 20⁰ off-nadir: 0.34 m
MS (Multispectral) Bands (8) in VNIR (Visible Near Infrared)	Coastal Blue	400 – 450 nm	Nadir: 1.24 m, 20⁰ off-nadir: 1.38 m
	Blue	450 – 510 nm	
	Green	510 – 580 nm	
	Yellow	585 – 625 nm	
	Red	630 – 690 nm	
	Red Edge	705 – 745 nm	
	Near-IR1	770 – 895 nm	
	Near-IR2	860 – 1040 nm	
Satellite data		Other data	
World view-3 data owned by Maxer Technologies		Field observation	

Results and discussion

A total of five categories of waterbodies were found in the study area (Fig. 3). There are three major rivers in this area, and canals are directly or indirectly connected with rivers. Tidal action was found in both rivers and canals. These canals play a vital role in water discharging from household activities and rainfall runoff. Both resources (river and canal) are the prime source of capture fish for both local as well as country people. Among all types of fisheries resources of this area, a large area is covered by fish farm/ ghear. The former Beel area has been converted to fish farm/ ghear. Both prawn and carp mix culture is practiced under controlled conditions. A plenty number of ponds are found in the research area and most of the ponds are under extensive aquaculture systems.

An anomaly found during field validation that is ponds closed to brick fields are excavated not for aquaculture, rather, those ponds are connected with rivers. The tidal action brings lots of sediments that fill the pond close to the brick field, and the brick field uses the soil of the pond through excavation. In another area pond-like reservoir has been identified; however, it is the Khulna WASA reservoir tank where water is purified through different treatment actions. These two different types of waterbodies are marked as other fisheries resources during on-screen digitization. The remaining Beel area located at the northeastern part of the upazila is still under capture fishery and indigenous fish species are the main aquatic species.

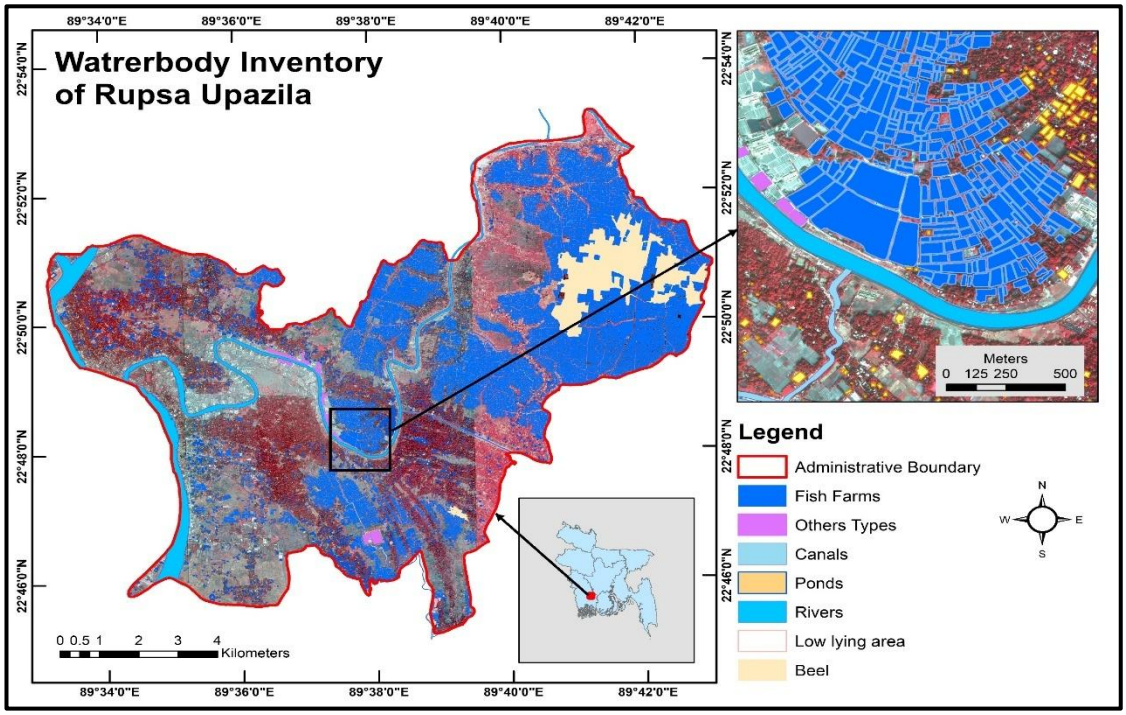

Fig. 3. Fisheries resources of Rupsa upazila of Khulna district.

Overall, the North-eastern part of this upazila bears most of the fisheries resources, i.e., fish farm and Beel area.

Conclusions

The present study focused on the identification of all types of fisheries resources in the selected upazila of Khulna district, which is a crucial task for fisheries management of that area. The output of this research could be used for sustainable management of resources that can enhance the overall fish production of that area. Further investigation will be conducted in the next fisacal year to complete the study objectives, which will be helpful to make the water area of this upazila up to date.

Acknowledgments

This research is supported by the Bangladesh Space Research and Remote Sensing Organization (SPARRSO).

References

Chen, Q., Zhang, Y., Ekroos, A., & Hallikainen, M. (2004). The role of remote sensing technology in the EU water framework directive (WFD). *Environmental Science & Policy*, *7*(4), 267-276. https://doi.org/10.1016/j.envsci.2004.05.002

Deoli, V., Kumar, D., Kumar, M., Kuriqi, A., & Elbeltagi, A. (2021). Water spread mapping of multiple lakes using remote sensing and satellite data. *Arabian Journal of Geosciences*, *14*(21), Article 2213. https://doi.org/10.1007/s12517-021-08597-9

Jiang, H., Feng, M., Zhu, Y., Lu, N., Huang, J., & Xiao, T. (2014). An Automated Method for Extracting Rivers and Lakes from Landsat Imagery. *Remote Sensing*, 6(6), 5067-5089. https://doi.org/10.3390/rs6065067

Li, L., Xia, H., Li, Z., & Zhang, Z. (2015). Temporal-Spatial Evolution Analysis of Lake Size-Distribution in the Middle and Lower Yangtze River Basin Using Landsat Imagery Data. *Remote Sensing*, 7(8), 10364-10384. https://doi.org/10.3390/rs70810364

Masser, I. (2001) Managing Our Urban Future: The Role of Remote Sensing and Geographic Information Systems. *Habitat International*, 25, 503-512. http://dx.doi.org/10.1016/S0197-3975(01)00021-2

Peng, J., Pan, Y., Liu, Y., Zhao, H., & Wang, Y. (2018). Linking ecological degradation risk to identify ecological security patterns in a rapidly

urbanizing landscape. *Habitat International*, 71, 110-124. https://doi.org/10.1016/j.habitatint.2017.11.010

Subramaniam, S., Babu, A.V.S., Roy, P.S. (2011). Automated Water Spread Mapping Using ResourceSat-1 AWiFS Data for Water Bodies Information System. *IEEE J. Sel. Top. Appl.* 4, :205–215. https://ieeexplore.ieee.org/document/5607324

Design and Manufacturing of a 1U CubeSat with Optimized Chassis Using 3D Printed Carbon Fiber Composite

Mohammad Mahdi Hasan[a*], Jagobandhu Some[a], Muhammad Sharif[a], Monirul Islam[b], Tanvir Shakil[c], Masuk Ridwan[d], Jeba Farjana[d], Farhan Tanvir[d], Imran Ahmed[d]

[a] Bangladesh Space Research and Remote Sensing Organization (SPARRSO), Agargaon, Sher-e-Bangla Nagar, Dhaka – 1207.
[b]North South University (NSU), Bashundhara, Dhaka-1229, Bangladesh.
[c]National Institute of Textile Engineering and Research (NITER), Savar, Dhaka, Bangladesh.
[d] Bangladesh University of Engineering and Technology (BUET), Dhaka-1000, Bangladesh.
**Corresponding author E-mail: mahdi@sparrso.gov.bd*

Abstract

This report presents the comprehensive design, manufacturing, and testing process of a 1U CubeSat developed by the Bangladesh Space Research and Remote Sensing Organization (SPARRSO) in collaboration with prominent educational and research institutions in Bangladesh. This is a significant initiative in Bangladesh's space and environmental monitoring capabilities. This CubeSat includes advanced materials and technology, showcasing innovative design principles while remaining cost-effective. It features a weather analysis module crucial for providing essential data for disaster management. Key components such as the G-Predict software for satellite tracking, Software Defined Radio (SDR) for communication, and an Artificial Intelligence (AI)-driven prediction model integrated with the Jetson Orin platform enable precise and reliable operation of the CubeSat. The project emphasizes the integration of cutting-edge technologies, including AI and advanced imaging systems, to enhance environmental monitoring and data analysis.

Keywords: G-predict software, Satellite tracking, Artificial Intelligence, Environmental monitoring.

Introduction

Recent years have seen an increase in the number of student satellites developed at universities around the world. To date, most university satellites require several years to develop significant financial resources, making them prohibitive for small programs (Heidt et al., 2000; Puig et al., 2001). The 1U CubeSat system, developed by SPARRSO (Bangladesh Space Research and Remote Sensing Organization), is a pioneering project to enhance Bangladesh's atmospheric research and disaster monitoring capabilities. The first CubeSats were launched in 2003, and just nine years

later, the one-hundredth CubeSat has been put in orbit (Swartwout, 2016). This system comprises a CubeSat for data collection and a Ground Segment for communication and retrieval. Launched via balloon, this CubeSat can monitor severe weather phenomena and capture images, providing critical data for disaster management and safeguarding lives and property in Bangladesh.

Materials and methods

The CubeSat system with ground station involves the Space Segment and the Ground Segment for Ground Communication. This integrated system will enable communication, data retrieval, and mission control for the CubeSat.

CubeSat Design

A CubeSat is a square-shaped, small, and low-cost satellite (typically 10 cm × 10 cm × 10 cm) 1U or 3U, or 6U designed for specific missions, such as Earth observation, Disaster Monitoring, or scientific research. The system includes essential components such as power supply, communication equipment, onboard computers, and scientific instruments, all integrated within the limited space (Fig. 1).

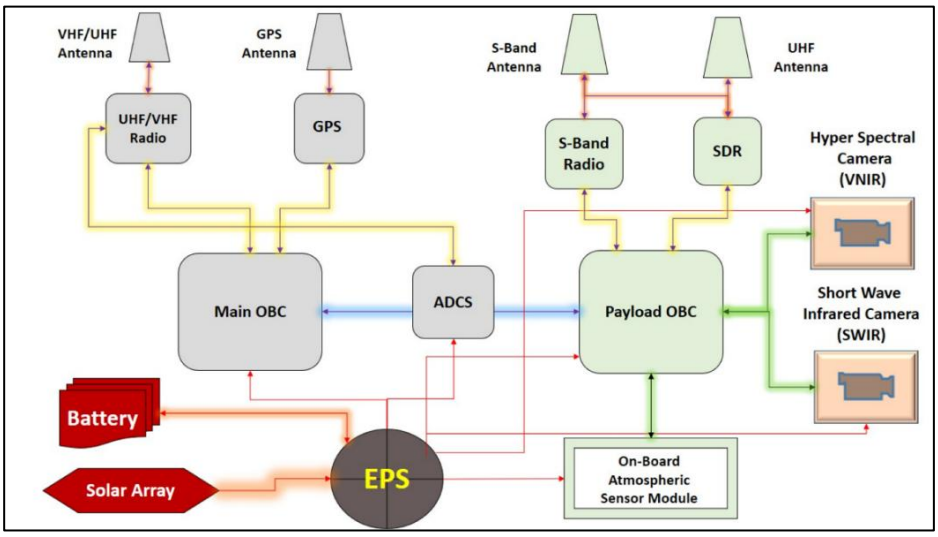

Fig. 1. CubeSat block diagram

Onboard Control System (OBC)

The NVIDIA Jetson Orin Nano was used as the CubeSat On-Board Computer (OBC) and serves as the brain of the CubeSat. It's based on a microcontroller connected to subsystems via a serial data bus and hardware devices.

Electric Power System (EPS)

The CubeSat Electrical Power System (EPS) manages power collection and distribution within the satellite. It integrates a Battery Management System (BMS) and controls power supply for subsystems and payloads (Fig. 2).

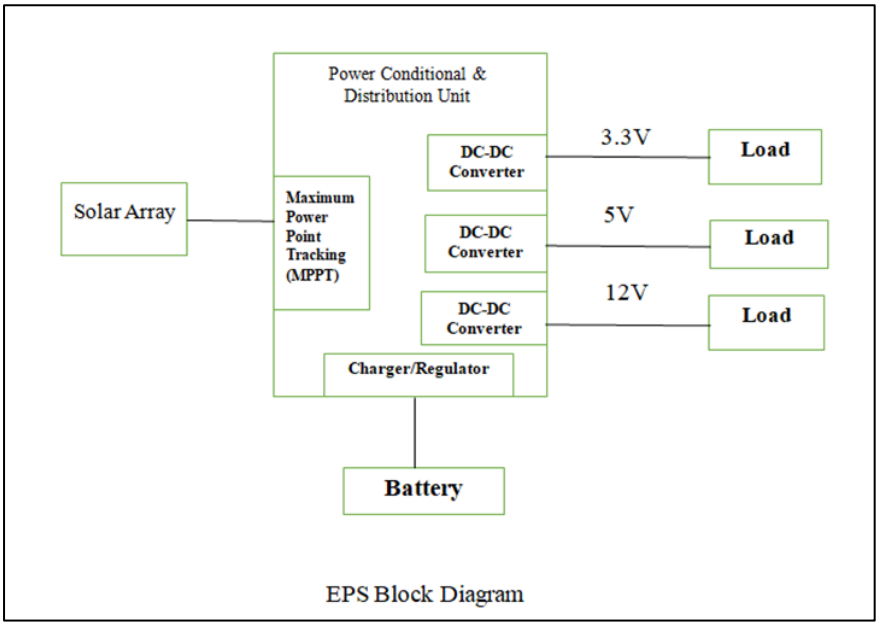

Fig. 2. Block Diagram of CubeSat electric power system controller

Communication Sub-System

The Communication Sub-System depicted in the image is designed for the CubeSat (Fig. 3) This sub-system facilitates robust and reliable communication between CubeSat and ground stations.

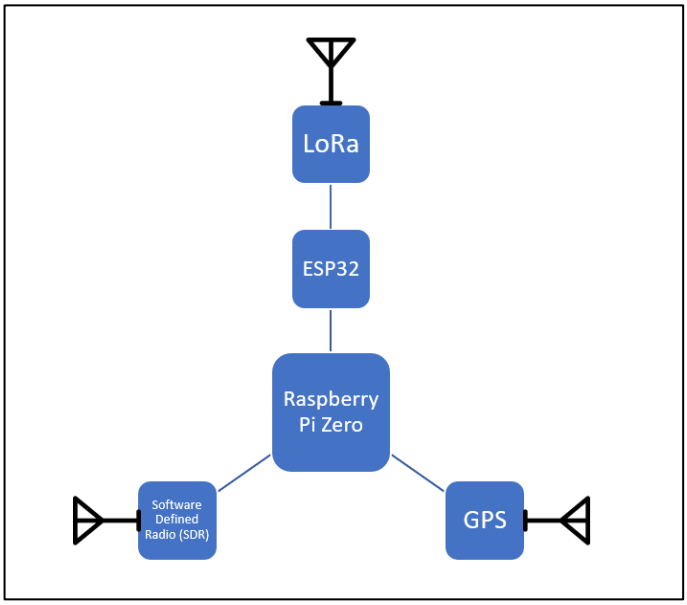

Fig. 3. CubeSat communication sub-system block diagram

Camera and Imaging Sub-System

The Camera and Imaging Subsystem for our CubeSat integrates advanced thermal and optical imaging capabilities, crucial for atmospheric research and object detection. The subsystem employs two primary cameras: the LWIR Thermal Imaging Camera and the High-Level 30x Optical Zoom Camera, each selected for their unique attributes and compatibility with CubeSat requirements (Fig. 4).

Fig. 4. The camera and thermal imaging sensors used in CubeSat.

CubeSat Structure Design

The CubeSat structure is a skeletal framework of a miniature satellite. The structure is characterized by its geometric precision and is typically made from lightweight yet durable materials like aluminum. It features a series of cutouts and patterns on each face, which are not only aesthetically pleasing but also functional, allowing for the attachment of various components and instruments.

Ground Station Design

A satellite ground station is a surface-based facility designed for real-time communication with satellites. These stations send radio signals to the satellite (uplink), receive data transmissions from the satellite (downlink), and, in some cases, serve as command-and-control centers for the satellite network (Fig.5). It includes a G-Predict module for satellite tracking, communication software for data handling, and an embedded system comprising an IMU sensor, embedded software, and hardware.

Communication Sub-System

The Communication Sub-System consists of a Power Supply Unit that feeds into both the Downlink Receiver and Uplink Transmitter, which are connected to an Antenna Tracking System.

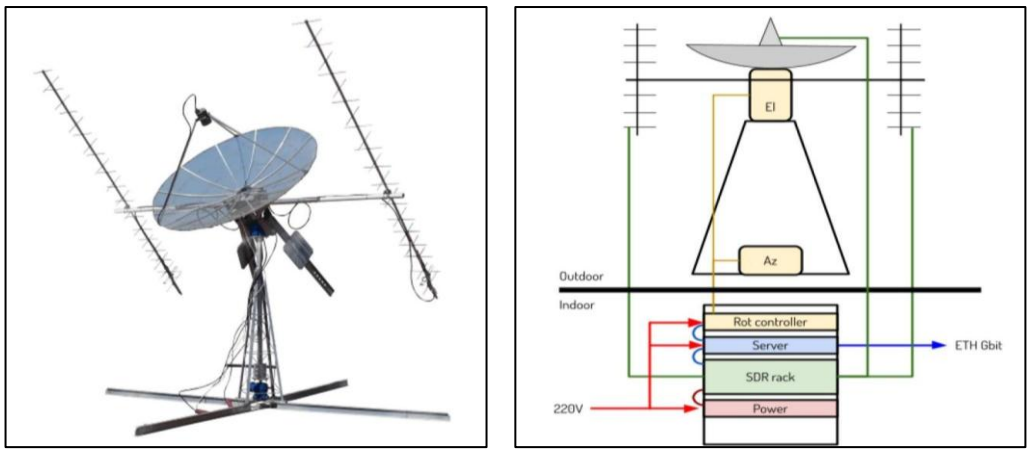

Fig. 5. Design of Ground Station Satellite Tracking Rotator Antenna

Ground Station Software Environment

The Ground Station Software Environment is a comprehensive suite designed for mission control operations. It encompasses modules for mission management, data handling, communication optimization, and system monitoring (Fig. 6).

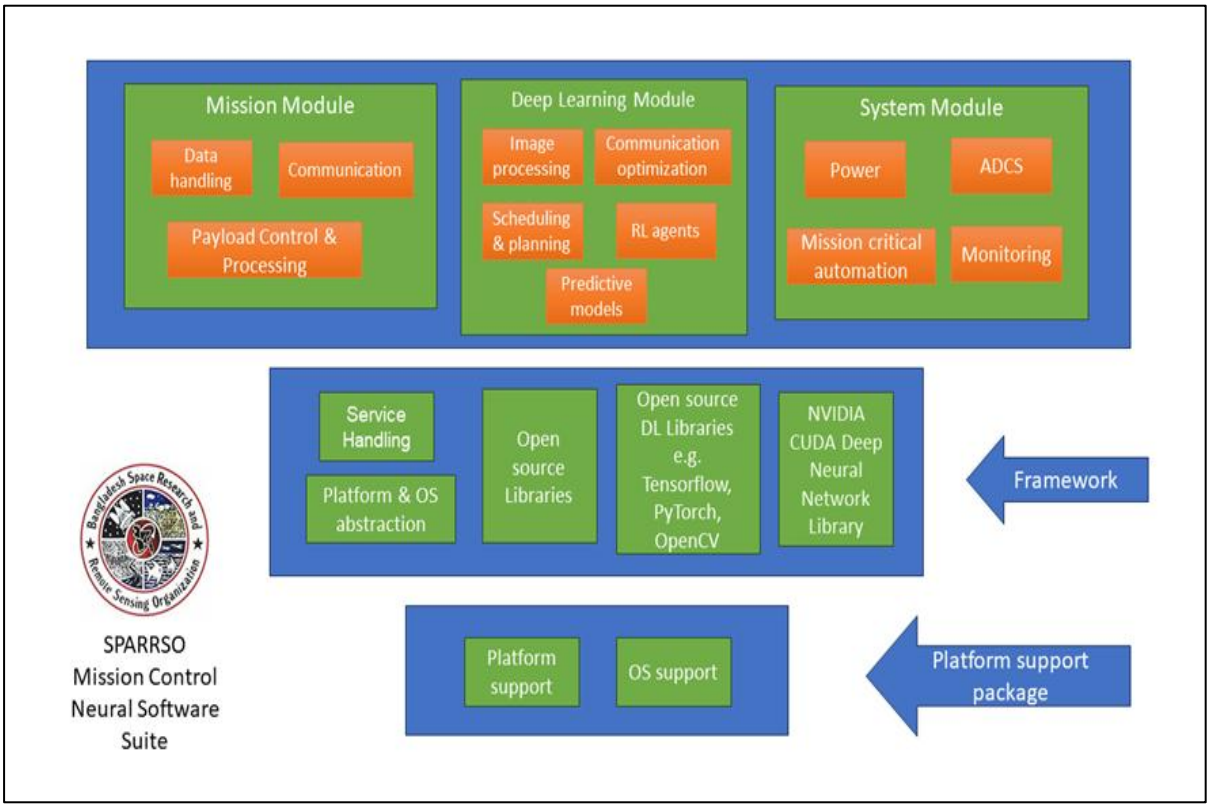

Fig. 6. Block Diagram of Ground Station Software environment

Ground Station Control System

The Ground Station Control System manages satellite communications using a diverse range of radios (S-band, UHF, and VHF). It features an antenna system, GPS receivers for positioning, a gyro and accelerometer module for orientation data, and precise azimuth and elevation gear motors (Fig. 7-10). A microcontroller unit (MCU) controls these components, while a user interface display and a dedicated database/server handle data processing.

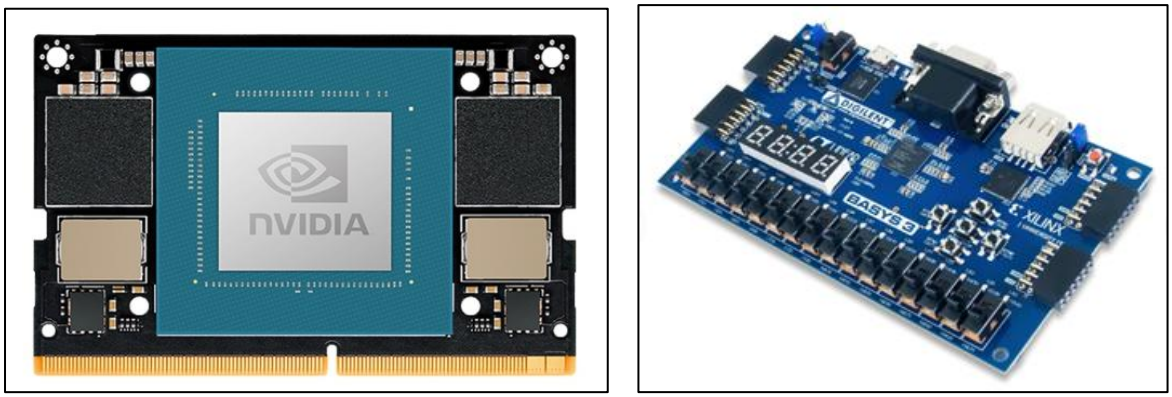

Fig. 7. Jetson Orin Nano used as the main OBC and Basys 3 Artix-7 FPGA Board used as Payload OBC or for weather module.

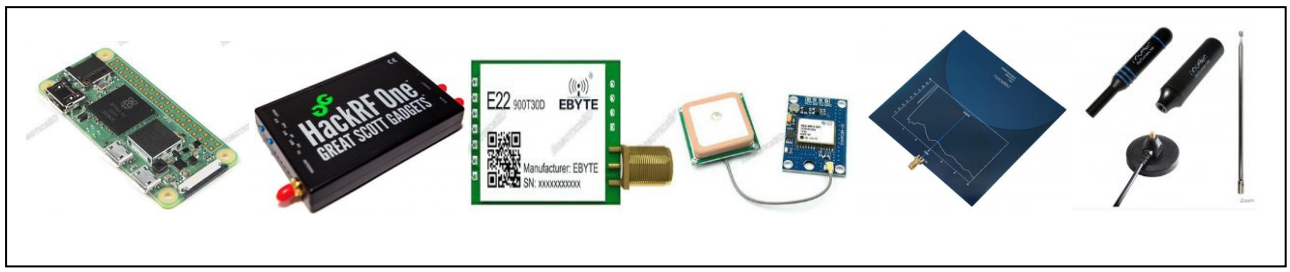

Fig. 8: Raspberry Pi Zero, HackRF SDR, LoRa module, GPS module, and antennas used for CubeSat communication sub-system.

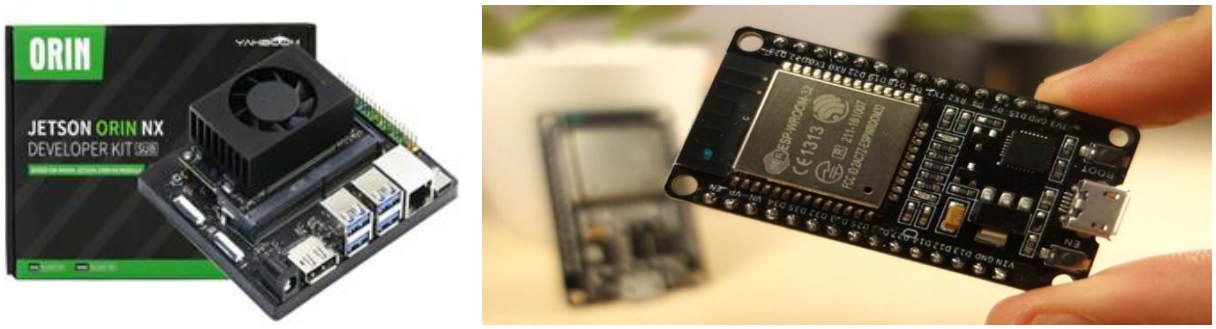

Fig. 9: Jetson Orin NX 16GB used as the main OBC of the ground station and ESP-32 as the microcontroller.

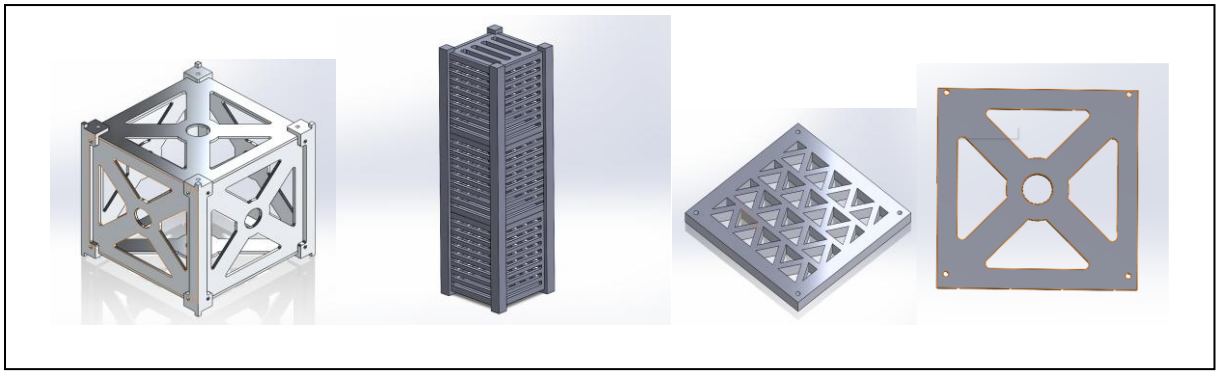

Fig. 10. Solid works design for cubesat structure developed for 3D printing with G-Code.

For communication, we are using Software Defined Radio (SDR) which is configured by GNU Radio and LORA communication Module for Telemetry and Data Communication (Fig.13).

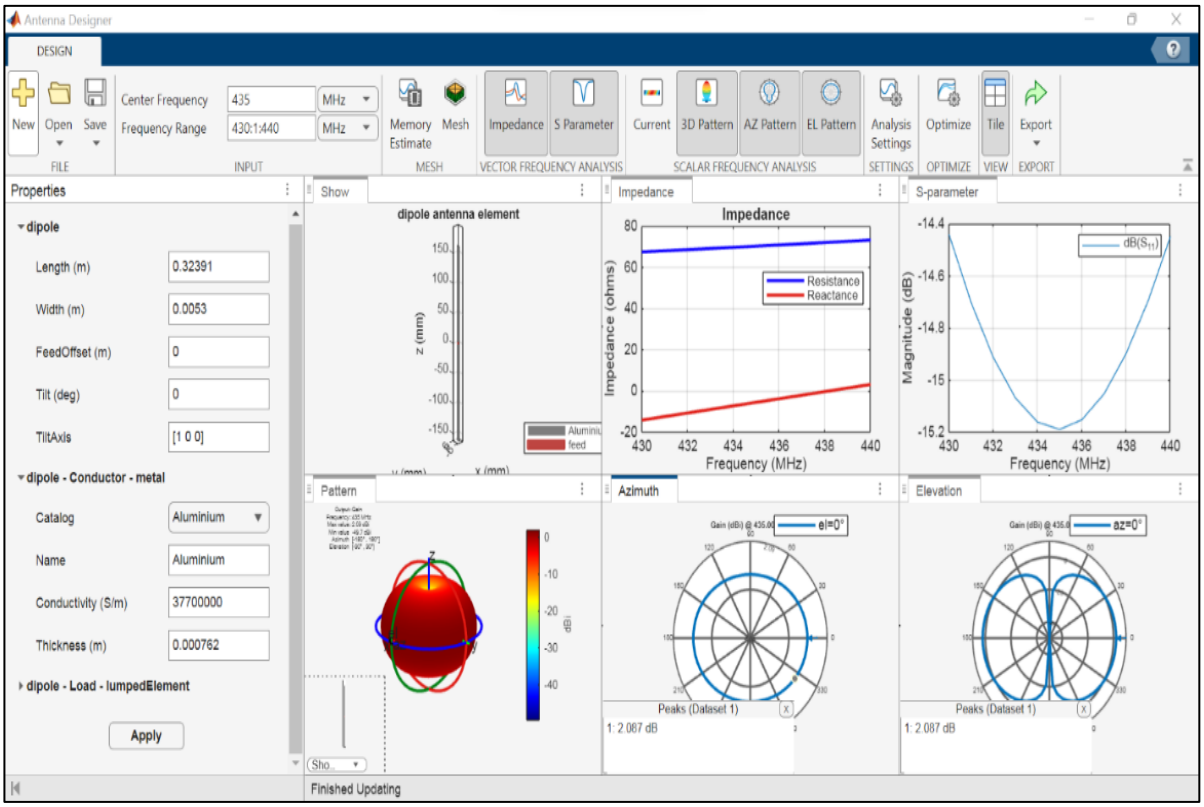

Fig. 11. Radiation pattern of CubeSat dipole antenna at 435 MHz

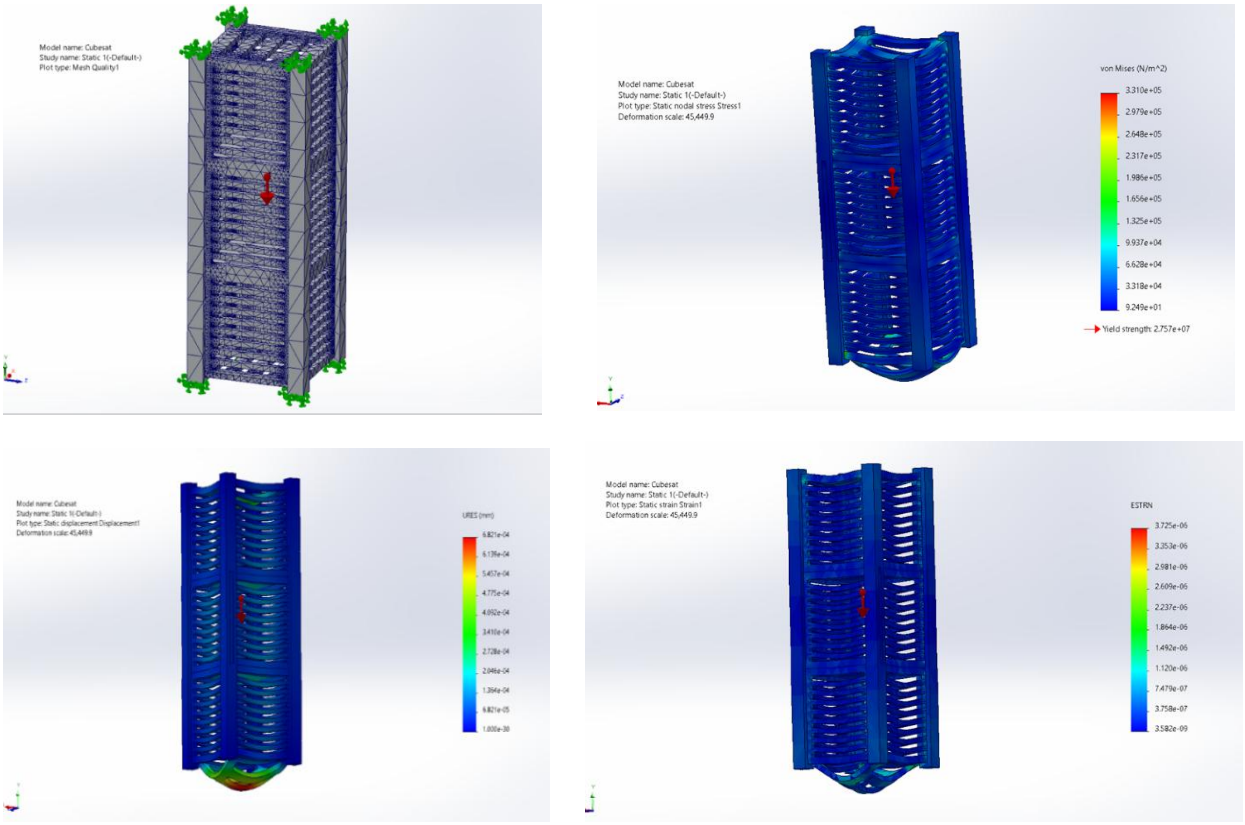

Fig. 12. Meshing for static structural simulation, results of static structural analysis (stress), results of static structural analysis (displacement) and results of static structural analysis (strain).

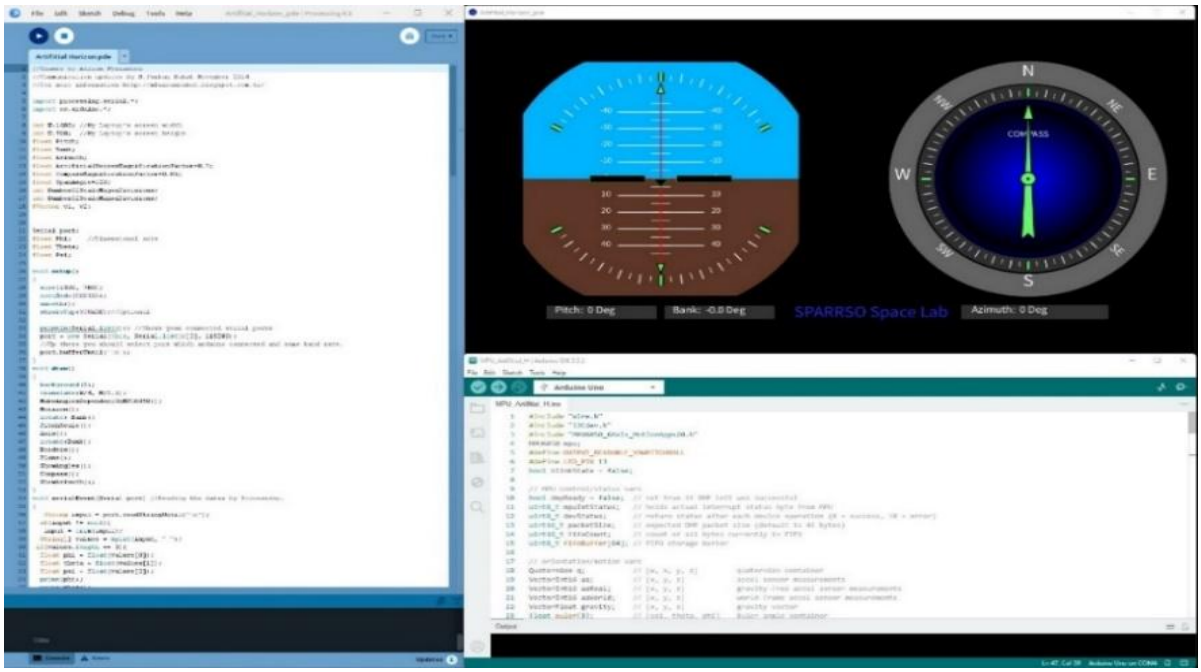

Fig. 13. SDR radio communication control by g-predict software.

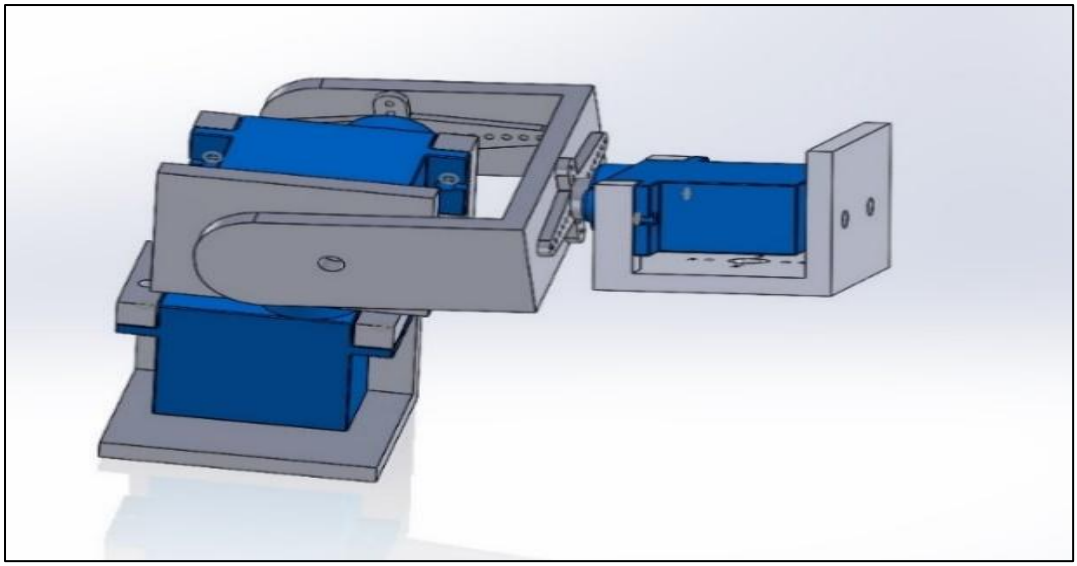

Fig. 14. Shows the design of a 3-axis rotator control module developed for the lab experiment.

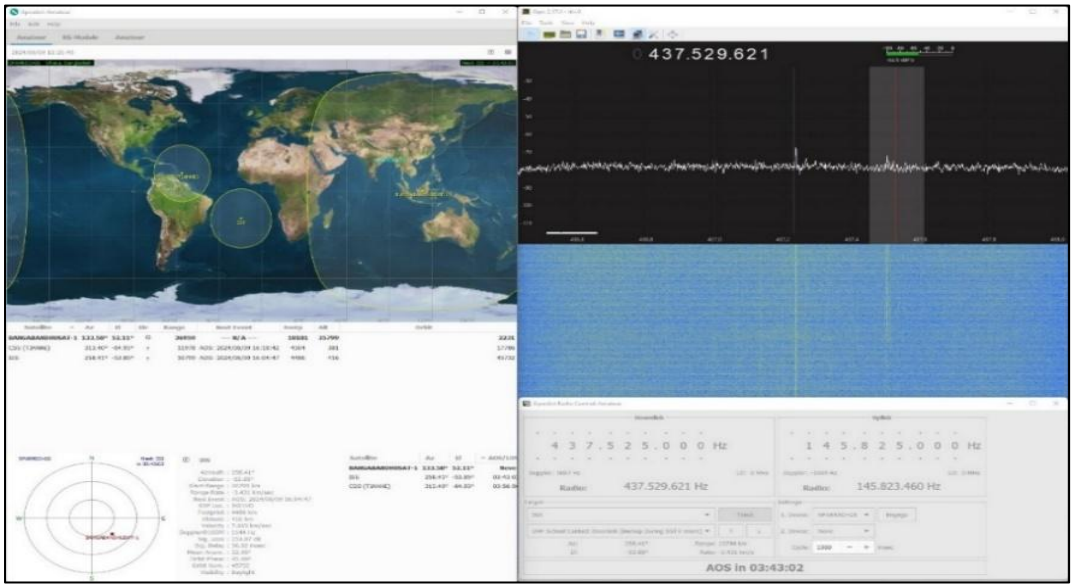

Fig. 15. Antenna direction and horizon visualizer.

Results and discussions

The development and testing phases of the 1U CubeSat project by SPARRSO have yielded promising results, demonstrating significant advancements in satellite technology and ground station capabilities. This section outlines the key findings, data analysis, and interpretations drawn from the comprehensive research and experiments conducted. The ground station's communication systems, which include multiple transceivers and antenna modules, were thoroughly tested and optimized. The G-Predict software, interfaced with the antenna motor control system, efficiently tracked and maintained communication with the CubeSat. Signal strength

and data integrity were consistently high, demonstrating the reliability of the Software Defined Radio (SDR) and LoRa communication modules used for telemetry and data communication.

Conclusions

The development of the 1U CubeSat by SPARRSO, in collaboration with prominent educational and research institutions, represents a significant milestone in Bangladesh's space research and environmental monitoring capabilities. This research aims for a successful demonstration of a cost-effective and robust satellite system to grow expertise in space technology and its application for environmental monitoring and disaster management. This project lays a strong foundation for future advancements in the country's space research capabilities. However, this project needs more time to accomplish as all the necessary components are not available in our local market. We hope to continue the development of this system in the future.

Acknowledgments

We extend our heartfelt gratitude to the team members for their dedicated efforts in the design, analysis, and manufacturing phases, who have supported the successful completion of this research. First and foremost, we are deeply thankful to SPARRSO for providing access to essential resources and facilities that were instrumental in the development of the 1U CubeSat and its optimized chassis.

References

Heidt, H., Puig-Suari, J., Moore, A., Nakasuka, S., & Twiggs, R. (2000). CubeSat: A new generation of picosatellite for education and industry low-cost space experimentation. Proceedings of the AIAA/USU Conference on Small Satellites, SSC00-V-5, 1-19. https://digitalcommons.usu.edu/cgi/viewcontent.cgi?article=2069&context=smallsat

Puig-Suari, J., Turner, C., & Twiggs, R. (2001). Development of the standard CubeSat deployer and a CubeSat class picosatellite. *Proceedings of the IEEE Aerospace Conference*, 1-8. https://ieeexplore.ieee.org/document/931726

Swartwout, M. (2016). The first one hundred CubeSats: A statistical look. *Journal of Small Satellites*, 2(2), 213-233. https://ui.adsabs.harvard.edu/abs/2013JSSat...2..213S

Design, Analysis & Simulation of an ML-based Remote Sensing Device and Antenna System

Mohammad Mahdi Hasan[a]*, Jagobandhu Some[a], Muhammad Sharif[a], Arnab Musabbir[b], Md Ashikur Rahman Any[b], Mishfaqur Rahman[c]

[a]Bangladesh Space Research and Remote Sensing Organization (SPARRSO), Agargaon, Sher-e-Bangla Nagar, Dhaka-1207.

[b]Bangladesh University of Engineering and Technology (BUET), Dhaka-1000, Bangladesh.

**Corresponding author E-mail: mahdi@sparrso.gov.bd*

Abstract

This study details the design, manufacturing, and testing processes of a Machine-learning (ML)-based Remote Sensing Device and Antenna System developed by the Bangladesh Space Research and Remote Sensing Organization (SPARRSO). Marking a pivotal step in the nation's space exploration and environmental monitoring efforts, the device incorporates advanced materials and technologies, demonstrating innovative and cost-effective design principles. It is equipped with a weather analysis module to deliver critical data for disaster management. Key components include Long-Range (LoRa) for communication and an Artificial Intelligence (AI)-driven prediction model. This project highlights the integration of cutting-edge technologies such as AI and advanced imaging systems, significantly enhancing environmental monitoring and data analysis capabilities.

Keywords: Machine-learning, Artificial Intelligence, UAVs, Rover.

Introduction

Bangladesh Space Research and Remote Sensing Organization (SPARRSO) is the focal space organization of the Government of Bangladesh. SPARRSO is about to enter the arena of space technology through its short, medium, and long-term planning. One of the momentous aims of this plan is to design, launch, and operate remote sensing devices like UAVs and Rover. The development of such systems is supported by research on LoRa communication and advanced materials in space systems.

Materials and methods

The design process had to undergo a lot of trial and error. Initially, the conceptual design was done using SolidWorks software. After that, some parts were printed using a Bambu Lab 3D printer and some metal parts and Testing were done at SPARRSO’s Space Technology Research Lab.

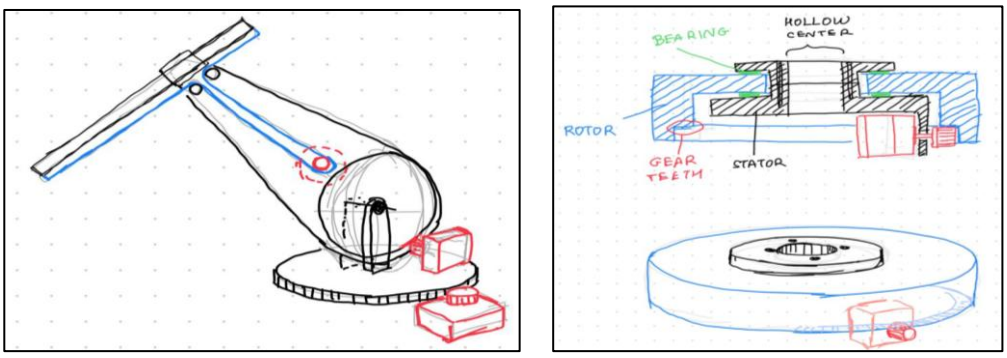

Fig. 1. Conceptualized rover arm and its base.

CAD Design of Tire, Chassis, Body, Arm, End Effector

The CAD design phase involved creating intricate designs for essential components of ROVER The CAD design phase involved creating intricate designs for critical components in ROVER (Fig. 2 & 3). The tire design was optimized for traction and durability following the Mars rover wheel (Dalmeida et al., 2024), while the chassis and body designs ensured structural integrity and weight distribution. The robotic arm was engineered for precision, critical for rover operations. In contrast, the chassis and body designs prioritized structural integrity and weight distribution to support the entire system. The arm and end effector designs were engineered for precision and strength, enabling versatile manipulation capabilities crucial for the rover's intended tasks.

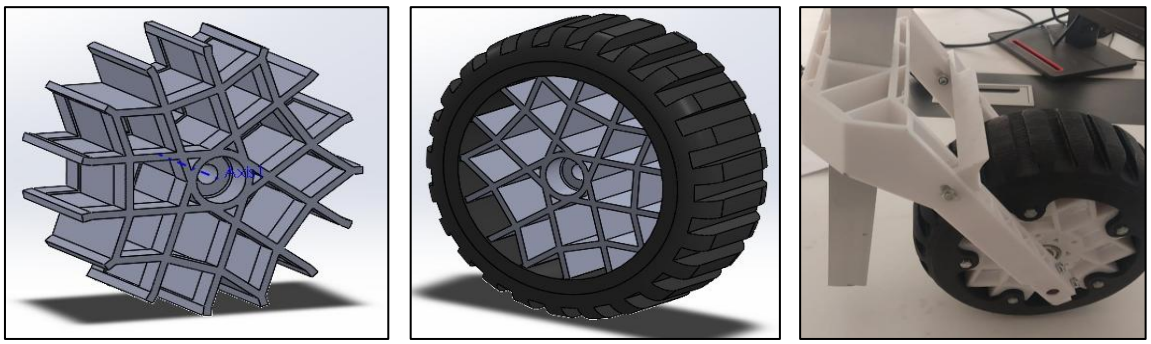

Fig. 2. CAD design of the wheel rim and tire, assembled wheel with 3D printed parts.

3D Print of Designed Parts

Following meticulous CAD design, the next step was translating these designs into physical components through 3D printing. This process utilized advanced materials to ensure each part met exact specifications for strength, durability, and weight considerations. The 3D printing phase facilitated rapid prototyping and iterative refinement, allowing for efficient adjustments based on initial testing and integration needs.

Electrical Subsystem Layout

The layout of ROVER's electrical subsystem was a critical aspect of its design. It involved strategic placement and routing of components to optimize space utilization and minimize electromagnetic interference Careful consideration was given to power distribution, ensuring efficient operation and reliability across the system. This phase laid the foundation for the seamless integration of sensors, actuators, and communication modules essential for ROVER's functionality.

Communication System

The development of ROVER's communication system focused on establishing robust connectivity between the rover and its operator. Wireless technologies were integrated to enable real-time data transmission and remote-control capabilities, essential for mission-critical operations and situational awareness. The communication system was designed to withstand environmental challenges and ensure continuous, reliable communication under varying operational conditions. LoRa communication is a recent communication technology under the Low Power Wide Area Network (LPWAN) that emphasizes long-range communication with high receiving sensitivity ability (Zourmand et al., 2019).

Initial Prototype Assembly

Assembly of the initial prototype marked a significant milestone in integrating mechanical, electrical, and software components into a cohesive system. This phase involved meticulous attention to detail to ensure proper alignment and functionality of all subsystems.

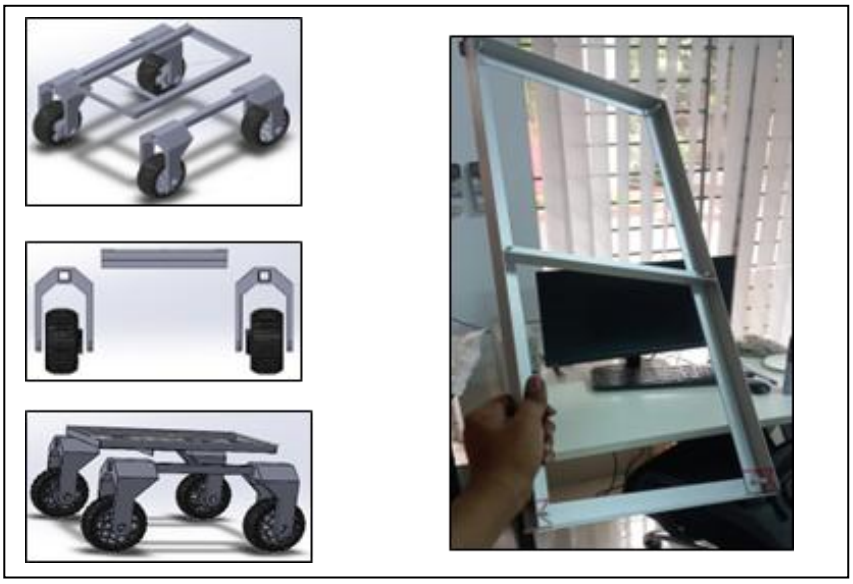

Fig. 3. CAD images of the rover chassis, manufactured chassis skeleton.

The prototype assembly aimed to validate design assumptions and identify potential areas for improvement through iterative testing and refinement.

Calibration of Sensors

Sensor calibration was essential to ensure accurate data acquisition and interpretation. This phase involved fine-tuning sensors such as cameras, LiDAR, and environmental sensors to optimize performance across different operational scenarios. Calibration processes focused on achieving precise measurements and minimizing errors, enhancing ROVER's ability to gather relevant data for decision-making and autonomous navigation.

Testing of Basic Functionalities

Rigorous testing of basic functionalities validated the operational capabilities of ROVER's integrated systems. This phase included comprehensive checks on movement controls, sensor data acquisition, and actuator responsiveness. Testing protocols were designed to simulate real-world conditions, providing insights into performance under various environmental factors and operational demands.

Integration of Telemetry Systems

The integration of telemetry systems enabled real-time monitoring of ROVER's operational parameters and environmental feedback. This capability facilitated remote diagnostics and proactive maintenance, enhancing operational efficiency and safety during field deployments. Telemetry systems provided critical insights into ROVER's performance metrics, guiding iterative improvements and ensuring reliability in mission-critical scenarios.

Preliminary Field Testing

Preliminary field testing provided crucial feedback on ROVER's performance in real-world environments. These tests focused on validating navigation algorithms, evaluating responses to control commands, and assessing durability under operational stresses. Data collected during field tests informed iterative refinements to hardware and software components, addressing identified issues and optimizing ROVER's overall functionality and reliability.

Results

Sensor Connections: Ongoing efforts are focused on optimizing sensor connections within ROVER's architecture. This task involves ensuring robust and reliable communication between sensors and the central processing

unit (CPU). Emphasis is placed on minimizing latency and maximizing data integrity to enhance situational awareness and decision-making capabilities during operations.

Electrical Subsystem: Continued development of ROVER's electrical subsystem is underway to further refine power distribution and component integration. This task includes implementing efficient power management strategies to extend operational endurance and reliability. Ongoing optimizations aim to minimize energy consumption while maintaining optimal performance across all subsystems. PV cells are used as a primary power source and batteries as the emergency power source following the design of the electrical power system of the Mars rover (Dongsheng and Pei, 2014).

Control System: The ongoing refinement of ROVER's control system encompasses software updates and algorithmic enhancements. This task focuses on improving response times, motion control accuracy, and autonomous navigation capabilities. Iterative adjustments based on field test data and user feedback aim to enhance ROVER's agility and adaptability in dynamic environments.

Fine-tuning of Communication Protocols: Efforts are ongoing to fine-tune communication protocols to ensure seamless and reliable data transmission between ROVER and its operator. This task includes optimizing bandwidth utilization, enhancing error detection and correction mechanisms, and integrating protocols that accommodate varying environmental conditions. Continuous improvements aim to maintain robust connectivity and operational efficiency.

User Interface Development: The user interface (UI) for ROVER is being developed to enhance operator interaction and control capabilities. This task involves designing intuitive interfaces that provide comprehensive real-time feedback on ROVER's status, sensor data, and operational parameters. Usability testing and iterative design refinements ensure the UI meets operational requirements and user expectations.

Motor Driver Configuration: Ongoing configuration of motor drivers is essential to optimize the performance and efficiency of ROVER's propulsion and actuation systems. This task includes adjusting motor parameters such as torque, speed, and acceleration profiles to achieve optimal operational characteristics. Continuous monitoring and adjustment ensure reliable and precise control over ROVER's movement and manipulation capabilities.

Integration of Power Management System (BMS): Integration efforts focus on enhancing ROVER's power management capabilities through the implementation of a Battery Management System (BMS). This task includes monitoring battery health, optimizing charging cycles, and implementing safety protocols to extend battery life and ensure reliable power supply. Ongoing refinements aim to maximize operational uptime and efficiency.

Testing of Navigation Algorithms: Ongoing testing of navigation algorithms is crucial to refine ROVER's autonomous capabilities. This task involves evaluating algorithm performance in diverse environments and scenarios, including obstacle avoidance, path planning, and localization. Data-driven adjustments aim to improve navigation accuracy, reliability, and adaptability to dynamic terrain and operational conditions.

Assembly of Robotic Arm: Continued assembly and integration of the robotic arm are ongoing tasks aimed at enhancing ROVER's manipulation capabilities. This task includes fine-tuning joint movements, gripper functionalities, and sensor integration to optimize dexterity and precision in object-handling tasks. Iterative adjustments based on practical testing ensure the robotic arm meets performance requirements and operational expectations.

Initial Field Calibration and Testing: Ongoing field calibration and testing are essential to validate ROVER's performance in real-world environments. This task involves fine-tuning sensor readings, verifying system reliability under operational stresses, and evaluating overall system robustness. Data collected from ongoing field tests informs iterative refinements and optimizations to enhance ROVER's operational readiness and reliability.

Power System BMS: Implementation of a Battery Management System (BMS) is planned to monitor and optimize ROVER's power supply and consumption. This includes implementing smart charging algorithms, battery health monitoring, and safety protocols to maximize battery lifespan and reliability during operations.

Discussions

The project encountered challenges due to malfunctions with the 3D printer, which delayed the fabrication of critical components. This issue necessitated troubleshooting and repairs, impacting the project timeline and requiring alternative manufacturing strategies to mitigate delays. Periodic unavailability of specific parts required for assembly and integration disrupted workflow continuity. This challenge necessitated

proactive sourcing alternatives and exploring substitute components without compromising system performance or functionality. Integration challenges arose when incorporating new components into existing subsystems, requiring iterative adjustments and compatibility testing. Rigorous testing and validation processes were essential to ensure seamless integration and functionality across the entire system architecture.

Compatibility issues encountered when integrating ROVER with existing systems or technologies posed interoperability challenges. Resolving these issues involved iterative testing, software updates, and interface modifications to ensure seamless communication and functionality across interconnected systems (Babcock & Smith, 2021; Rahman & Chowdhury, 2022). Plans include conducting rigorous mechanical stress testing to validate the durability and structural integrity of ROVER's components. This testing will simulate extreme conditions and operational stressors to assess performance limits and identify areas for reinforcement or design improvements.

Enhancements to ROVER's mechanical structure will involve iterative design refinements and material selection to achieve optimal balance between weight, strength, and flexibility. This includes integrating modular components for scalability and adaptability to varying mission requirements and environmental conditions.

Conclusions

The design, analysis, and testing of the ML-based Remote Sensing Device and Antenna System represent a significant milestone for the Bangladesh Space Research and Remote Sensing Organization (SPARRSO) and its collaborators. This initiative underscores the potential of integrating machine learning, advanced materials, and innovative design principles to address critical challenges in space exploration and environmental monitoring. The development process involved meticulous planning, from CAD modeling and 3D printing to comprehensive sensor calibration and rigorous field testing. Despite encountering challenges such as component delays and integration difficulties, the project team demonstrated resilience and adaptability, employing alternative manufacturing strategies and iterative design refinements to maintain progress. Key outcomes include the creation of a robust communication system, an AI-driven weather analysis module, and a modular, scalable architecture (Babcock & Smith, 2021) capable of supporting diverse applications. Preliminary testing validates the system’s capability to operate in complex environments,

paving the way for further enhancements in autonomous navigation, power management, and user interface development. This research not only advances SPARRSO's capabilities but also establishes a foundational framework for future endeavors in satellite technology, disaster management, and environmental data analysis. By leveraging innovative technologies, the project contributes to the nation’s broader scientific and technological goals, providing a template for cost-effective, high-performance systems that align with global standards.

Acknowledgments

We extend our heartfelt gratitude to the team members for their dedicated efforts in the design, analysis, and manufacturing phases who have supported the successful completion of this research. First and foremost, we are deeply thankful to SPARRSO for providing access to essential resources and facilities that were instrumental in the development of the ROVER.

References

Dalmeida, J., Sequeira, F. S., Abrar, M., Crasta, J. (2024). Design and analysis of Mars rover wheel. *International-Journal-of-Innovative-Research-in-Advanced-Engineering*, 11 (2),741-746. https://doi.org/10.26562/ijirae.2024.v1107.03

Dongsheng, J., and Pei, Z. (2014). An electrical power system of Mars rover. 2014 IEEE Conference and Expo Transportation Electrification Asia-Pacific (ITEC Asia-Pacific), Beijing, pp. 1-4. https://ieeexplore.ieee.org/document/6940651

Zourmand, A., Hing, A.L.K., Hung, C.W. and AbdulRehman, M. (2019). Internet of Things (IoT) Using LoRa Technology. 2019 IEEE International Conference on Automatic Control and Intelligent Systems (I2CACIS), Selangor, 29-29 June 2019, 324-330. https://doi.org/10.1109/I2CACIS.2019.8825008

Design and Assemble of Optical Telescope for Space Observation and Astronomical Research Capacity Building in SPARRSO

Md. Naim Islam Talukder*, S.A.M. Arif-Ul-Haque

Bangladesh Space Research and Remote Sensing Organization (SPARRSO), Agargaon, Sher-e-Bangla Nagar, Dhaka-1207.
**Corresponding author E-mail: talukder.naim@sparrso.gov.bd*

Abstract

Astronomy is the scientific study of celestial objects, phenomena, and the distribution of matter and energy across the universe, encompassing visible and invisible elements such as stars, planets, galaxies, nebulae, and cosmic dust. This field, which has evolved from ancient traditions to modern space exploration, is a vital tool for understanding the universe. A key milestone in astronomy's development was the telescope's invention in the 17th century by Galileo Galilei, which revolutionized our understanding of the solar system and laid the foundation for future discoveries. Modern astronomy is divided into two primary branches: observational and theoretical astronomy. Observational astronomy focuses on gathering data from astronomical phenomena through instruments such as telescopes, while theoretical astronomy uses the principles of astrophysics to analyze and interpret this data, aiming to uncover the underlying mechanisms of the universe's formation, evolution, and future. Nowadays, modern space observation systems are at the core of the current advanced space research organization of all developed countries. This research is one of the fundamental research projects in the field of astronomy, which will build the capacity of SPARRSO researchers in space observation, exploration, and further valuable astronomical research in this arena.

Keywords: Observational astronomy, Optical Telescope, Universe formation, Space exploration.

Introduction

Astronomy is the study of celestial objects, structures, matter, and energy distribution in the universe, including both visible and invisible universe like the Sun, the moon, the planets, the stars, the galaxy, the nebula, and the interstellar and intergalactic dust and cloud beyond earth's atmosphere. Astronomy is introduced as an interesting and amazing science from ancient to modern period (Barmby, 2018). Today’s advanced human civilization has stepped beyond the earth and modern astronomy has become a vital source of space exploration and learning of the unknown matter of our extremely mysterious universe. The first true breakthrough

in humankind's exploration of the universe was the invention of the telescope in the 17th century. Italian astronomer Galileo Galilei was an early adopter and developer of that technology, which enabled him to make major strides in the understanding of our solar system. Astronomy is a broad discipline encompassing many subfields including observational astronomy, theoretical astronomy, planetary science, astrophysics, cosmology and astrobiology.

Professional astronomy is divided into two major parts, one is theoretical, and the other is observational. Observational astronomy is focused on acquiring data from observations of astronomical objects. This data is then analyzed theoretically using basic principles of astrophysics. Astrophysicists apply the laws and theories of physics to astronomical observations. It's an attempt to understand the mechanism behind how the universe was created and how it has and will evolve. Space observation with ground-based optical telescope also includes astrometry and astrophotography in observational astronomy.

Astrometry is the science of positional astronomy, which measures the location of a celestial object and its movement within the plane of the sky. This was one of the first techniques used to search for planets around other stars. Astrophotography, also known as astronomical imaging, is the photography or imaging of astronomical objects, celestial events, or areas of the night sky. High quality scientific data are gathered and analyzed by using powerful telescope and various astronomy image processing tools (Burns, 2021).

Materials and Methods

This research utilized different materials and some of the major components have been given below.

1. Computerized Newtonian Reflector Telescope (Dobsonian Sky watcher Go-To Telescope; Aperture: 400 mm & Focal length: 1800 mm).
2. Dobsonian mount with motorized Alt-Az rotation system.
3. SynScan Hand Control with 42,000+ Celestial Object Database.
4. Digital Single Lens Reflector (DSLR - Canon 90D) camera.
5. Different types of Telescope related accessories (Finder scope, Eyepieces, Barlow lens, Astronomy Filter, Focal Reducer, etc.).
6. Astronomy Software-Stellarium, PIPP, Autostakkert3, GIMP, Registax6.
7. The Interactive-Sky-Chart from Sky & Telescope (American Astronomical Society).

The methodological workflow of this research has been outlined in Fig.1.

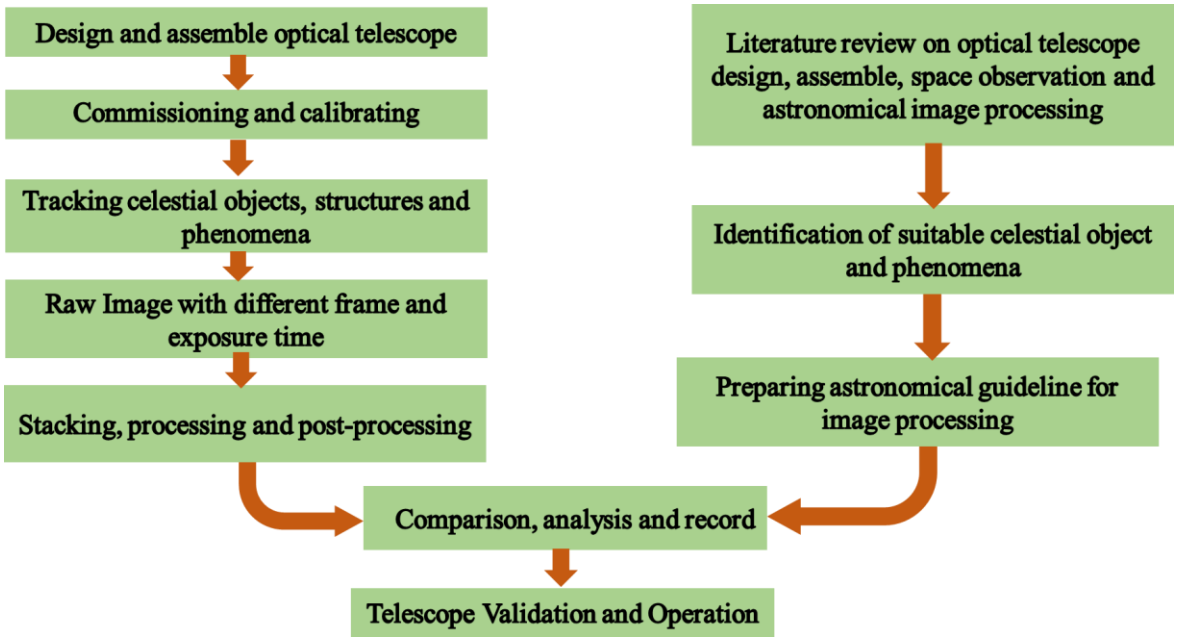

Fig. 1. Research methodology

Results and Discussion

The specific results of this project are a) Complete ground-based Optical space observation system; b) capacity building of optical telescope design, assembles, and observation; c) astronomical guideline for image processing from telescope data; and d) radical celestial events and objects data record.

The aim of this research project is space observation through a ground-based optical telescope. The main tasks of this research project are to purchase a 400 mm/16-inch diameter optical telescope for space observation and build a 12-inch diameter optical telescope for capability building. The research work is divided into two phases. In the first year (phase-I) a 16-inch diameter telescope has been purchased and set up, and installation, validation, and commissioning work has been completed. In the second year (Phase-II) we make a 12-inch diameter optical telescope for capacity building, and a dome to house it and record the scientific results of space observations. With the telescope, some test images from the observation are given in Fig. 2 and Fig. 3.

Fig. 2. Telescope calibration and validation in the rooftop.

Fig. 3. Test images of curved moon with craters and highlands.

Conclusions

Ground-Based Optical Space observation is one of the thumbs of the established space organization. As a national focal point of space organization in Bangladesh, SPARRSO have the mandate to take fundamental research for the further development of space science and technology in Bangladesh. Through this research project we wish to build the capacity to start our journey from the earth surface to our desire deep space exploration. Researcher in Bangladesh will get Practical deep space scenario from here which will increase the interest in the practice of

astronomy among the common people in Bangladesh. An opportunity will be created in the future to use our astronomy data in research, which will play an important role in the field of further research in Astronomy and astrophysics in Bangladesh.

Acknowledgements

First of all, we would like to express our gratitude to our esteemed Chairman Md. Rashedul Islam and all the board members for accepting, approving and providing facilities for this research project. We are grateful to everyone involved in the financial and procurement process of the optical telescope with related accessories. We are also grateful to all our colleagues for their scientific and sincere advice.

References

Barmby, P. (2018). Astronomical observations: a guide for allied researchers. *ArXiv*. https://doi.org/10.21105/astro.1812.07963

Burns, M. S. (2021). A Practical Guide to Observational Astronomy. CRC Press. https://doi.org/10.1201/9781003203919

The Interactive Sky Chart. Sky & Telescope. https://skyandtelescope.org/interactive-sky-chart/

Formulation of Draft National Space Legislation in Bangladesh

Rubel Kanti Dey*, Muhammad Sharif, Md. Nur Hossain Sharifee

Bangladesh Space Research and Remote Sensing Organization (SPARRSO), Agargaon, Sher-e-Bangla Nagar, Dhaka-1207.
**Corresponding author E-mail: rubelkanti@sparrso.gov.bd*

Abstract

Developing national space legislation is essential for countries aiming to establish a robust space industry, and Bangladesh is no exception. Despite acceding to the Outer Space Treaty of 1967 in 1986, Bangladesh has not ratified other international space laws or treaties nor established a comprehensive national legal framework for space activities. This lack of legislation poses significant challenges, including technical expertise, institutional collaboration, and regulatory alignment with international standards. Bangladesh seeks high-income status through industrialization and highlighting the potential benefits of space legislation, such as economic growth, foreign investment, and the development of a commercial space industry. Previous research has proposed a draft space act tailored to Bangladesh's needs, but gaps remain. This study reviewed the necessary documents related to space legislation and outlined a framework for developing national space legislation in Bangladesh, proposing eight (8) relevant chapters and twenty-five (25) sections. This study emphasizes the necessity of aligning domestic space laws with international standards to fully realize the country's space research, technological development, and economic potential.

Keywords: Space law, Outer space, Framework, Space legislation, Bangladesh.

Introduction

The development of national space legislation is crucial for any country looking to establish a viable space industry. Bangladesh, a rapidly developing country, is also exploring the prospects of expanding its space program. In the year of 1986, Bangladesh became a state party of the Outer Space Treaty 1967 through accession (UNOOSA, 1967). Except for this treaty, Bangladesh has not ratified any of the other international space law treaties, nor has it established any major national legal framework in this area. However, the country faces significant challenges in this endeavor, including the need for technical expertise, knowledge, collaboration between institutions, and regulatory alignment with international space laws. Regarding many issues relating to space affairs, Bangladesh does not have any legal framework that would guide any authority to act in accordance with a specified formal procedure (Hossain,

2019). There are no proper rules, regulations or acts in Bangladesh which will guide us on comprehensive issues related to space law. As a result, Bangladesh faces constant challenges and complications to deal with matters related to space law. Moreover, Bangladesh vision 2041 aims at achieving high-income status through industrialization and encourages expansion and investment in various ranges of industries. Nevertheless, the potential benefits of developing national space legislation, such as foreign or private company investment, economic development, commercial use of the space industry, establishment of spaceport and spacecraft manufacturer, collaboration between institutions, environment protection etc., are substantial. The previous research works examine the prospects and challenges of developing national space legislation in Bangladesh and formulate a draft space act considering the various countries' legislation primarily considering fundamental needs from Bangladesh's perspectives. The proposed research aims to review the draft legal framework, identify gaps, and propose a comprehensive legislative framework for the space sector in Bangladesh. It concludes that, despite the difficulties, the country must pursue this goal to realize the full potential of its space research and technological development, eyeing the space economy and industrial prospects. So Bangladesh needs to develop domestic space legislation in accordance with international space law and other model laws around the world.

The objectives of this research are (a) to find out and fill up the required reforms, additions, and amendments of the previous phase draft Space Activities Act of Bangladesh; (b) to assess feedback from different organizations/ministries and organize stakeholder meetings/seminars in favor of space affairs and legislation; and (c) To finalize the national space legislation covering all the issues related to space law.

Materials and methods

A qualitative, doctrinal approach to research methodology follows the research. The paper likely adopts a multi-disciplinary approach, drawing upon legal research, comparative analysis, and studies to inform the formulation of the draft national space legislation (Jakhu & Dempsey, 2017; Lyall & Larsen, 2018). The report analyses international space law treaties, legal frameworks of various space-faring nations, and the prospects and challenges for developing national space legislation in Bangladesh. The study aims at investigating new possibilities of space law in Bangladesh. It also tends to search for potential solutions and steps for the development of the space industry of Bangladesh. The study explores the scope and

benefits of adopting a national space law and finding out the challenges to doing so.

Results and discussion

Draft Space Activities Act

The following draft act has been outlined by reviewing and analyzing different countries' space activities related to legal documents. Whereas, making provisions promoting the responsible and sustainable development of space activities, remote sensing, and geographical information system (GIS); outlining the provisions of authorization, supervision, registration, liability, insurance, environment protection, space debris mitigation of such activities, penalties; incorporation of UN principles, guidelines, and international space treaties such as, Outer Space Treaty, Registration Convention, Liability Convention, etc. and for matters ancillary has been counted for further space activities (UNOOSA, 1967; APRSAF, 2020; Freeland, 2020; IISL, 2021).

This draft act proposes 8 chapters and 25 sections (Table 1) and is entitled "Bangladesh Space Activities Act, 2023." This act applies to space activities, remote sensing, and GIS activities carried out within the People's Republic of Bangladesh or outside of Bangladesh on (a) space object, aircraft, vessel, vehicle, or facilities registered in Bangladesh; or (b) by operators, owners, or companies registered in Bangladesh. The following sections have been listed in the proposed chapters, which are listed below.

Table 1: Potential chapters proposed for the Bangladesh Space Activities Act 2023

Chapter	Title	Section
Chapter 1	Preliminary	1.1 Short title, application, and commencement 1.2 Definitions
Chapter 2	Authorization, Formulation, and Supervision of Space Activities	2.1 Compliance with International Law 2.2 Formulation of Policy, Rules, Regulations, and Guidelines, 2.3 Authorization for Space Activities, Remote Sensing and GIS 2.4 Prerequisites for authorization 2.5. Application for authorization 2.6 Withdrawal, suspension or amendment of authorization 2.7 Supervision

Chapter	Title	Section
Chapter 3	Registration	3.1 Registry of Space Objects, Remote Sensing and Geographical Information System
Chapter 4	Liability and insurance	4.1 Liability for damage done by operator or owner 4.2 Insurance
Chapter 5	Protection of Environment	5.1 Environmental Protection 5.2 Space Debris Mitigation
Chapter 6	Remote Sensing and GIS Data Management	6.1 Approval of Remote Sensing and GIS Activity 6.2 Supervision of Remote Sensing and GIS Data 6.3 Acquisition and Distribution of Remote Sensing and GIS Data 6.4 Remote Sensing Data Distribution Standard
Chapter 7	Penalties	7.1 Punishment for unauthorized space activity 7.2 Punishment for unauthorized remote sensing and GIS activity 7.3 Punishment for misinformation and false document 7.4 Punishment for non-compliance with supervising authority 7.5 Punishment for non-compliance with environment protection and space debris mitigation rules
Chapter 8	Miscellaneous	8.1 Intellectual property rights 8.2 Right of authority for information

Development of Questionnaire for Stakeholder Meeting/Seminar

To assess feedback from different organizations/ministries and organizing stakeholder meetings/seminars in favor of space affairs and legislation, the following questions have been prepared in accordance with present and future perspectives of space-related affairs of Bangladesh.

Space Law and Policy Questionnaire

a) What kind of "Space Activity" works are being conducted in your institution?)

b) Are the "Space Activity" related works conducted by Government funding/non-government/foreign funding?

c) In conducting such activities, do you follow any policy/guideline/rule?

d) Does your institution have any relation with any domestic or foreign institution in conducting "space activity"?

e) Which stages of space activities would your institution like to be covered in its intended national space legislation?

f) Would your institution prefer to enact a general law on outer space activities or a specialized one?

g) Which of the following options resembles the legislative requirements of your institution?

h) Which national authority shall be entrusted with authority according to your institution to conduct space activities?

i) Which of the following regulative categories does your institution wish to be included in national space legislation?

j) What are the priorities of your institution for space legislation?

Conclusions

Creating effective and comprehensive space laws will require significant effort, resources, and expertise, particularly in policy development and legal infrastructure. After reviewing the draft act and comprehensive questionnaire, further progressive development will continue until the next financial year. Despite the challenges, Bangladesh has the potential to become a prominent player in the space sector through the development of national space legislation. While developing national space legislation in Bangladesh is a complex and challenging task, it is also a necessary step towards ensuring the country's participation and competitiveness in the global space community. In conclusion, developing national space legislation in Bangladesh presents both promising opportunities and significant challenges. After considering feedback from different organizations/ministries organizing stakeholder meetings/seminars in favor of formulating space affairs and legislation, it will create a strong impact in finalizing this research output.

Acknowledgements

The research study was conducted with financial support from Bangladesh Space Research and Remote Sensing Organization (SPARRSO)'s annual research budget of 2023-2024.

References

Asia-Pacific Regional Space Agency Forum (APRSAF). (2020). Space policy development in the Asia-Pacific region: Lessons for emerging space nations. Retrieved from https://www.aprsaf.org on Jan 2025.

Freeland, S. (2020). The role of international law in regulating space activities. *Journal of Space Law*, 44(1), 1-25. https://doi.org/10.1017/S0000000000000000

Hossain, K. (2019). Space activities in Bangladesh: Legal and policy challenges. *Asian Journal of International Law*, 9(2), 345-360. https://doi.org/10.1017/S0000000000000000

International Institute of Space Law (IISL). (2021). Proceedings of the International Astronautical Congress: Space law and policy for developing nations. Paris, France.

Jakhu, R. S., & Dempsey, P. S. (2017). Space law and policy: A comprehensive guide to the legal and regulatory framework for space activities. McGill University Press.

Lyall, F., & Larsen, P. B. (2018). Space law: A treatise (2nd ed.). Routledge. https://doi.org/10.4324/9781315558942

United Nations Office for Outer Space Affairs (UNOOSA). (1967). Treaty on Principles Governing the Activities of States in the Exploration and Use of Outer Space, including the Moon and Other Celestial Bodies (Outer Space Treaty). Retrieved from https://www.unoosa.org

Bangladesh Space Research and Remote Sensing Organization (SPARRSO)

Mohakash Biggyan Bhaban, Agargaon, Sher-e-Bangla Nagar, Dhaka 1207, Bangladesh
Phone: +88-02-48117692, Fax: +88-02-48111169
E-mail: admin@sparrso.gov.bd
Website : www.sparrso.gov.bd